

PREPARATION AND CHARACTERIZATION OF POLYMERIC HARD TISSUE SUPPORTS

A THESIS SUBMITTED TO
THE GRADUATE SCHOOL OF NATURAL AND APPLIED SCIENCES
OF
MIDDLE EAST TECHNICAL UNIVERSITY

BY

TUĞBA ENDOĞAN

IN PARTIAL FULFILLMENT OF THE REQUIREMENTS
FOR
THE DEGREE OF DOCTOR OF PHILOSOPHY
IN
POLYMER SCIENCE AND TECHNOLOGY

MARCH 2013

Approval of the thesis:

**PREPARATION AND CHARACTERIZATION OF POLYMERIC HARD TISSUE
SUPPORTS**

submitted by **TUĞBA ENDOĞAN** in partial fulfillment of the requirements for the degree of
**Doctor of Philosophy in Polymer Science and Technology Department, Middle East Technical
University** by,

Prof. Dr. Canan Özgen
Dean, Graduate School of **Natural and Applied Sciences**

Prof. Dr. Teoman Tinçer
Head of Department, **Polymer Science and Technology**

Prof. Dr. Nesrin Hasırcı
Supervisor, **Chemistry Dept., METU**

Prof. Dr. Vasif Hasırcı
Co-supervisor, **Biological Sciences Dept., METU**

Examining Committee Members:

Prof. Dr. Serpil Aksoy
Chemistry Dept., Gazi University

Prof. Dr. Nesrin Hasırcı
Chemistry Dept., METU

Assoc. Prof. Dr. Caner Durucan
Metallurgical and Materials Engineering Dept., METU

Prof. Dr. Teoman Tinçer
Chemistry Dept., METU

Prof. Dr. Necati Özkan
Polymer Science and Technology Dept., METU

Date: 01/03/2013

I hereby declare that all information in this document has been obtained and presented in accordance with academic rules and ethical conduct. I also declare that, as required by these rules and conduct, I have fully cited and referenced all material and results that are not original to this work.

Name, Last name : Tuğba Endoğan

Signature :

ABSTRACT

PREPARATION AND CHARACTERIZATION OF POLYMERIC HARD TISSUE SUPPORTS

Endođan, Tuđba
Ph.D., Department of Polymer Science and Technology
Supervisor: Prof. Dr. Nesrin Hasırcı
Co-supervisor: Prof. Dr. Vasıf Hasırcı

March 2013, 118 pages

In recent years, the demand for the use of artificial materials have increased drastically in biomedical field since autografts have limited availability and allografts lead to immune response problems. The aim of this thesis was to prepare polymer based materials which will be used for either supportive or regenerative materials for hard tissue applications.

In the first part of the thesis, hydroxyapatite (HAp) containing acrylic based bone cements as supportive materials were prepared. In this thesis, bone cements with different compositions were prepared by using PMMA microspheres and ground and sieved PMMA particles, with particle sizes in the range of 50–150 μm (BC1), 1–50 μm (BC2) and 1 μm (BC3). Formulations were obtained by addition of HAp to enhance the biocompatibility and mechanical strength of the cements. Various bone cement formulations were obtained by application of oxygen plasma to increase the compatibility of polymeric and inorganic components. Some formulations contained ammonium nitrate, zeolite or chitosan. Plasma application improved the mechanical properties of all groups but increased the maximum curing temperature which is undesirable for bone cements. Addition of zeolite served as reinforcement and increased the mechanical strength of bone cements. Chitosan containing bone cement formulation was used in the in vivo applications in rats and new bone tissue formation was observed.

In the second part of the thesis, 2D and 3D porous scaffolds were prepared as regenerative materials for bone tissue engineering applications. In the preparation of scaffolds, chitosan and poly(lactic acid-co-glycolic acid) (PLGA) were used as the biodegradable polymeric component and HAp as the mineral component. Scaffolds were produced by three different techniques: microfabrication, freeze drying and electrospinning. They were characterized by chemical, thermal, mechanical and in vitro tests. Microfabrication technique yielded porous 2D membranes with regular square holes at micron level. 3D scaffolds having interconnected macroporous structure and 77-89% porosity were produced by freeze drying. PLGA and HAp containing scaffolds had the highest compressive modulus in the hydrated state. Fibers with diameters in the range of 180–525 nm were obtained with electrospinning technique. It was shown that degradation rate of chitosan scaffolds could be controlled by addition of PLGA. Cell culture tests showed that SaOs-2 cells properly attached and proliferated on all the prepared scaffolds. The results indicated that CH-PLGA blend scaffolds that combined the advantages of both the polymers could be good candidates for use in bone tissue engineering applications.

Keywords: Acrylic bone cement, PMMA, chitosan, zeolite, PLGA, hydroxyapatite, hard tissue support, scaffold, bone tissue engineering

ÖZ

POLİMERİK SERT DOKU DESTEKLERİNİN HAZIRLANMASI VE KARAKTERİZASYONU

Endođan, Tuđba
Doktora, Polimer Bilimi ve Teknolojisi Bölümü
Tez Yöneticisi: Prof. Dr. Nesrin Hasırcı
Ortak Tez Yöneticisi: Prof. Dr. Vasıf Hasırcı

Mart 2013, 118 sayfa

Son yıllarda, otogreftlerin sınırlı miktarda bulunması, allogreftlerin ise bađışıklık sisteminde tepkilere neden olmasından dolayı biyomalzeme alanında yapay malzemelerin kullanımı için talep büyük ölçüde artmıştır. Bu tezin amacı, sert doku uygulamaları için destekleyici veya yenileyici malzeme olarak kullanılmak üzere polimer esaslı matrisler hazırlamaktır.

Tezin ilk kısmında, destekleyici malzeme olarak hidroksiapatit içeren akrilik kemik çimentoları hazırlanmıştır. Bu çalışmada, sentezlenen poli(metil metakrilat) (PMMA) mikroküreleri ve öđütölüp elenmiş PMMA tanecikleri kullanılarak deđişik kompozisyonlara sahip kemik çimentoları hazırlanmıştır. Kullanılan PMMA parçacık boyutları 50–150 µm arası (BC1), 1–50 µm arası (BC2) ve 1 µm dir (BC3). Kompozisyonlar, biyoyumluluđu ve mekanik dayanımı arttırmak için hidroksiapatit (HAp) kullanılarak hazırlanmıştır. Çeşitli kemik çimentosu formülasyonlarında polimerik ve inorganik bileşenler arasında uyumu arttırmak için oksijen plazma uygulaması yapılmıştır. Bazı kompozisyonlar amonyum nitrat, zeolit, kitosan eklenerek hazırlanmıştır. Plazma uygulaması bütün grupların mekanik özelliklerini geliştirmesinin yanında istenmeyen bir durum olan maksimum kür sıcaklıklarını da arttırmıştır. Ek olarak, zeolit güçlendirici madde olarak davranıp kemik çimentolarının mekanik gücünü arttırmıştır. Kitosan içeren kemik çimentosu formülasyonu sıçanlarda in vivo uygulamaları için kullanılmış ve yeni kemik oluşumu gözlenmiştir.

Tezin ikinci kısmında, kemik doku mühendisliđi uygulamaları için yenileyici malzeme olarak 2D ve 3D gözenekli destek yapılar hazırlanmıştır. Destek yapıların hazırlanmasında biyobozunur polimer olarak kitosan ve poli(laktik asit-ko-glikolik asit) (PLGA), mineral bileşen olarak HAp kullanılmıştır. Destek yapılar mikrofabrikasyon, liyofilizasyon ve elektroöđirme olmak üzere üç farklı teknik kullanılarak hazırlanmış ve kimyasal, termal, mekanik ve in vitro testler ile karakterize edilmiştir. Mikrofabrikasyon tekniđi ile mikron boyutlu düzenli kare boşluklara sahip iki boyutlu gözenekli membranlar elde edilmiştir. İçiçe geçmiş ve makrogözenekli, %77-89 gözenekliliđe sahip üç boyutlu destek yapılar liyofilizasyon yöntemi ile hazırlanmıştır. Islak PLGA ve HAp içeren destek yapılar en yüksek sıkıştırma modülüne sahiptir. Ayrıca, elektroöđirme yöntemi ile 180–525 nm arası çapa sahip fiberler elde edilmiştir. Kitosan destek yapıların bozunma hızlarının PLGA eklenerek deđiştirilebileceđi gözlenmiştir. Hücre kültürü deneyleri, SaOs-2 hücrelerinin hazırlanan bütün destek yapılar üzerinde uygun bir şekilde yapıştığı ve çođaldığını göstermiştir. Sonuçlar, her iki polimerin avantajlarını birleştiren CH-PLGA karışımı doku destek yapılarının, kemik doku mühendisliđi alanında kullanılmak için iyi bir aday olduğunu göstermiştir.

Anahtar Kelimeler: Akrilik kemik çimentosu, PMMA, kitosan, zeolit, PLGA, hidroksiapatit, sert doku desteđi, destek yapı, kemik doku mühendisliđi

To My Family...

ACKNOWLEDGEMENTS

I would like to express my deepest gratitude to my supervisor Prof. Dr. Nesrin Hasırcı for her continuous guidance, encouragement and advices during all the stages of my thesis. I am deeply thankful for her motivation and support to complete this thesis.

I am also deeply thankful to Prof. Dr. Vasıf Hasırcı for his support, leadership and guidance in METU-BIOMAT Biomaterials and Tissue Engineering Research Group. I am also thankful to him for giving me the possibility of joining many international academical organizations supported by this team.

I am grateful to my thesis progress committee members, Prof. Dr. Serpil Aksoy and Assoc. Prof. Dr. Caner Durucan for their helpful comments and suggestions throughout this thesis.

I wish to thank Prof. Dr. Claudio Migliaresi for providing me a good opportunity to work in his research laboratory at the Department of Materials Engineering and Industrial Technologies, Trento University, Italy. I am grateful to Prof. Dr. Antonella Motta, Dr. Eleonara Carletti and Dr. David Maniglio for their guidance during the stage of polymer fabrication with microfabrication technique and characterization studies at Trento University. I also would like to thank to all members of Prof Dr. Claudio Migliaresi's research group for their support during my stay in Italy.

I deeply thank to special lab mates Aysel Kızıltay, Eda Ayşe Aksoy, Cantürk Özcan, Aysun Güney, Şeniz Uçar, Özge Özgen, Ümran Aydemir, Gülçin Çiçek, Filiz Kara and other lab members of D-148 for the good memories and support during my experiments.

I am thankful to Aysel Kızıltay who teached me cell culture techniques and supported me. I am deeply grateful to Eda Ayşe Aksoy for her valuable friendship, continuous motivation and support throughout all the stages of my life.

I deeply thank all the members of METU-BIOMAT group, especially Halime Kenar, Deniz Yücel, Albana Ndreu, Hayriye Özçelik, Pınar Yılgör, Arda Büyüksungur, Aysu Küçükürhan and Menekşe Ermiş. I also would like to thank Zeynel Akın for his technical support throughout my research.

I am thankful for their support and understanding of Prof. Dr. Hayrettin Yücel and Prof. Dr. Necati Özkan. I would like to thank to METU Central Laboratory for characterization tests.

This study was supported by FP6 European Network of Excellence project EXPERTISSUES and grants are gratefully acknowledged. I also would like to acknowledge the financial support from TUBITAK through project 104M432.

I would like to thank to my dear friends Eylem Yalçınkaya, Elif Kanbertay, Mine Kalkancı for their friendship and support in every part of my life.

Finally, I would like to thank to my mother, my father, my sister and my fiancé for their patience, encouragement and endless love they have shown.

TABLE OF CONTENTS

ABSTRACT.....	v
ÖZ.....	vi
ACKNOWLEDGEMENTS.....	viii
TABLE OF CONTENTS.....	ix
LIST OF TABLES.....	xiii
LIST OF FIGURES.....	xiv
ABBREVIATIONS.....	xvi
CHAPTERS	
1 INTRODUCTION.....	1
1.1 Bone.....	1
1.1.1 Types of Bone.....	1
1.1.2 Types of Cells in Bone.....	2
1.1.3 Mechanical Properties of Bone.....	3
1.1.4 Bone Remodeling.....	4
1.2 Bone Supporting Materials.....	4
1.2.1 Bone Cements.....	5
1.2.1.1 Inorganic Bone Cements.....	6
1.2.1.2 Acrylic Bone Cements.....	7
1.2.1.2.1 Preparation of Acrylic Bone Cements.....	9
1.2.1.2.2 Mechanical Properties of Acrylic Bone Cements.....	9
1.2.1.2.3 Setting and Curing Properties of Acrylic Bone Cements.....	10
1.2.1.2.4 Modifications of Acrylic Bone Cement Formulations.....	11
1.2.1.2.4.1 Modification of Chemical Composition.....	11
1.2.1.2.4.2 Modification with Bioactive Agents.....	12
1.2.1.2.4.3 Modification with Different Additives.....	12
1.2.1.2.4.4 Modification with Plasma.....	13
1.2.2 Bone Tissue Engineering Scaffolds.....	14
1.2.2.1 Essential Properties of Scaffolds.....	15
1.2.2.2 Materials for Scaffold Production.....	15
1.2.2.2.1 Chitosan.....	16
1.2.2.2.2 Poly(lactic acid-co-glycolic acid).....	17
1.2.2.3 Processing Techniques of Scaffolds.....	18
1.2.2.3.1 Microfabrication.....	18
1.2.2.3.2 Freeze Drying.....	19
1.2.2.3.3 Electrospinning.....	19
1.3 The Aim of This Thesis.....	21
2 ACRYLIC BONE CEMENTS.....	23
2.1 Experimental.....	23
2.1.1 Materials.....	23
2.1.2 Preparation of PMMA Particles.....	24
2.1.3 Characterization of PMMA Particles.....	25
2.1.3.1 Fourier Transform Infrared Spectroscopy.....	25

2.1.3.2	Morphological Investigations.....	25
2.1.3.3	Particle Size Analysis.....	25
2.1.4	Preparation and Modification of Acrylic Bone Cements.....	25
2.1.5	Characterization of Acrylic Bone Cements	27
2.1.5.1	Mechanical Analysis	27
2.1.5.1.1	Tension Tests.....	27
2.1.5.1.2	Compression Tests.....	27
2.1.5.2	Thermal Analysis	28
2.1.5.3	In Vivo Tests.....	29
2.2	Results and Discussion.....	30
2.2.1	Fourier Transform Infrared Spectroscopy Results.....	30
2.2.2	Morphological Analysis Results of PMMA Particles.....	31
2.2.3	Particle Size Analysis Results	32
2.2.4	Modification of Acrylic Bone Cements with Oxygen Plasma.....	33
2.2.4.1	Effect of Oxygen Plasma on Mechanical Properties	34
2.2.4.2	Effect of Oxygen Plasma on Curing Properties	35
2.2.5	Modification of Acrylic Bone Cements with DDM and AN	37
2.2.5.1	Effect of DDM and AN Addition on Mechanical Properties	37
2.2.5.2	Effect of DDM and AN Addition on Curing Properties.....	38
2.2.6	Modification of Acrylic Bone Cements with Zeolite	40
2.2.6.1	Effect of Zeolite Addition on Mechanical Properties.....	40
2.2.6.2	Effect of Zeolite Addition on Curing Properties	41
2.2.7	Modification of Acrylic Bone Cements with Chitosan.....	42
2.2.7.1	Effect of Chitosan Addition on Mechanical Properties.....	42
2.2.7.2	Effect of Chitosan Addition on Curing Properties	43
2.2.8	In Vivo Tests	45
2.2.9	Morphological Analysis Results of Crosssections of Bone Cements	47
3	BONE TISSUE ENGINEERING SCAFFOLDS.....	49
3.1	Membranes Prepared by Microfabrication	49
3.1.1	Experimental.....	49
3.1.1.1	Materials	49
3.1.1.2	Microfabrication System.....	50
3.1.1.3	Preparation of Microfabricated Membranes.....	51
3.1.1.4	Characterization of Microfabricated Membranes.....	51
3.1.1.4.1	Rheological Tests	51
3.1.1.4.2	Morphological Investigations	51
3.1.1.4.3	Fourier Transform Infrared Spectroscopy	51
3.1.1.4.4	Differential Scanning Calorimetry	52
3.1.1.4.5	Dynamic Mechanical Thermal Analysis.....	52
3.1.1.4.6	Preliminary Cell Culture Tests	52
3.1.2	Results and Discussion	52
3.1.2.1	Microfabricated Chitosan Membranes	52
3.1.2.1.1	Morphological Analysis Results.....	52

3.1.2.1.2	Rheological Test Results	53
3.1.2.1.3	Fourier Transform Infrared Spectroscopy Results.....	54
3.1.2.1.4	Differential Scanning Calorimetry Results.....	55
3.1.2.1.5	Dynamic Mechanical Thermal Analysis Results.....	56
3.1.2.1.6	Preliminary Cell Culture Test Results	58
3.1.2.2	Microfabricated PLGA Membranes.....	59
3.1.2.2.1	Morphological Analysis Results.....	59
3.1.2.2.2	Rheological Test Results	61
3.1.2.2.3	Fourier Transform Infrared Spectroscopy Results.....	61
3.1.2.2.4	Differential Scanning Calorimetry Results.....	62
3.1.2.2.5	Dynamic Mechanical Thermal Analysis Results.....	64
3.1.2.2.6	Preliminary Cell Culture Test Results	65
3.2	Scaffolds Prepared by Freeze Drying	68
3.2.1	Experimental	68
3.2.1.1	Materials	68
3.2.1.2	Synthesis of Hydroxyapatite	68
3.2.1.3	Characterization of Hydroxyapatite	69
3.2.1.4	Preparation of Freeze Dried Scaffolds	69
3.2.1.5	Characterization of Freeze Dried Scaffolds	69
3.2.1.5.1	Morphological Investigations	69
3.2.1.5.2	Fourier Transform Infrared Spectroscopy	69
3.2.1.5.3	Differential Scanning Calorimetry	70
3.2.1.5.4	Porosity and Pore Size Distribution Determination.....	70
3.2.1.5.5	Mechanical Tests	70
3.2.1.5.6	Water Uptake Capacity.....	71
3.2.1.5.7	In vitro Degradation Tests	71
3.2.1.5.8	Cell Culture Tests.....	71
3.2.2	Results and Discussion	72
3.2.2.1	XRD Results of HAp	72
3.2.2.2	Morphological Analysis Results	72
3.2.2.3	Fourier Transform Infrared Spectroscopy Results	76
3.2.2.4	Differential Scanning Calorimetry Results	76
3.2.2.5	Porosity and Pore Size Distribution Results	78
3.2.2.6	Mechanical Test Results	80
3.2.2.7	Water Uptake Capacity Results	81
3.2.2.8	In vitro Degradation Results	82
3.2.2.9	Cell Culture Test Results	83
3.3	Fibers Prepared by Electrospinning.....	88
3.3.1	Experimental	88

3.3.1.1	Materials	88
3.3.1.2	Preparation of Electrospun Fibers	88
3.3.1.3	Characterization of Electrospun Fibers	89
3.3.1.3.1	Morphological Investigations	89
3.3.1.3.2	Fourier Transform Infrared Spectroscopy	89
3.3.1.3.3	Differential Scanning Calorimetry	89
3.3.1.3.4	In vitro Degradation Tests	89
3.3.1.3.5	Cell Culture Tests	89
3.3.2	Results and Discussion	91
3.3.2.1	Morphological Analysis Results	91
3.3.2.2	Fourier Transform Infrared Spectroscopy Results	92
3.3.2.3	Differential Scanning Calorimetry Results	93
3.3.2.4	In vitro Degradation Results	94
3.3.2.5	Cell Culture Test Results	95
4	CONCLUSIONS.....	99
	REFERENCES	101
	APPENDICES	
	A POLYMERIZATION REACTION	115
	B CALIBRATION CURVE	117
	CURRICULUM VITAE.....	118

LIST OF TABLES

TABLES

Table 1.1 Properties of bone cells	3
Table 1.2 Mechanical properties of bone	3
Table 1.3 Compositions of some commercial acrylic bone cements	8
Table 2.1 Composition of CMW1 commercial bone cement.....	24
Table 2.2 Types of PMMA used in bone cement preparation.....	24
Table 2.3 Bone cement formulations	26
Table 2.4 Mechanical properties of bone cements before and after O ₂ plasma	34
Table 2.5 Curing properties of bone cements before and after O ₂ plasma	36
Table 2.6 Mechanical properties of DDM or AN containing bone cements	38
Table 2.7 Curing properties of DDM or AN containing bone cements	39
Table 2.8 Mechanical properties of zeolite containing bone cements.....	40
Table 2.9 Curing properties of zeolite containing bone cements	41
Table 2.10 Mechanical properties of chitosan containing and CMW1 bone cements	43
Table 2.11 Curing properties of chitosan containing and CMW1 bone cements	44
Table 3.1 Results of DSC analysis of scaffolds	78
Table 3.2 Porosity of scaffolds	78
Table 3.3 Compressive elastic modulus of dry and hydrated scaffolds	81
Table 3.4 Average diameter of fibers.....	91
Table 3.5 Results of DSC analysis of fibers	93

LIST OF FIGURES

FIGURES

Figure 1.1 Structure of bone.....	1
Figure 1.2 Morphology of bone cells.....	2
Figure 1.3 Schematic representation of A) total hip replacement, B) vertoblasty.....	6
Figure 1.4 Chemical structure of PMMA.....	7
Figure 1.5 Representation of plasma surface modification.....	13
Figure 1.6 Schematic presentation of bone tissue engineering.....	14
Figure 1.7 Chemical structure of chitosan.....	16
Figure 1.8 Chemical structure of PLGA (X: PLA, Y: PGA).....	17
Figure 1.9 Schematic presentation of scaffold preparation with microfabrication system.....	19
Figure 1.10 Electrospinning instrument.....	20
Figure 2.1 Bone cement dough preparation.....	25
Figure 2.2 Tension test samples and test set up.....	28
Figure 2.3 Compression mold and test set up.....	28
Figure 2.4 Typical temperature versus time graph of setting of acrylic cements.....	29
Figure 2.5 Illustration of bone cement application.....	30
Figure 2.6 FTIR spectrum of PMMA microspheres.....	31
Figure 2.7 SEM micrographs of PMMA particles A) 50–150 μm , B) 0–50 μm , C) 1 μm	31
Figure 2.8 Particle size distributions of PMMA particles.....	32
Figure 2.9 Particle size distribution of HAp particles.....	32
Figure 2.10 Particle size distribution of BaSO ₄ particles.....	33
Figure 2.11 Particle size distribution of PMMA microspheres.....	33
Figure 2.12 UTS, UCS and T _{max} values of O ₂ plasma applied bone cements.....	37
Figure 2.13 UTS, UCS and T _{max} values of DDM or AN containing bone cements.....	39
Figure 2.14 UTS, UCS and T _{max} values of zeolite containing bone cements.....	42
Figure 2.15 UTS, UCS and T _{max} values of chitosan containing bone cements.....	45
Figure 2.16 Microscopic images of neighboring tissue 4 weeks after the implantation of bone cements. Arrows show newly formed osteoid. A) Control, B) BC1, C) BC1-CH1, D) CMW1.....	46
Figure 2.17 SEM micrographs of cross-sections of bone cements. A) BC1; B) BC2; C) BC3.....	47
Figure 3.1 The photograph of microfabrication device.....	50
Figure 3.2 Images of chitosan membranes A) Light micrograph, B) and C) SEM micrographs.....	53
Figure 3.3 Rheological test results of chitosan solution.....	54
Figure 3.4 FTIR-ATR spectra of chitosan A) powder, B) film, C) membrane.....	55
Figure 3.5 DSC thermograms of chitosan powder (A. 2nd run and B. 1st run); film (C. 2nd run and D. 1st run); and membrane (E. 2nd run and F. 1st run).....	56
Figure 3.6 Storage Modulus and tan δ curves of chitosan. A) membrane, B) film.....	57
Figure 3.7 SEM micrographs of chitosan membranes after MG63 cell seeding. A, B, C after 4 days, D, E, F after 10 days.....	58
Figure 3.8 SEM micrographs of chitosan membranes after MRC5 cell seeding. A, B, C after 4 days, D, E, F after 10 days.....	59
Figure 3.9 Light micrographs of PLGA membranes microfabricated from PLGA solution prepared in A, B) DCM, C, D) DMF.....	60
Figure 3.10 Images of PLGA membrane A) light microscopy, B) SEM.....	60
Figure 3.11 Rheological test results of PLGA solution.....	61
Figure 3.12 FTIR-ATR spectra of PLGA A) powder, B) film, C) membrane, D) DMF.....	62
Figure 3.13 DSC thermogram of PLGA powder.....	63
Figure 3.14 DSC thermogram of PLGA film.....	63
Figure 3.15 DSC thermogram of PLGA membrane.....	64
Figure 3.16 Storage Modulus and tan δ curves of PLGA. A) membrane, B) film.....	65
Figure 3.17 SEM micrographs of PLGA membranes after MG63 cell seeding. A, B) 4 days,	

C, D) 10 days in the culture	66
Figure 3.18 SEM micrographs of PLGA membranes after MRC5 cell seeding. A, B) 4 days, C, D) 10 days in the culture	66
Figure 3.19 XRD patterns of A) nsHAp, B) sintered HAp powder	72
Figure 3.20 SEM micrographs of A, B) HAp, C, D) nsHAp powder	73
Figure 3.21 SEM micrographs of scaffolds A) CH; B) CH-HAp; C) CH-PLGA; D) CH-HAp-PLGA; E) CH-HAp; F) CH-HAp-PLGA at higher magnification.....	74
Figure 3.22 SEM micrographs of the crosssections of scaffolds A) CH; B) CH-HAp; C) CH-PLGA; D) CH-HAp-PLGA.....	75
Figure 3.23 FTIR-ATR spectra of HAp, PLGA powder and scaffolds.....	76
Figure 3.24 DSC thermograms of scaffolds A) 1st scan, B) 2nd scan.....	77
Figure 3.25 Pore size distributions of scaffolds A) CH; B) CH-HAp; C) CH-PLGA; D) CH-HAp-PLGA	79
Figure 3.26 Representative force–extension curve for scaffolds	80
Figure 3.27 Water uptake capacity of the scaffolds	82
Figure 3.28 Degradation behavior of scaffolds in lysozyme containing PBS.....	83
Figure 3.29 Proliferation of SaOs-2 cell line on the scaffolds	84
Figure 3.30 SEM micrographs of cell seeded foams. A, B) CH; C, D) CH-HAp; E, F) CH-PLGA; G, H) CH-HAp-PLGA. Day 1	85
Figure 3.31 SEM micrographs of cell seeded foams. A, B) CH; C, D) CH-HAp; E, F) CH-PLGA; G, H) CH-HAp-PLGA. Day 7	86
Figure 3.32 SEM micrographs of fibers A) CH; B) CH-PLGA; C) CH-PLGA-HAp; D) PLGA.....	92
Figure 3.33 FTIR-ATR spectra of fibers.....	93
Figure 3.34 DSC thermograms of fibers A) 1st run, B) 2nd run	94
Figure 3.35 Degradation behavior of fibers in lysozyme containing PBS	95
Figure 3.36 Proliferation of SaOs-2 cells on the electrospun fibers.....	96
Figure 3.37 SEM micrographs of cell seeded fibers on day 1 A, B) CH; C, D) CH-HAp; E, F) CH-PLGA; G, H) CH-HAp-PLGA presented with different magnifications.....	97
Figure 3.38 SEM micrographs of cell seeded fibers on day 7 A, B) CH; C, D) CH-HAp; E, F) CH-PLGA; G, H) CH-HAp-PLGA presented with different magnifications.....	98
Figure A.1 Redox reaction between BPO and DMPT	115
Figure A.2 Radical formation	115
Figure A.3 Initiation step of MMA polymerization	116
Figure A.4 Propagation step of MMA polymerization	116
Figure A.5 Termination step	116
Figure B.1 Calibration curve of SaOs-2 with Alamar Blue Assay.....	116

ABBREVIATIONS

AN	Ammonium nitrate
ATR	Attenuated total reflectance
BaSO ₄	Barium sulphate
BC	Bone cement
BPO	Benzoyl peroxide
CH	Chitosan
DDM	1-Dodecyl mercaptan
DHPT	Dihydroxyl-propyl-p-toluidine
DMPE	N,N-dimethyl-amino-phenethanol
DMPT	N,N-dimethyl-p-toluidine
DMTA	Dynamic mechanical thermal analysis
DSC	Differential scanning calorimetry
E _C	Compressive modulus of elasticity
E _T	Tensile modulus of elasticity
EGDMA	Ethylene glycol dimethacrylate
FTIR	Fourier transform infrared spectroscopy
HAp	Hydroxyapatite
HQ	Hydroquinone
KBr	Potassium bromide
MMA	Methyl methacrylate
MW	Molecular Weight
N ₂	Nitrogen
PEGDMA	Poly(ethylene glycol) dimethacrylate
PEMA/n-BMA	Poly(ethyl methacrylate)/n-butyl methacrylate
PLGA	Poly(lactic acid-co-glycolic acid)
PMMA	Poly(methyl methacrylate)
P(MMA/BMA)	Poly(methyl methacrylate/butyl methylacrylate)
P(MMA/MA)	Poly(methyl methacrylate/methylacrylate)
P(MMA/sty)	Poly(methyl methacrylate/styrene)
PP	Poly(propylene)
PVA	Poly(vinyl alcohol)
SaOs-2	Sarcoma osteogenic
SEM	Scanning electron microscopy
T _{amb}	Ambient temperature
T _g	Glass transition temperature
T _{max}	Maximum curing temperature
t _{set}	Setting time
UCS	Ultimate compressive strength
UHMWPE	Ultra high molecular weight polyethylene
UTS	Ultimate tensile strength
XRD	X-ray diffraction
Z	Zeolite
ZrO ₂	Zirconium dioxide

CHAPTER 1

INTRODUCTION

1.1 Bone

Bone is the main component of the skeletal system. Its main functions are providing support and protection, movement, mineral storage and indirectly, blood cell formation. Bone is a complex composite material, which is made up of inorganic and organic constituents. Organic component is composed of proteoglycans, glycoproteins and collagen fibers, and this part represents about 20–40% of the bone matrix. These molecules affect tensile strength and flexibility of bone. Inorganic part is composed of mineral salts, which are mainly calcium phosphates and represent about 50–70% of the bone matrix. Tiny calcium phosphate crystals are found inside and outside of the collagen fibers and provide stiffness and compressive strength to the bone. The suitable combination of organic fibers and inorganic salts makes bone tough and strong and able to carry whole body.

1.1.1 Types of Bone

There are two kinds of bone structure; compact and spongy bone. They are composed of the same matrix elements and the same type of cells, however, they differ in structure and function. The main difference is that in spongy bone the mineralized portion is about 15–25% of matrix while it is 80–90% in compact bone. The rest of the volume is made up by bone marrow, blood vessels and connective tissue (Baron 1999). A scheme of general bone structure is presented in Figure 1.1.

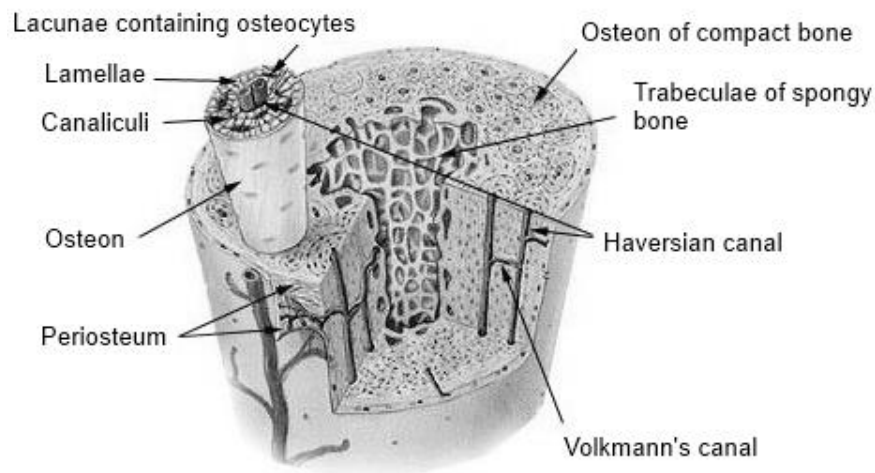


Figure 1.1 Structure of bone (Spence 1990)

The rigid surface of bone is made up of compact bone tissue. This tissue is the reason for smoothness, whiteness, solid appearance of the bone, has a porosity of 5–30%. Main structural unit of compact bone is osteon which is composed of 20–30 concentric lamellae. Each osteon is an elongated cylinder, approximately having diameter between 200 μm and 250 μm . There is a

Haversian canal in the center of each osteon, which comprises nerve fibers and blood vessels. Extra canals called Volkmann canals extending from the central canal into the osteon matrix are present in order to supply nutrients to osteons deeper in the bone and to the marrow cavity (Martini 1995). Volkmann canals are covered with a thin connective tissue membrane named as endosteum. The outside of bone is covered with a thin connective tissue layer and is named as the periosteum. There are small cavities inside the concentric lamellae called lacunae where osteocytes exist. Canaliculi canals join the lacunae to each other and to the central canal, and serve as a narrow passage for diffusion of nutrients to lacunae. There is a 1–2 μm thick mineralized tissue layer surrounding each osteon which does not contain collagen fibers. Spongy bone is less arranged compared to compact bone. It is composed of trabeculae which are thin plates of bone. Trabecular bone makes up the 20% of total bone mass and it has a porosity of 30–90%.

1.1.2 Types of Cells in Bone

Bone tissue is made up of four cell types: osteoblasts, osteocytes, osteoclasts and bone lining cells (Table 1.1). Osteoblasts are bone forming cells which are seen around high bone metabolism areas, for example next to the medullary cavity and under the periosteum. Osteocytes are mature cells which secrete bone tissue and preserve the bone with enzymatic secretions. Osteoclasts are multinuclear cells that breakdown bone tissue enzymatically, inducing growth of bone, remodelling and curing. Bone lining cells adjust movement of calcium and phosphate ions and are seen at the surface of many adult bones. The morphology of these cells is in given Figure 1.2.

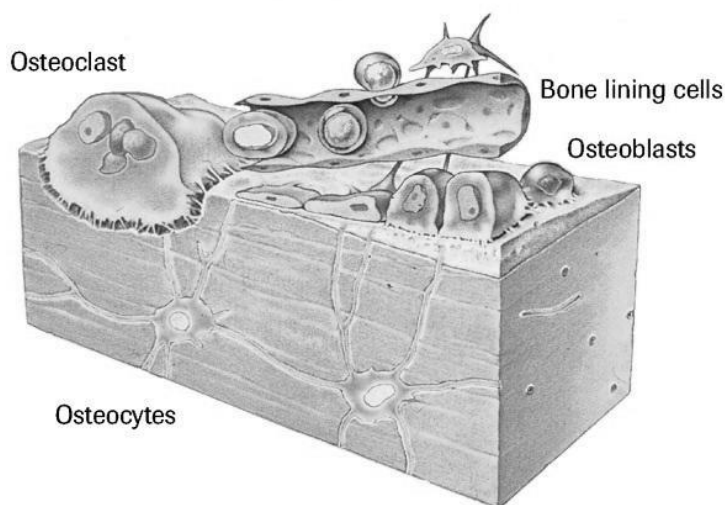


Figure 1.2 Morphology of bone cells (www.roche.com)

Table 1.1 Properties of bone cells (Jee 1999)

	Osteoblast	Osteocyte	Osteoclast	Bone lining
Size	15–30 μm	$\sim 20 \mu\text{m}$	20–100 μm	1 μm thick 12 μm long
Shape	Cuboidal	Elliptical with processes	Multinucleated	Flattened ellipsoidal
Function	Synthesize and secrete bone matrix	Regulate mineral content and architecture of bone mass	Erode bone	Cover inactive bone surfaces
Location	Mineralization front	Lacunae	Cavities on bone surface	Inactive bone surface
Precursor	Mesenchymal progenitors	Osteoblast	Macrophage	Inactive osteoblasts

1.1.3 Mechanical Properties of Bone

Bone has a dynamic structure and an ability to change its shape and structure according to external and internal stimuli. Hormones, nutrition, health condition, exercise and several environmental elements affect the preservation or bone loss. Bone structure is anisotropic, and therefore, its properties are anisotropic; this means its properties change in character or quantity according to direction. The anisotropic mechanical property is believed to develop as a form of adaptive response to functional loading. An extensive range of mechanical values have been stated in literature as given in Table 1.2.

Table 1.2 Mechanical properties of bone (Nalwa 2004)

Property	Compact bone	Spongy bone
Compressive strength (MPa)	140–193	7–10
Compressive elastic modulus (GPa)	14–20	0.01–0.5
Tensile strength (MPa)	50–150	10–20
Fracture toughness ($\text{MPa}\cdot\text{m}^{1/2}$)	2–12	0.1
Strain to failure (%)	1–3	5–7

The intrinsic strength of bone is affected by the bone type, architecture, species, age, gender, composition, porosity, density and mineralization. The compact and spongy bone amount at a given skeletal site influences the strength of bone. It is reported that at the ages of 40 and 70, bending strength of cortical bone is decreased to 15–20% and compressive strength of cancellous bone is approximately decreased to 50% (Martin 1993).

1.1.4 Bone Remodeling

The skeleton experiences continual remodeling all through lifetime. Old tissue is replaced by an equivalent mass of bone matrix by bone remodeling and by this way the physiological preservation of bone is accomplished and the repair of microdamages in bone is possible. In bone remodeling osteoclasts eliminates the mineralized bone and then osteoblasts forms the new bone matrix. Bone remodeling process is composed of three sequential stages: resorption, reversal and formation phase. First stage is the digestion of the old bone by osteoclasts which is called resorption phase. Second mononuclear cells are seen on the surface of bone (reversal phase), and then formation of new bone by osteoblasts is observed until the resorbed bone is completely substituted (formation phase).

1.2 Bone Supporting Materials

Bone replacement materials are needed when a part of a bone is lost by an accident or after the removal of the damaged area in orthopedics, neurosurgery, oral and maxillofacial surgery; and the gap needs to be filled in. The necessity for bone replacement materials is predicted to increase as the population gets older. A suitable bone replacement material must have osteoconduction, osteoinduction and osteogenesis ability (Moore *et al.* 2001).

Current therapies used in bone tissue loss and damage are based on autografts, allografts and implants. The demand for the use of implants has increased significantly in the biomedical field since use of autografts and allografts has some disadvantages. Autografts have limited accessibility and two surgical procedures are required (to harvest and implant the tissue), causing more pain and a higher risk of infection is involved while allografts lead to higher risks of infection and rejection of the implant.

Metals, ceramics, polymers and their combinations are commonly used materials to repair or replace injured bone parts. In orthopedic applications cobalt–chromium, stainless steel and titanium alloys are commonly employed as supporting materials. Metals have the toughness and strength which are necessary for supporting or replacing load carrying parts. There are concerns about the ion release and corrosion of metal in body (Park 1995). However, there are intense studies to modify the composition or surface of the metallic implants for biomedical applications (Schrooten and Helsen 2000, Nguyen *et al.* 2004, Sun and Haruman 2008). Ceramics such as alumina, zirconia, calcium phosphate and bioglass find use in bone and joint surgeries. They are compatible with body because they contain ions generally exist in the physiological medium (such as calcium, potassium, magnesium, sodium ions). Brittle nature and low bending and tensile strength of ceramics limit their use in clinical applications. HAp, which is a bioactive ceramic, due to its biological properties has been extensively used in bone cement formulations (Serbetci *et al.* 2004, Zou *et al.* 2008, Ni *et al.* 2010, Hamizah *et al.* 2012). There are several polymers such as acrylics (Kawashita *et al.* 2010, Lam *et al.* 2011), polyesters (Chen *et al.* 2011), polyethylene (Pourdeyhimi *et al.* 1989) and polyurethane (Boxberger *et al.* 2011) that have been used in bone repair. Polymers are resilient and easy to fabricate but they may not be strong enough and some may degrade or deform with time. Use of a combination of different materials such as ceramic-polymer composites may have advantages like combining their osteoconductive property and the mechanical strength (Espigares *et al.* 2002).

In orthopedic applications, metallic plates, screws, wires, ceramic fillers, polymeric fibers, plates and cements are the most widely used bone support or substitute materials. Among these materials, bone

cements are used to fill cavities and to stabilize the implants. Bone cements are used to transmit body weight and loads from the implant to the bone and improve the load carrying ability of the implant-cement-bone system.

Bone tissue engineering is a different approach for bone replacement, repair, and regeneration. Various systems for bone tissue engineering applications may be improved to imitate the lost tissue of the wound site, maintain the functions of the injured bone tissues in an efficient way. Scaffolds are one of the necessary components of a tissue engineered product and they regenerate a new tissue. Metals and ceramics are not degradable in biological environment and it is not easy to process them therefore their use for tissue engineering applications is disadvantageous. Alternatively, polymers are attractive materials for scaffold production because they may be designed to have the required flexibility and their composition can be changed to meet specific requirements of the target tissue (Liu and Ma 2004).

1.2.1 Bone Cements

Bone cements have been employed clinically in orthopedic and dental purposes for the stabilization of the orthopedic implant or as filling agent for bone defects and dental cavities (Lewis 2009). They provide mechanical attachment and do not function as an adhesive (Katti *et al.* 2008). They are introduced to the desired area as a flowable dough mixture, then harden with time in situ and provide immediate immobilization of the implant.

In addition to fixing prostheses in joint replacement surgeries, recently bone cements have also been used in stabilizing compression fractures of the vertebrae and treating vertebral tumors by percutaneous vertebroplasty (Provenzano *et al.* 2004). Schematic representation of total hip replacement and vertebroplasty are given in Figure 1.3. Vertebral body fractures are one of the most common complications of osteoporosis from which a large number of patients are affected. The occurrence of vertebral body fractures is higher in women and can cause chronic pain, functional impairment and decrease the quality of life (Deb 2008). In vertebroplasty applications, powder and liquid components of bone cement are mixed and the resultant dough is drawn into a syringe and the syringe is connected to a biopsy needle by a flexible tube. Cements to be used in vertebroplasty and kyphoplasty must be radiopaque, easily injectable into the collapsed vertebral body, have a low curing temperature and adequate mechanical properties that would lead to immediate reinforcement and provide early ambulation of the patient. PMMA has been a good material for these purposes and PMMA based cements have been used for vertebroplasty and kyphoplasty procedures successfully (Lieberman *et al.* 2005).

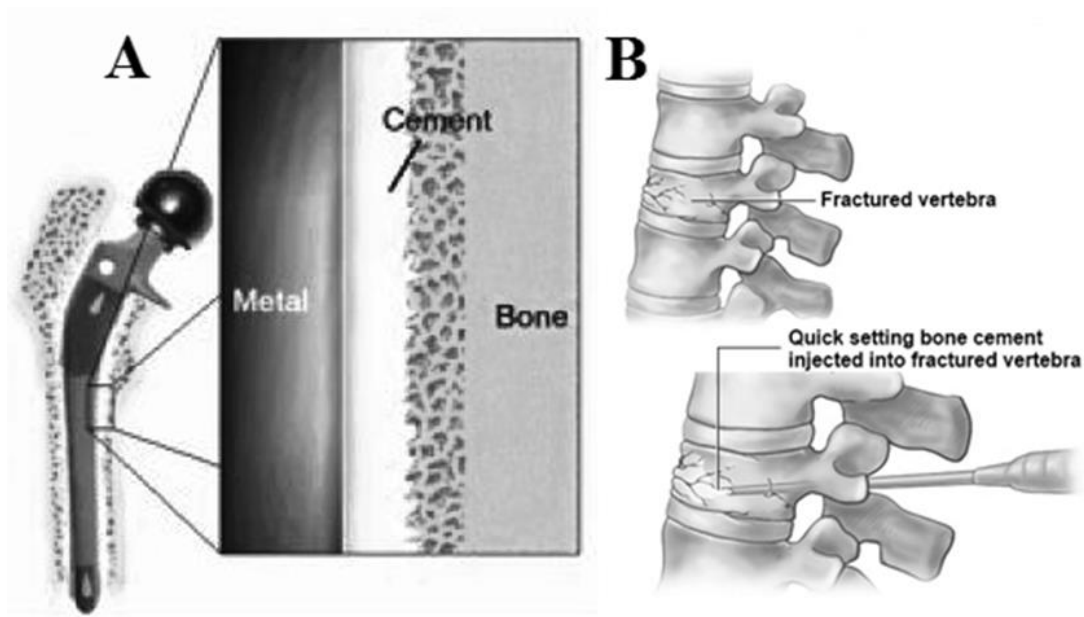


Figure 1.3 Schematic representation of A) total hip replacement, B) vertebroplasty

1.2.1.1 Inorganic Bone Cements

For some orthopedic or dental applications injectable or moldable inorganic cements are suitable choices. A number of inorganic cements have been produced forming a cementitious reaction and capable of setting in the body and were used in different clinical applications (Bohner 2010). Various cement compositions containing zinc phosphate, calcium sulphate, calcium phosphates, calcium carbonate, magnesium oxide and phosphate compounds have been developed (Mestres and Ginebra 2011). Among these cements, calcium phosphate cements (CPCs) are generally employed in orthopedics, maxillofacial surgery and dentistry due to their biocompatibility and bioactive properties (Drosos *et al.* 2012). CPCs consist of varied mixtures of calcium phosphate salts that can form hydroxyapatite and brushite. The fraction of calcium phosphate salt combination affects the solubility, reactivity, resorption and bonding of these materials to bone tissue. CPCs are prepared by mixing the reactive powder with liquid which is generally water, at ambient conditions forming a paste that is then used to fill a bone defect. After setting reaction of this mixture a calcium deficient hydroxyapatite or brushite is produced (Canal *et al.* 2011, Cicek *et al.* 2011). The setting reaction of CPCs is a dissolution–precipitation process which occurs in three stages: dissolution, nucleation, crystal growth. Powder part liberates calcium and phosphate ions and forms a supersaturation in the solution during dissolution. The new phase starts to nucleate usually surrounding the powder particles when the ionic concentration approaches a critical value. The new phase grows as the dissolution continues. Setting reaction is affected by the dissolution kinetics of the raw materials during the first hours, but when the new phase is formed, the process is affected by diffusion of reactants across the new phase (Chen *et al.* 2003).

CPCs are commercially available as granules, pre-shaped blocks or as injectable cement materials. The setting reaction is not exothermic unlike acrylic bone cements, and consequently, lets drug and biological molecule incorporation and making CPCs suitable carriers for drug delivery. However, due to brittleness and low mechanical strength, CPCs use is restricted to non-load bearing applications. To solve the low mechanical property problem, different kinds of fibers have been added to improve the strength and fracture resistance of CPCs (Nezafati *et al.* 2010).

1.2.1.2 Acrylic Bone Cements

PMMA is employed in many medical applications due to its high degree of compatibility with human tissue and ease of manipulation. It has been used in the manufacture of ocular and contact lenses because of optical properties (Park 1995). PMMA has also found a place in dental applications because of its dimensional stability, low water absorption and ease of preparation (Saha and Pal 1984). One other important area in which PMMA is widely used is orthopedic applications, mostly as bone cement. Chemical structure of PMMA is given in Figure 1.4. Acrylic bone cement usage to stabilize hip replacements to bone was advanced by Dr. John Charnley an orthopedic surgeon (Charnley 1960).

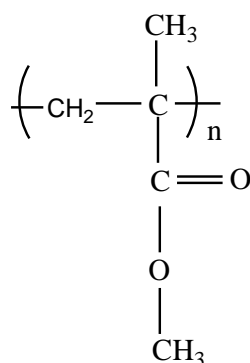


Figure 1.4 Chemical structure of PMMA

All commercially available acrylic bone cements are composed of two components; a white solid powder and a transparent liquid, which are packaged separately. Cement is prepared by mixing the powder and liquid components in situ prior to use. The liquid and powder part formulations may have differences but mainly the powder part is composed of PMMA, benzoyl peroxide (BPO), radioopaque and sometimes antibiotics. In addition to PMMA, powder part of the bone cements may contain low proportions of copolymers of styrene (Morejon *et al.* 2005), methyl acrylate (Liu *et al.* 2001), ethyl methacrylate (Liu *et al.* 2001), butyl methacrylate (Kindt-Larsen *et al.* 1995) or 2-(4-iodobenzoyl)-oxo-ethyl methacrylate (Hooy-Corstjens *et al.* 2004). BPO is an initiator that is necessary to start the polymerization process and can be incorporated within the polymer particles or can be physically mixed. As radioopaque agents generally barium sulfate (BaSO_4) is added as X-ray contrast agents which allow visualization of the cement at the implant site by X-ray imaging as required by the surgeons.

The liquid part consists of methyl methacrylate (MMA), N,N-dimethyl-p-toluidine (DMPT) and hydroquinone (HQ). Liquid component is volatile having a characteristic penetrant smell. In some bone cement formulations other esters of acrylic acid or methacrylic acid are used as the monomer. DMPT is an accelerator for the polymerization reaction of MMA monomer; it activates the initiator found in the powder part. Alternative initiator or accelerators are used in some bone cement formulations. For example, in Duracem® cement, in the liquid part 2-4-dimethylamino phenyl ethanol is present instead of DMPT. Liquid part may also contain a crosslinking agent such as ethylene glycol dimethacrylate, poly(ethylene glycol) dimethacrylate and poly(MMA-co-AA-co-allyl methacrylate) and possibly a colorant such as chlorophyllin. The presence of a crosslinking agent is expected to provide anchoring points for PMMA matrix causing formation of insoluble network during polymerization and cause an increase in stiffness of the cement matrix and a decrease in shrinkage.

There are more than 30 commercial acrylic bone cements accepted by the Food and Drug Administration (FDA). They have several differences such as polymer molecular weight, particle

size, amount of polymer, presence of a copolymer, type of radioopacifiers, amounts of accelerator and initiator and presence of additives such as antibiotics, colorants, etc. In Table 1.3 components of powder and liquid parts of some commercial bone cements are given.

Table 1.3 Compositions of some commercial acrylic bone cements

Cement type	Powder part (% , w/w)	Liquid part (% , w/w)
Palacos R	P(MMA/MA): 84.25 ZrO ₂ : 15 BPO: 0.75	MMA DMPT: 2
Simplex P	P(MMA/Sty): 75 PMMA: 15 BaSO ₄ : 10 BPO	MMA DMPT: 2.6 %, v/v
CMW1	PMMA: 88.85 BaSO ₄ : 9.10 BPO: 2.05	MMA DMPT: 1.5
CMW3	PMMA: 88 BaSO ₄ : 10 BPO: 2	MMA DMPT: 2.487
Endurance	PMMA: 67.05 P(MMA/Sty): 21.10 BaSO ₄ : 10 BPO: 1.85	MMA DMPT: 2
Zimmer dough type	PMMA: 89.25 BaSO ₄ : 10 BPO: 0.75	MMA DMPT: 2.75 %, v/v
Osteobond copolymer cement	P(MMA/Sty): 87.5 BaSO ₄ : 10 BPO: 1.2 – 2.5	MMA DMPT: 0.75 %, v/v
Sulfix-60	PMMA: 79.65 P(BMA/MMA): 8.84 ZrO ₂ : 9.83 BPO: 0.84 d-CEPHT: 0.84	MMA: 83.62 BMA: 14.77 DMPE: 1.61

PMMA: poly(methyl methacrylate); P(MMA/MA): poly(methyl methacrylate/ methylacrylate); P(MMA/Sty): poly(methyl methacrylate/styrene); P(MMA/BMA): poly(methyl methacrylate/butyl methylacrylate); BPO: benzoyl peroxide; MMA: methyl methacrylate; BMA: butyl methacrylate; DMPT: N,N-dimethyl-p-toluidine; DMPE: N,N-dimethylamino-phenyl-ethanol, d-CEPHT: di-cyclo-esilphtalate

Bone cement supply fast recovery of the patient by providing excellent adhesion of the bone to the implant. However, bone cements have some disadvantages. Tissue damage caused by the chemical reactions during setting of cement, leaching of unreacted monomer, and the differences in stiffness

values of the bone and the cement are some of the shortcomings of bone cements (Katti et al. 2008). Polymerization reaction of MMA monomer is exothermic and temperature rise up to 120°C is observed and this is higher than the threshold levels of thermal tissue damage. Temperature rise during polymerization causes necrosis of the tissue and damage blood circulation. Despite the drawbacks, the success rate of cemented implanted hips and knees are very high; on average 90% are successful for 15 years post implantation (Deb 2008).

1.2.1.2.1 Preparation of Acrylic Bone Cements

The preparation of the bone cement begins when both powder and liquid parts are mixed in a bowl or in a specific mixing device at room temperature. When these two parts are mixed MMA monomer dissolves some of the solid PMMA particles and polymerizes in a matrix surrounding these particles and other insoluble ingredients such as radioopacifiers, antibiotic or bioactive agent forming solid cement. Mixing of powder and liquid part first forms a highly fluid, low viscosity mass, and by time it becomes more viscous and the dough completely hardens into a solid matrix.

The setting process of acrylic bone cements can be divided into four basic phases: mixing, waiting, working and setting. In mixing phase, liquid part wets the powder part forming low viscosity cement. In waiting phase, swelling takes place, polymerization begins, and viscosity starts to increase. Polymer chains form and a sticky dough is obtained. In the working phase, because of chain propagation, mobility of chains is reduced and increases the viscosity. Heat generation occurs in this stage. Setting phase is the last step, in which the chain growth is finished and cement is hardened (Kühn 2000).

After mixing the powder and liquid components, the reaction between the initiator and the activator starts forming primary free radicals, and this initiates the polymerization of MMA. Free radicals are produced with the homolytic disintegration of the BPO initiator molecules present in the powder and accelerated with DMPT accelerator present in the liquid. Since the carbon-carbon double bonds of the monomer have a relatively low stability, the formed radicals react with the MMA to start the polymerization and then propagate the chain. Propagation continues until the supply of the monomer is finished, and free radicals lose their activity and termination takes place. Polymerization reaction mechanism is given in Appendix A.

Bone cements cannot be produced from just methyl methacrylate monomer since polymerization would take a long time and the shrinkage due to polymerization would be extremely high. For these reasons bone cements are produced as two-component systems. During the polymerization process of acrylic bone cement formulations density alters; MMA, with a density of 0.937 g.mL⁻¹, is converted to PMMA having higher density, 1.18 g.mL⁻¹, and this leads to volume shrinkage. Pure PMMA exhibits volume shrinkage of approximately 21%, however, the presence of pre-polymerized powder in acrylic bone formulations reduces the theoretical value by up to 6–7% (Deb 2008). Moreover, if the bone cements were prepared from only monomer, it would be hard to control the heat produced during the polymerization of MMA monomer and the temperature would rise to much higher levels than it now does (Kühn 2000).

1.2.1.2.2 Mechanical Properties of Acrylic Bone Cements

Bone cements are subjected to repetitive loading and the cyclic loads that the cemented total hip implants experience is up to five to eight times of body weight (Nordin and Frankel 1989). There is a mechanical connection among the bone and the cement as well as among the cement and the implant, where the cement layer acts as an elastic buffer. Bone cement transmits the applied load homogeneously from the implant to the bone. If external stress factors are greater than the ability of the cement to transfer the force, cement fracture will occur. Bone cement fracture is a major reason of mechanical failure, and therefore, aseptic loosening of implant. The occurrence of this failure is

connected to the bone cement strength. Therefore, mechanical properties of bone cements should be determined to decide if the bone cements will be able to tolerate the loads applied.

There are several static tests performed at low rates of loading, such as tensile, compressive, shear and bending tests. As a result of these tests ultimate strength, elastic modulus values are determined. These values are sensitive to testing method, test temperature, environment, specimen preparation method, and strain or loading rate (Saha *et al.* 1984). In addition to static mechanical tests, fatigue and impact tests are also conducted. These tests can be done at different times after polymerization; specimens can be kept in water or ringer's solution at 37°C to simulate body conditions before testing.

Acrylic bone cements are known to be brittle, weak in tension but strong in compression and have low fatigue strength (Rentería-Zamarrón *et al.* 2009). Other reasons of low mechanical strength of bone cement can be weak interfaces between the inorganic additives and the polymer, agglomeration of ingredients, formation of bubbles. Different components affecting the mechanical properties of bone cements have been investigated by numerous researchers (Litsky *et al.* 1990, Topoleski *et al.* 1995, Pascual *et al.* 1996, Kim and Yasuda. 1999, Heini *et al.* 2001, May-Pat *et al.* 2012, Franco-Marques *et al.* 2012).

Cement mixing method is very important. High porosity is observed when cement is mixed inefficiently. Pores acts as stress raisers and starts sites for cracks and promotes breakdown of the cement. Porosity occurs due to the initial air surrounding the powder and liquid components, entrapped air during wetting, mixing and dough transfer into the replacement site, evaporation of MMA during setting reactions. In order to reduce cement porosity and improve mechanical properties, vacuum mixing has been used in the preparation of PMMA bone cements (Lelovics and Liptakova 2010, Lewis 2011, Zivic *et al.* 2012).

Many studies were conducted to increase mechanical strength of acrylic bone cements such as using different mixing methods, and incorporation of additives such as fibers or mineral particles to the cements (Topoleski *et al.* 1995, Zivic *et al.* 2012). It was stated that although they are not the main cause of failure, agglomeration of additives may take part in crack formation with pores. Therefore, it is important to distribute the additives evenly in the cement formulations and to keep the maximum curing temperature, setting time and handling characteristics in acceptable ranges.

1.2.1.2.3 Setting and Curing Properties of Acrylic Bone Cements

The setting parameters that characterize the polymerization reaction are maximum temperature, dough time and setting time. Maximum curing temperature (T_{max}) is the maximum temperature reached by the bulk during polymerization reaction. The setting time (t_{set}) is the time passed to attain a temperature halfway between room temperature and maximum temperature. Dough time is the time passed between the beginning of mixing until the dough is able to detach easily from a glove. At setting time, the cement would no longer plastically deform under hand pressure. Another important parameter that describes the handling characteristics of the cement is the working time which has been defined as the difference between both setting and dough times.

The setting time is affected by the amount and type of components, polymer-to-monomer ratio, mixing type, particle size and shape of the powder, the temperature of the powder and liquid parts and mixing environment. Therefore, temperature of the mixing environment should be stable to prevent the changes in setting time due to environment. It was observed that setting time was extended by lowering the operating room temperature. In addition, it was reported that increase in the monomer/polymer ratio increased the setting time and dough time, while this did not affect the working time significantly (Meyer *et al.* 1973).

Polymerization reaction of MMA is highly exothermic, high level of heat is generated during polymerization and cause significant temperature rise ranging from 80°C to 120°C. During polymerization, the carbon to carbon double bond in the MMA monomer is broken and replaced by a single bond; this process leads to the release of 544 J.g⁻¹ of heat for each broken bond (Pascual *et al.* 1996). Elevated temperature causes tissue necrosis and damage at the bone-cement interface and can eventually lead to aseptic loosening (Kuehn *et al.* 2005). The amount of temperature rise depends on the mass, thickness of the cement, ambient temperature and efficiency of heat dissipation to the surrounding. The temperature at the bone and bone cement interface was reported to be lower than the bulk because of thin layer of cement mantle, the wet environment and dissipation of heat by metallic implant (Kühn 2000). The highest maximum temperature (T_{max}) accepted by standards in vitro is 90°C.

Many research groups have done extensive investigations in order to decrease the maximum curing temperature. Cooling the cement components and prosthesis before implantation and mixing cement at 4°C caused a decrease in maximum curing temperature at the bone and bone cement interface (Meyer *et al.* 1973, Toksvig-Larsen *et al.* 1991).

1.2.1.2.4 Modifications of Acrylic Bone Cement Formulations

Despite the successful use of acrylic bone cements clinically, there are still some disadvantages. Main disadvantages are high curing temperature and comparatively low mechanical properties with respect to natural bone. As a result, improvements in the mechanical and curing properties are needed to provide achievement of a cemented implant. Many researchers have been studying to overcome these drawbacks with various chemical modifications, incorporation of various additives or physical modifications such as using different mixing methods. In literature various bone cement formulations were prepared by using alternative or combination of different amounts of comonomers of methyl methacrylate, accelerators, copolymers of PMMA, initiators, radioopacifiers, crosslinking agents, antioxidants, antibiotics and reinforcement agents. Some of these modifications are summarized in the following sections.

1.2.1.2.4.1 Modification of Chemical Composition

Several studies were carried out to decrease the maximum curing temperature by substituting the MMA monomer partially or completely with others (Pascual *et al.* 1999, Mendez *et al.* 2002). It was shown that use of hydrophilic monomers decreased maximum curing temperature and also improved toughness of the cements. Recently, comonomers soluble in MMA containing amine groups were used as partial replacement of methyl methacrylate (May-Pat *et al.* 2012). They observed that bending and compressive strength decreased with increasing comonomer amount while fracture toughness increased with respect to the control. In the control groups the liquid part was composed only of MMA and DMPT. They claimed that the reduction in mechanical strength was because of the remaining monomer that acted as a plasticizer in the bone cement matrix. Improvement in fracture toughness was explained by the observation that the glass transition temperatures (T_g) of copolymers were lower than T_g of PMMA. As a result, cements containing any of these comonomers had higher residual monomer contents and shorter setting times, higher maximum curing temperatures and lower compressive strengths. In addition, incorporation of amine containing comonomers led to improved surface interaction between cell and cement (Cervantes-Uc *et al.* 2005).

As an alternative to PMMA/MMA bone cements, poly(ethyl methacrylate)/n-butyl methacrylate (PEMA/n-BMA) bone cements were developed. It was claimed that PEMA/n-BMA cements had a lower exotherm (50-55°C), less polymer shrinkage and 20% less extractable monomer compared to PMMA cements (Litsky *et al.* 1990). Formulations containing poly(ethyl methacrylate) polymer and combinations of ethyl methacrylate and ethoxyeugenyl methacrylate or eugenyl methacrylate were

also reported to bring bioactivity properties to the bone cements due to eugenol's analgesic, antimicrobial and antiinflammatory effects (Rojo *et al.* 2009).

1.2.1.2.4.2 Modification with Bioactive Agents

Lack of sufficient osteointegration and bioinert nature of bone cements may lead implant loosening after some time making long term stability questionable (Heini *et al.* 2001, Urrutia *et al.* 2008). Therefore, extensive studies were carried out with incorporation of bioactive fillers in order to increase bioactivity of cements.

Titania is a nondegradable and bioactive material and in simulated body fluid HAp forms on the surface of titania and it has been used to obtain bioactive bone cements (Uchida *et al.* 2003, Goto *et al.* 2008, Fukuda *et al.* 2010 and 2011). It was stated that bioactive titania layer formed on the surface of cements caused bonding of the cement to the bone interface (Fukuda *et al.* 2010).

Another filler is HAp which is bioactive and osteoconductive, it integrates with bone and supports the new bone formation making chemical bonds directly with the bone. In addition to biocompatibility, HAp incorporation improves compressive strength of bone cements (Opara *et al.* 2003, Serbetci *et al.* 2004). However particle size, surface properties and amount of HAp influences mechanical and curing properties.

In order to enhance bone cement properties researches change the formulations of commercial cements. Vertecem V+ commercial PMMA bone cement was modified by adding various amounts of bone marrow taken from sheep to be used in vertebroplasty (Arens *et al.* 2011). It was claimed that addition of bone marrow to PMMA cement had positive effects on mechanical properties and bioactivity, and also decreased the curing temperature.

1.2.1.2.4.3 Modification with Different Additives

In addition to bioactive agents additives such as carbon (Cao *et al.* 2009), aramid (Saha *et al.* 1984), ultra high molecular weight polyethylene (UHMWPE) (Pourdeyhimi and Wagner 1989, Ladizeyski and Ward 1995), PMMA fibers (Wright *et al.* 1999), biodegradable polymers (Pereira *et al.* 1998, Zou *et al.* 2008, Franco-Marques *et al.* 2012) has been used to improve bone cement properties. In addition, chain transfer agents may be used to reduce the molecular weight of PMMA matrix and maximum curing temperature (Brauer *et al.* 1986, Race *et al.* 2008, Endogan *et al.* 2009). Chain stopping agent avoids the formation of high molecular weight macromolecules and formation of a highly exothermic polymerization reaction and therefore controls the setting of the bone cement.

Researchers proposed addition of biodegradable materials to acrylic bone cement formulations in order to create pores in the cement matrix, so that as the degradable material degrades bone regeneration could be facilitated in the pores. Traditional bone cement was modified with the addition of carboxymethyl cellulose to obtain porous acrylic bone cement. Animal experiments indicated that hard and soft tissues readily grew into the pores of the cement and therefore anchored the implant strongly to the host tissues (Van Mullen *et al.* 1988). In addition to degradable material, presence of bioactive particles may induce new bone growth not only on the interface of bone and cement but also into the cement matrix as the degradable polymer is removed. This may cause better healing around the prosthesis as degradation of additives takes place and at the same time simultaneously maintain the mechanical integrity. In the light of this idea corn starch/cellulose acetate blend containing partly biodegradable cements were developed with addition of various amounts of HAp (Espigares *et al.* 2002).

Several studies have shown that zeolites are appropriate to be used as biomaterials (Ceyhan *et al.* 2007, Saghiri *et al.* 2012). Zeolites are microporous crystalline aluminosilicate minerals. Some

molecules can penetrate into zeolites because of their microporous structure. Therefore various agents such as antibiotics or silver may be incorporated into these materials and can be used as antibacterial agents. The silicon-containing zeolite was observed to increase eggshell thickness in hens and reported that silicon in trace amounts improves bone formation. Zeolites may have therapeutic function in osteoporotic individuals due to their ability to stimulate bone formation (Pavelic and Hadzija 2005). Therefore, zeolites may be candidate additives into acrylic bone cements to increase their mechanical stability and biocompatibility.

1.2.1.2.4.4 Modification with Plasma

Plasma is a commonly used technique for surface modification of various materials without changing the bulk properties. In low pressure glow discharge plasma an inert vessel is evacuated and then filled using a low pressure gas. Techniques like radiofrequency energy, microwaves, alternating current or direct current are used to energize the low pressure gas. As a result of this process energetic species such as ions, electrons, radicals, metastables and photons are produced. These energetic species are capable of bombarding the surfaces of materials in depths from several hundred angstroms to 10 μm and transfer their energy to the surfaces (Loh and Sheu 1995). Surface modification is resulted from these energy transfers within the solid by several chemical and physical reactions as shown in Figure 1.5.

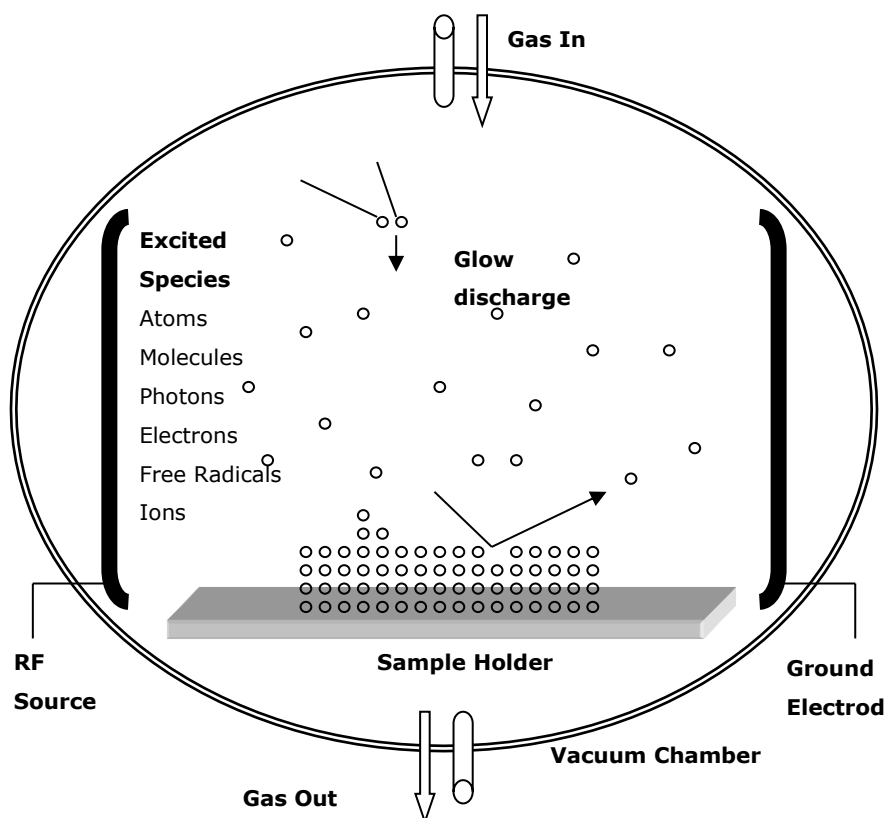


Figure 1.5 Representation of plasma surface modification (Ozcan 2006)

Plasma surface modification has been used for several biomedical applications such as changing the surface properties or sterilization for various applications such as ocular prostheses, orthopedic

implants or tissue culturing. In orthopedic applications plasma is employed for modifying the surface of metal implants to increase cell adhesion and proliferation on bone cements.

Bone cements are composite materials. Interfaces between matrices and fillers affect the physical properties of composite materials because effective transfer of stress from the matrix to the fillers strongly depends on good interfacial adhesion. In order to improve the interfacial adhesion between constituents of composites, many studies such as chemical modification of the constituents, addition of compatibilizers or plasma treatment have been done. Plasma treatment is advantageous among other techniques because lower number of chemicals is used and treatment times are low in this technique. It was shown that fatigue properties of acrylic bone cement were improved when radioopaque agent and reinforcing fibers were treated with plasma (Kim and Yasuda 1999). Therefore plasma application can be useful to reinforce mechanical properties of bone cements by improving interfacial adhesion between additives.

1.2.2 Bone Tissue Engineering Scaffolds

Another type of bone supporting materials is those used in the production of scaffolds to be used in bone tissue engineering applications. Bone tissue engineering combines the principles of engineering and the life sciences in order to develop biological substitutes that restore, maintain or improve function of bone tissue (Langer and Vacanti 1993). It is a promising approach for bone repair. The leading basis of bone tissue engineering approach is to have a porous biodegradable 3 dimensional matrix and seed it with cells and biomolecules, culture and then implant the matrix into the defect to facilitate new bone formation. Biomolecules like growth factors control osteogenesis, bone tissue regeneration and extracellular matrix (ECM) formation. It was proposed that addition of biomolecules in scaffolds (matrix) could lead to decrease in wound healing period and therefore support patient recovery (Bose *et al.* 2012). The cells adhere to the scaffold, grow, differentiate and form healthy bone while the degradation and elimination of scaffold takes place. Ultimate shape of the formed new bone will depend on the architecture of the scaffold. The principal of bone tissue engineering is given in Figure 1.6.

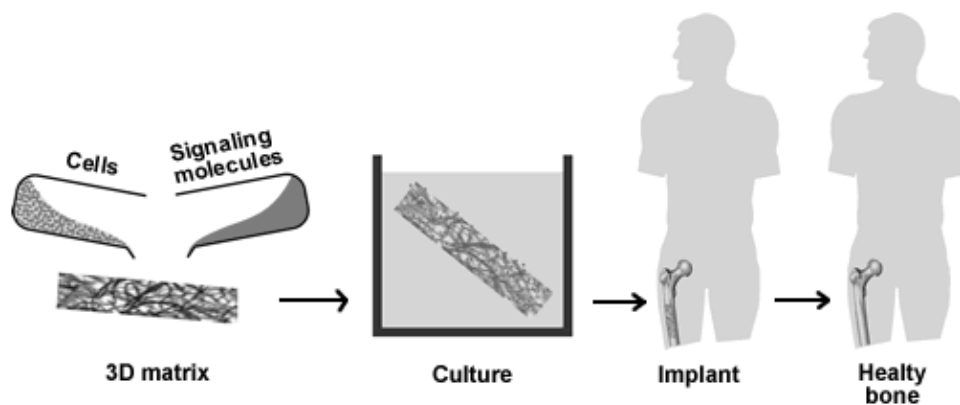


Figure 1.6 Schematic presentation of bone tissue engineering (www.btec.cmu.edu)

Bone tissue engineering is classified into six stages. First stage is the fabrication of the scaffold. In this stage; the scaffold should be prepared from a biocompatible and biodegradable material which will degrade at a controlled rate. Second stage is the osteoblast cell seeding into the prepared scaffold in a static culture. Third stage is the growth of premature tissue in a dynamic culture media. Fourth stage is the growth of mature tissue in a computer controlled bioreactor. Fifth and sixth stages

are the surgical transplantation and assimilation/remodelling of the tissue-engineered transplant, respectively.

3D matrices which are called scaffold are needed for tissue engineering applications since cells need support to grow in 3D manner form a bone. Ideally, these materials should be porous, which provide space for cells penetrate and proliferate to develop tissue, also led transportation of nutrients and metabolites and offer temporary mechanical support. These scaffolds should degrade slowly as the tissue grows.

1.2.2.1 Essential Properties of Scaffolds

Scaffolds are one of the necessary components for bone tissue engineering; they provide three dimensional growth space for transportation of nutrients and metabolites. It is not easy to define an ideal scaffold design since every single tissue needs a particular scaffold design (Hutmacher 2004). Also mechanical properties of cancellous and cortical bone differ extensively. For example when compressive properties are compared; cortical bone has an elastic modulus of 14-20 GPa while cancellous bone has an elastic modulus of 0.01-0.5 GPa (Nalwa *et al.* 2004). These large differences in mechanical strength and complex shape make it harder to produce one type of ideal scaffold. Therefore it can be said that scaffold design should at least meet several requirements depending on the application region.

Biocompatibility is important for a scaffold to be able to support the cells to attach, grow and form ECM. They should have enough mechanical strength and stiffness to endure wound contraction forces. Mechanical strength is also important to provide safe handling during sterilization, packaging and transportation to surgery room. Interconnected porosity is another requirement for scaffolds to provide cell adhesion and migration into the scaffold, transport of nutrients and metabolites and cell distribution throughout the porous scaffold. It was stated that pore size should be at least 100 μm for proper transportation of important nutrients and oxygen for cells (Rouwkema *et al.* 2008). Nevertheless, 200–350 μm pore sizes are shown to be suitable for bone tissue ingrowth (Murphy *et al.* 2010). It was stated that 50 μm pore size was sufficient for bone ingrowth (Bong-Soon *et al.* 2000). Moreover, researches have shown that both micro and macro porosities can perform better than only macro porous scaffolds (Woodard *et al.* 2007). It is believed that optimum pore size varies with cell type (Zeltinger *et al.* 2001). The degradation rate of scaffold should be balanced with the tissue growth; the degradation of scaffold should be completed when the injured tissue is totally renewed. Finally, material used in scaffold fabrication should be easily processed to form the chosen shape with required porosity and size and should be sterilized with ease (Salgado *et al.* 2004).

1.2.2.2 Materials for Scaffold Production

It is important to choose the most suitable material when producing scaffolds to obtain the desired properties. Several materials such as ceramics, natural and synthetic origin polymers have been employed in scaffold fabrication for tissue engineering applications.

Synthetic and natural biodegradable polymers are good candidates for the production of scaffolds. Chitosan, gelatin, collagen, starch, silk, fibrinogen, hyaluronic acid, alginate and poly(hydroxy butyrate) are some examples of natural biodegradable polymers. There are several advantages of using natural polymers. They have low immunogenic potential, and have better interactions with cells because of their bioactive properties. Poly(α -hydroxy acids) such as poly(L-lactic acid) (PLLA) and poly(L-lactic acid-co-glycolic acid) (PLGA), poly(ϵ -caprolactone) (PCL), poly(propylene fumarates), poly(carbonates), poly(phosphazenes) and poly(anhydrides) are examples of synthetic polymers. They can be synthesized under controlled conditions, their degradation time and mechanical properties can be tailored for intended use. However degradation products of the

synthetic polymers decrease the pH of the environment, increase the polymer degradation rate induce inflammatory response and may have toxic effects (Khang *et al.* 2012).

There are several additives used in scaffold preparation in order to give some specific properties. For example, 3D polyurethane scaffolds were prepared with incorporation of fluorinated zeolite particles to increase oxygen delivery to cells (Seifu *et al.* 2011). There are researches concentrating on producing scaffolds with the incorporation of therapeutic drugs to provide the growth of new tissue as well as in situ controlled drug delivery. Zhang *et al.* prepared porous chitosan/collagen scaffolds by freeze drying and added plasmid and growth factor. Cell culture tests showed that TGF-beta1 containing scaffolds has the highest cell proliferation (Zhang *et al.* 2006). Furthermore, the use of metallic ions like silver, copper, cobalt, strontium, iron and zinc as therapeutic agents in tissue engineering applications has been investigated (Mourino *et al.* 2012).

Ceramics have been extensively used for bone regeneration applications. They are biocompatible, corrosion resistant and have high compressive strength (Barrere *et al.* 2006). However, they are brittle, not easy to fabricate, and also most of them are not biodegradable. Ceramics employed in implant production can be categorized as nonabsorbable, bioactive and resorbable. Alumina, zirconia and carbons are nonabsorbable while some glass ceramics and dense HAp are bioactive ceramics. Calcium phosphates, zinc sulphate calcium phosphates, ferric calcium phosphorus oxides, calcium aluminates and tricalcium phosphates are examples of resorbable ceramics (Lyons *et al.* 2008). HAp [$\text{Ca}_{10}(\text{PO}_4)_6(\text{OH})_2$] has been used in bone fillers and replacements since its highly reactive surface causes better attachment and bioactivity; it has osseointegrative and osseointegrative effects (Aoki 1994, Albrektsson and Johansson 2001, He *et al.* 2013). There are some limitations in its usage since its brittleness makes it hard to shape. To overcome these disadvantages, polymer/ceramic composites have been studied in tissue engineering applications, considering that natural bone consists of organic and inorganic materials. The polymer/ceramic composites are believed to have better mechanical strength than polymers and higher flexibility and structural integrity compared to ceramics. Biocompatibility will be improved in the presence of ceramics with the initial flash spread of serum proteins compared to the more hydrophobic polymer surface (Endres *et al.* 2003, Hutmacher *et al.* 2007).

1.2.2.2.1 Chitosan

Chitosan is a cationic natural polymer and it is a partially deacetylated form of chitin. It can be found in the exoskeletons of sea crustaceans like shrimp and crab, and in the cell walls of some fungi. Although chitin is abundant, chitosan is only present in nature in limited amounts, such as in some fungi. For that reason chitosan is produced from chitin through chemical or enzymatic treatments. Chemical structure of chitosan is shown in Figure 1.7.

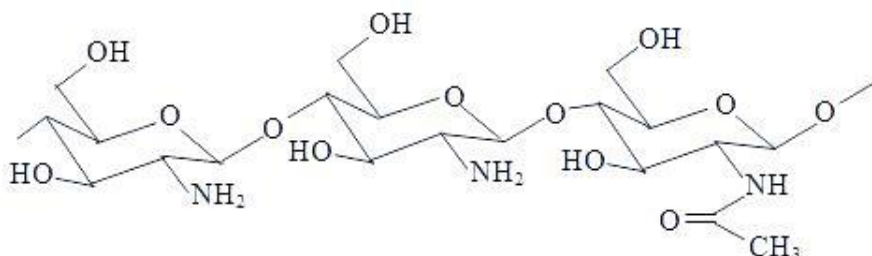


Figure 1.7 Chemical structure of chitosan

The deacetylation of chitin usually produces a chitosan with 70–95% deacetylation degree. Degree of deacetylation determines the amount of free amino groups in the polymer chain. Chitosan gains its

positive charge from the free amino groups. The amino and the hydroxyl group of chitosan provide functionality which yields a reactive polymer. Chitosan has many electrostatic interactions with negatively charged molecules because of its positive charge. The processability of chitosan depends on its solubility which is directly related to its crystallinity (Hudson and Jenkins 2001, Dvir *et al.* 2005).

Chitosan is structurally similar to glycosaminoglycan (GAG) which is one important constituent of extracellular matrix (ECM) playing a key role in controlling cell morphology, cell functions and cell differentiation (Nishikawa *et al.* 2000, Pulieri *et al.* 2008). Chitosan is a biodegradable, nontoxic, nonimmunogenic, antibacterial and antifungal, bioactive, osteoconductive polymer and therefore has been widely studied in biomedical applications. Chitosan is also used in some industrial applications like waste water treatment since it has ability to chelate many metal cations, cholesterol, fats, proteins and even tumor cells (Li *et al.* 1992, Elsabee *et al.* 2012).

Chitosan is a degradable polymer; as the crystallinity amount increases degradation rate decreases. Thermal degradation arises, polymer chains rapidly break down above 280°C. In biological media enzymatic degradation is the principal way of controlling the breakdown of chitosan. Hydrolytic enzymes, mostly lysozyme which is present in some secretions, like tears, saliva and mucus, can be used to naturally degrade chitosan. Aminosugars are formed due to the degradation of chitosan (Hudson and Jenkins 2001, Alberto *et al.* 2005). Fibers, films, sponges and gels can be produced by using chitosan. Due to many attractive properties, it is a good candidate to fabricate 3D scaffolds for tissue engineering applications (Li *et al.* 1992).

1.2.2.2 Poly(lactic acid-co-glycolic acid)

Poly(lactic acid-co-glycolic acid) (PLGA) is a synthetic copolymer of polylactic acid (PLA) and polyglycolic acid (PGA). The structure of PLGA is shown in Figure 1.8; x is the number of lactic acid units while y shows the glycolic acid units. It is FDA approved synthetic biodegradable polymer. It shows a wide range of erosion times and has adjustable mechanical properties changing with the composition of PGA and PLA units. Its physical properties can be changed by changing polymer molecular weight and ratio of lactide to glycolide (Mohamed and van der Walle 2008). It is widely used as suture material, as controlled release device and currently it is being used as scaffold for tissue engineering applications.

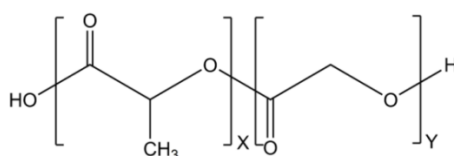


Figure 1.8 Chemical structure of PLGA (X: PLA, Y: PGA)

Due to the appropriate properties, PLGA has been used for tissue engineering applications but as a major disadvantage, because of its hydrolytic degradation, it decreases the local pH and produces undesirable inflammatory and allergenic reactions (Khang *et al.* 2012). In vivo, if the surrounding tissue can not eliminate immense release of acidic degradation products inflammatory reactions may occur (Bergsma *et al.* 1995, Niiranen *et al.* 2004). It is stated that the basic resorption products of inorganic fillers such as HAp may buffer the acidic degradation products of polyesters and possibly avoid pH decrease of the environment (Agrawal and Athanasiou 1997, Shikinami and Okuno 1998, Niiranen *et al.* 2004). Therefore, PLGA may be blended with other polymers or ceramics to overcome disadvantages and result in a material with suitable properties which can be used in tissue engineering (Wan *et al.* 2007).

1.2.2.3 Processing Techniques of Scaffolds

The technique that is going to be used to process the chosen material for scaffold preparation is important. There are many different processing methods like solvent casting, particulate leaching, membrane lamination, freeze drying, electrospinning, melt based technologies, gas foaming, rapid prototyping etc. (Mikos *et al.* 1994, Vozzi *et al.* 2003, Vrana *et al.* 2007, Zhang *et al.* 2008, Yilgor *et al.* 2008, Yucel *et al.* 2010). As a result of these processing techniques scaffolds in the forms of meshes, fibers, sponges and foams are obtained. Polymer is treated with heat or pressure or dissolved in an organic solvent to give a desired shape in most of the techniques. Each processing technique has some advantages and disadvantages and all of them may not be applicable to some polymers.

Thin membranes or 3D samples with thin wall sections can be obtained with solvent casting and particle leaching technique (Mikos *et al.* 1994, Suh *et al.* 2002, Sin *et al.* 2010). In this technique; salt particles with a specific particle size is added into polymer solution to produce a homogeneous mixture, then the solvent is evaporated. The composite is then immersed in water in order to get rid of salt particles. Thin membranes can also be obtained with lamination technique but it is a time consuming process. In phase separation method; molten phenol or naphthalene is used to dissolve the polymer. Then two-phase solid is obtained by lowering the temperature and by sublimation the solvent is removed to have a porous matrice. Fiber bonding technique which is a textile technology was developed to obtain interconnected fiber networks.

1.2.2.3.1 Microfabrication

Microfabrication technique is a computer controlled fabrication technique that can produce complex 3D objects by the help of computer assisted design (CAD) systems. In these techniques 3D objects are produced layer by layer with the processing of solid sheet, liquid or powder. It is considered as an effective method for producing scaffolds in a reproducible, controlled and cost-effective way (Hutmacher 2001). Their leading advantages for the use in tissue engineering are customized design, computer controlled production and anisotropic scaffold microstructures. Computerized systems were classified according to their processing technology (Hutmacher 2004). There are systems based on laser technology such as stereolithography, selective laser sintering, print technology such as 3D printing, extrusion technology such as fused deposition modelling and 3D plotting. A rapid prototyping robotic dispensing system functioning with the same principles as the bioplotter was also developed to produce scaffolds.

In microfabrication technique, it is possible to produce scaffolds having a micrometric resolution for tissue engineering applications (Figure 1.9). Polymer solution or melt is injected over a platform which can move in three directions. Scaffold is built on layer over layer in the vertical direction and each layer is orthogonal to the following one. Well ordered scaffolds can be produced adjusting process parameters controlled through a computer programme. Fabrication of PDLA scaffolds with controlled geometry and micro size porosity by a microfabrication system is reported in literature (Carletti *et al.* 2011). Vozzi *et al.* (2003) used pressure-assisted microsyringe based microfabrication technique to produce 2D and 3D PLGA scaffolds with feature sizes of 10-200 μm . Microfabricated scaffolds were prepared from alginate, gelatin and poly(N-isopropylacrylamide)-based copolymer to be used in myocardial tissue engineering. The microfabricated scaffolds provided the mechanical strength requirements for ventricular myocardium, and supported the alignment of myoblast without external stimuli (Rosellini *et al.* 2010). Daoud *et al.* (2011) microfabricated geometrically-controlled PLGA scaffolds and seeded them with human islets embedded in an extracellular matrix (ECM). In order to obtain different porosities spacing between strands was changed. Presence of ECM components in scaffolds improved prolonged culture.

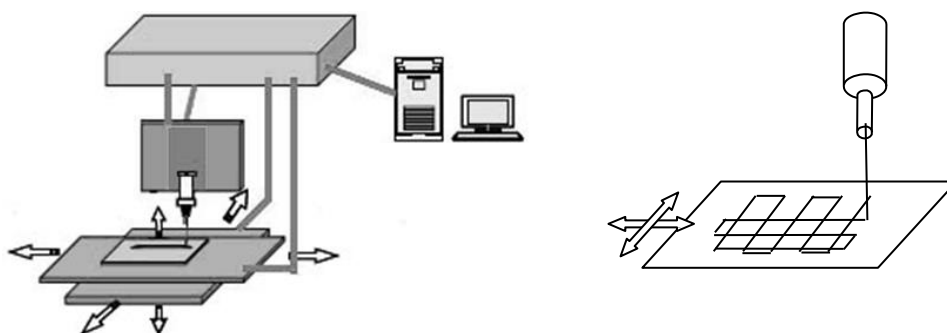


Figure 1.9 Schematic presentation of scaffold preparation with microfabrication system

1.2.2.3.2 Freeze Drying

Freeze drying is a thermally induced phase separation technique. In this technique; a homogeneous polymer solution is poured into a mold and then its temperature is lowered. Polymeric foam is produced by removing the solvent by vacuum sublimation after the phase-separated system is stabilized. Scaffolds from polymers such as chitosan (Nwe *et al.* 2009, Venkatesan *et al.* 2012), collagen (Kane and Roeder 2012), agarose (Joshy *et al.* 2013), fibroin (Bhardwaj *et al.* 2011), gelatin (Thakur *et al.* 2012), poly(D,L-lactic acid) (Patist *et al.* 2004) were obtained by this technique. This technique does not necessitate high temperature or a separate leaching step. Low mechanical stability and sensitivity of the technique are its main disadvantages. In this technique the pore size can be adjusted by changing the freezing rate, for example smaller pores may be obtained by applying a fast freezing rate. Venkatesan *et al.* prepared chitosan/functional multiwalled carbon nanotube composite scaffolds by freeze drying. Composite scaffolds had higher porosity, cell proliferation, alkaline phosphatase activity, protein concentration and mineralization (Venkatesan *et al.* 2012). Freeze dried collagen matrices were reinforced with addition of various amounts of HAp (Kane and Roeder 2012). Thakur *et al.* prepared gelatin scaffolds with this method and crosslinked them with genipin at different crosslinking temperatures and studied the delivery of indomethacin. Gelatin scaffolds crosslinked at 25°C showed highest crosslink density, lowest water uptake capacity and the slowest release of indomethacin (Thakur *et al.* 2012). Joshy *et al.* (2013) produced agarose, gelatin and HAp composite scaffolds. It was reported that incorporation of HAp had significant effect on the water uptake capacity, drug release and haemolytic activity. Scaffolds showed extended drug release, increased mechanical property, haemocompatibility.

1.2.2.3.3 Electrospinning

Electrospinning is a technique used to obtain nano and micron sized fibers. Nanofibers have high surface to volume ratio and high porosity with small pore size. They can be used in wound dressing, drug delivery and bone tissue engineering applications (Zhang *et al.* 2008, Ndreu *et al.* 2008, Yucel *et al.* 2010, Meng *et al.* 2011, Kenar *et al.* 2011).

Electrospinning setup is mainly composed of three constituents; a high voltage power supply, a needle and a collector (Kumar *et al.* 2010). Basic electrospinning instrument is given in Figure 1.10. Polymer solution or melt placed in a syringe is fed through a needle with the help of a syringe pump into an electric field which is created by applying a high voltage. There are two electrodes; one is located on the needle and the second is placed on the collector. With application of electric field, the repulsive electrostatic force overcomes the surface tension of polymer and a charged jet of fluid is ejected. The discharged polymer solution jet undergoes a whipping process during which the solvent evaporates, and a charged polymer fiber is collected on a grounded metal collector. Electrospinning

is a cost effective method. Mostly uniform and continuous fibers are obtained by electrospinning and no further purification is needed (Elsabee *et al.* 2012).

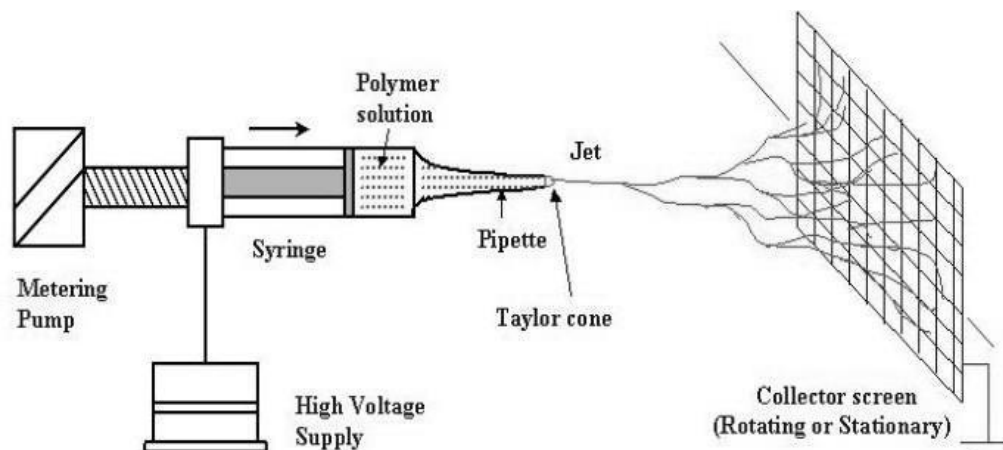


Figure 1.10 Electrospinning instrument

There are solution and process parameters affecting fiber formation and morphology during electrospinning. Solution parameters can be given as polymer type, polymer molecular weight, viscosity, conductivity, solvent type, surface tension while process parameters are voltage, distance from the needle to the collector, flow rate, room temperature and humidity (Huang *et al.* 2003, Li *et al.* 2005).

Both synthetic and natural polymers are used for electrospinning. Synthetic polymers are electrospun due to their cost, availability and wide range of acceptable solvents. They also tend to be easier to engineer for specific applications and do not require complicated purifications that can be necessary for some natural polymers (Dvir *et al.* 2005).

PLGA fibers having a wide range of fiber diameter from 400 nm to 2 μm were produced using several solvents such as dimethyl formamide, methylene chloride, chloroform, hexafluoro-2-propanol (Xin *et al.* 2007, Duan *et al.* 2007). Biocompatibility of the electrospun PLGA nanofibers was studied with in vitro cell culture tests and claimed that PLGA nanofiber mesh could be a possible scaffold material for tissue engineering. It was stated that addition of different amounts of HAp (1, 5, 10 and 20 wt%) increased the average fiber diameter more than two-fold and agglomeration of HAp was observed at higher concentrations (Jose *et al.* 2009).

It is reported that obtaining electrospun fibers from a natural polymer is usually harder than obtaining fibers from a synthetic polymer (Huang *et al.* 2004). Therefore, there are relatively less reports about electrospinning of some natural biopolymers. Chitosan which is a natural polymer is also hard to electrospin. It does not dissolve in common organic solvents because of hydrogen bonds, high crystallinity and high viscosity in solution (Elsabee *et al.* 2012). There are several studies in order to electrospin chitosan fibers using different solvents like dilute and concentrated acetic acid, formic acid and trifluoroacetic acid (Ohkawa *et al.* 2004, Geng *et al.* 2005). Blends with other polymers such as poly(vinyl alcohol) (PVA) (Ohkawa *et al.* 2004), poly(ethylene oxide) (Subbiah *et al.* 2005), collagen (Chen *et al.* 2007) or chemically modified chitosan into soluble derivatives such as hexanoyl chitosan, carboxymethyl chitosan were used to improve the electrospinnability of chitosan (Zhao *et al.* 2012).

1.3 The Aim of This Thesis

The ultimate goal of this thesis was to prepare polymer based acrylic bone cements and tissue engineering scaffolds to be used as supportive or replacement materials for hard tissue applications.

In the first part of the thesis acrylic bone cements with different compositions were prepared. For this purpose, three groups of PMMA particles either synthesized or grounded and sieved were used. The sizes of the particles were in the range of 50–150 μm (BC1), 1–50 μm (BC2) and 1 μm (BC3) (synthesized PMMA microspheres). All of the compositions contained HAp as inorganic load carrying substance and barium sulphate (BaSO_4) as radioopaque agent. Several modifications were done by application of oxygen plasma or incorporation of 1-dodecyl mercaptan (DDM), ammonium nitrate, zeolite or chitosan additives. Mechanical and curing properties were examined and in vivo tests were performed with chitosan containing bone cement formulation and the obtained results were compared with the results of commercial CMW1 bone cement. Application of oxygen plasma to the powder part of bone cements and addition of additives such as zeolite and ammonium nitrate are the novelties of the first part of the thesis.

In the second part of the thesis; 2D and 3D porous scaffolds were prepared for bone tissue engineering. In the preparation of scaffolds, chitosan and poly(lactic acid-co-glycolic acid) (PLGA) as the biodegradable biopolymeric component and HAp as the mineral component were used. Scaffolds were produced by three different techniques which are microfabrication, freeze drying and electrospinning. Resultant polymeric matrices were characterized by chemical, thermal and mechanical tests and in vitro cell culture experiments were carried out using SaOs-2 osteoblast cells. Preparation of scaffolds using chitosan, PLGA and HAp and combining their advantages by electrospinning technique is the novelty of the second part of the thesis.

CHAPTER 2

ACRYLIC BONE CEMENTS

The main purposes of the acrylic bone cements are to serve as an interfacial phase between implant and the bone and homogeneously transfer the applied loads to the rest of the system. Therefore mechanical properties of bone cements are vital to be able to endure applied stresses. Another important factor is the temperature rise because of exothermic polymerization reaction during preparation of bone cement which can cause damage at the application area of host tissue. Thus, suitable bone cement should have low curing temperature besides its desirable mechanical strength.

In this part of the thesis, different acrylic bone cement formulations were prepared by using either ground poly(methyl methacrylate) (PMMA) particles or homogeneously synthesized PMMA microspheres. In some formulations plasma was applied and/or various ingredients were added. The effects of applied modifications on mechanical and curing properties were investigated. The selected compositions were applied to the rat knees to examine the biological effects.

2.1 Experimental

2.1.1 Materials

Acrylic bone cements were produced by combining the solid and liquid parts of the cement formulation. In the solid part the main component is poly(methyl methacrylate) (PMMA) and as polymer either ground and sieved PMMA (MW: 120 000, Sigma-Aldrich Chemie, Munich, Germany) particles or synthesized PMMA microspheres were used. In the solid part of the cement, besides PMMA, benzoyl peroxide (BPO, Scharlau Chemie, Barcelona, Spain), barium sulphate (BaSO_4 , Merck, Darmstadt, Germany) and hydroxyapatite (HAp, Riedel-de Haën A.G., Hanover, Germany) were added. The liquid part involved methyl methacrylate monomer (MMA, Acros Organics, USA) and N,N-dimethyl-p-toluidine activator (DMPT, Sigma-Aldrich Chemie, Steinheim, Germany).

In the synthesis of PMMA microspheres; methyl methacrylate monomer (MMA, Acros Organics, New Jersey, USA), poly(vinyl alcohol) (PVA, MW: 88 000, Acros Organics, USA), benzoyl peroxide (BPO, Scharlau Chemie, Barcelona, Spain) and technical grade ethanol (Tekel Sincan Organize Sanayi, Ankara, Turkey) were used. MMA was washed with 10 wt% aqueous sodium hydroxide (J.T. Baker, Deventer, Holland) solution to eliminate the inhibitor prior to each PMMA microsphere synthesis experiment.

Other chemicals used in the preparation of different bone cement formulations are 1-dodecyl mercaptan (DDM, Acros Organics, New Jersey, USA), chitosan (CH, low viscosity, 75–85% deacetylated, Fluka, Osaka, Japan), zeolite (Z, ZSM-5, Acros Organics, New Jersey, USA) and ammonium nitrate (NH_4NO_3 , Acros Organics, New Jersey, USA). As a control group CMW1 bone cement that is product of DePuy International Ltd. (Blackpool, England) was used in in vivo tests. The composition of CMW1 commercial bone cement is given in Table 2.1.

Table 2.1 Composition of CMW1 commercial bone cement*

Powder part		Liquid part	
Material	wt%	Material	wt%
PMMA	88.85	MMA	98.50
BPO	2.05	DMPT	1.50
BaSO ₄	9.10	HQ	75 ppm

* Information provided from manufacturer's package insert

2.1.2 Preparation of PMMA Particles

PMMA particles used in the thesis were prepared by two methods. In the first method, fine PMMA powder was obtained by grinding commercial PMMA particles using water-cooled analytical mill (Tekmar®, Janke and Kunkel GMBH Co. KG), the obtained powder was sieved through meshes with 150 µm and 50 µm pore size before use. Bone cement formulations which were prepared with PMMA particles in the diameter range of 50–150 µm sized particles were assigned as BC1 group and 0–50 µm were assigned as BC2 group.

In the second method, PMMA microspheres were synthesized from its monomer MMA by suspension polymerization (Endogan *et al.* 2009). The polymerization was carried out in ethanol/water (50/50 v/v) media by using BPO as initiator and PVA as stabilizer. BPO initiator (160 mg) was dissolved in MMA (16 mL) monomer and nitrogen gas was purged through the solution for 15 min to exclude air. Distilled water (80 mL), ethanol (80 mL) and aqueous PVA solution (24 mL, 5% w/v) were mixed in a round bottom two necked flask fitted with a nitrogen inlet and condenser. Nitrogen (N₂) gas was bubbled through the solution for 15 min. Then monomer solution was added to the flask and nitrogen was bubbled for 15 more minutes. The flask was immersed in an oil bath at 70°C and the polymerization medium was mixed with a magnetic stirrer during the reaction. N₂ purging through the solution was continued during all process to exclude air from the medium to prevent its inhibition effect on the polymerization of MMA monomer. The medium was homogenous and clear at the beginning of the polymerization since the monomer is soluble in alcohol. However after 10–15 min, solution became white opaque because of formation of PMMA microspheres. The reaction continued for 6 hours at 70°C. The synthesized PMMA microspheres were filtered, washed with water and alcohol, and then dried in vacuum oven at room temperature. Microspheres were prepared as several batches and then combined as the stock source and the characterization studies were performed on the stock batch. Bone cement formulations prepared with this synthesized microspheres were assigned as BC3 group. Type and particle size of all PMMA particles used in bone cement preparation are summarized in Table 2.2 .

Table 2.2 Types of PMMA used in bone cement preparation

Sample code	PMMA type	Particle size (µm)
BC1	Commercial polymer, powder	50–150
BC2	Commercial polymer, powder	0–50
BC3	Synthesized polymer, microsphere	~1

2.1.3 Characterization of PMMA Particles

Chemical structure of synthesized PMMA microspheres was examined by Fourier Transform Infrared Spectrometer (FTIR). Morphology of PMMA particles were examined by Electron Microscopy (SEM). The average particle size and size distribution curves for ground and sieved PMMA particles were obtained by a particle size analyser.

2.1.3.1 Fourier Transform Infrared Spectroscopy

The FTIR spectra of the microspheres were recorded by using a FTIR spectrometer (Spectrum One Spectrometer, Perkin Elmer, Maryland, USA). KBr pellets were prepared by mixing the microspheres and potassium bromide (KBr). The mixture was pressed to form a pellet and the spectrum was recorded over the wavenumber range from 400 to 4000 cm^{-1} at 32 scans.

2.1.3.2 Morphological Investigations

Morphological shapes of PMMA particles used in cement preparation and fractured surfaces of tensile test samples were examined by Scanning Electron Microscopy (SEM, FEI Quanta 400F, Eindhoven, Holland). The samples were mounted on aluminium stubs, sputter-coated with gold-palladium (AuPd) under an argon atmosphere before analysis.

2.1.3.3 Particle Size Analysis

The average particle size and size distribution curves of PMMA powders, HAp and barium sulphate particles were examined by particle size analyzer (Malvern TM Mastersizer, Malvern Instruments Ltd, Worcestershire, UK) while PMMA microspheres were examined by Zeta Sizer (Malvern Nano ZS90, Worcestershire, UK). Distilled water was used as dispersant and the analysis was performed at room temperature for all analyses.

2.1.4 Preparation and Modification of Acrylic Bone Cements

Bone cement is a two component system and it is obtained by mixing the liquid and the powder parts. Liquid part was prepared by mixing MMA monomer and DMPT accelerator and also 1-dodecyl mercaptan was added to some compositions as chain stopping agent. Powder part consisted of PMMA polymer, BPO initiator and HAp and barium sulphate (BaSO_4). Moreover, powder part of some compositions contained various amounts of zeolite (Z), ammonium nitrate (AN) and chitosan (CH). For bone cement preparation, weighed amounts of powder part were mixed in a polypropylene bowl and then liquid part was added. In all compositions 4 g PMMA, 604 mg BaSO_4 , 45 mg BPO initiator, 168 mg HAp and 56 μL DMPT were used and these amounts were kept constant in all experiments. Bone cements were prepared by hand mixing with a spatula as shown in Figure 2.1.

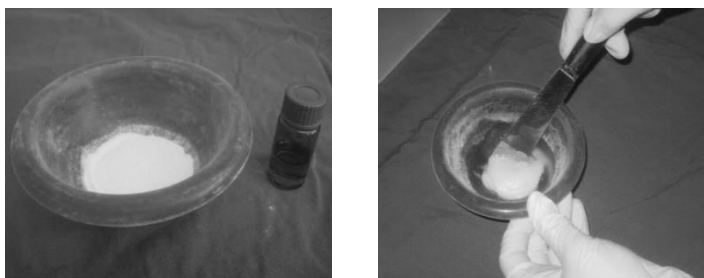


Figure 2.1 Bone cement dough preparation

The prepared bone cement compositions are summarized in Table 2.3. For BC2 and BC1 groups, 2 mL MMA monomer was used for 4 g PMMA polymer. For group BC3, 6 mL MMA monomer was used for 4 g PMMA polymer since more monomer was needed to wet the total microspheres because of higher surface to volume ratio of these microspheres compared to BC2 and BC1 groups.

Table 2.3 Bone cement formulations

Sample Code	O ₂ plasma application		DDM	AN	Z	CH1*	CH2*
	50 W	100 W					
BC1	-	-	-	-	-	-	-
BC1-P50	+	-	-	-	-	-	-
BC1-P100	-	+	-	-	-	-	-
BC1-P50-DDM	+	-	+	-	-	-	-
BC1-P50-AN	+	-	-	+	-	-	-
BC1-P50-DDM-Z	+	-	+	-	+	-	-
BC1-P50-AN-Z	+	-	-	+	+	-	-
BC1-CH1	-	-	-	-	-	+	-
BC1-CH2	-	-	-	-	-	-	+
BC2	-	-	-	-	-	-	-
BC2-P50	+	-	-	-	-	-	-
BC2-P100	-	+	-	-	-	-	-
BC2-P50-DDM	+	-	+	-	-	-	-
BC2-P50-AN	+	-	-	+	-	-	-
BC2-P50-DDM-Z	+	-	+	-	+	-	-
BC2-P50-AN-Z	+	-	-	+	+	-	-
BC2-CH1	-	-	-	-	-	+	-
BC2-CH2	-	-	-	-	-	-	+
BC3	-	-	-	-	-	-	-
BC3-P50	+	-	-	-	-	-	-
BC3-P100	-	+	-	-	-	-	-
BC3-P50-DDM	+	-	+	-	-	-	-
BC3-P50-AN	+	-	-	+	-	-	-
BC3-P50-DDM-Z	+	-	+	-	+	-	-
BC3-P50-AN-Z	+	-	-	+	+	-	-
BC3-CH1	-	-	-	-	-	+	-
BC3-CH2	-	-	-	-	-	-	+

* CH1: 0.05 g chitosan per gram of PMMA, CH2: 0.1 g chitosan per gram of PMMA

Oxygen plasma application was performed to powder part of some bone cement formulations to activate the surface of the particles. It was aimed to create active groups on the surface of powder components and increase interaction between the powder and liquid constituents and eventually to increase the mechanical properties. For this purpose, powder part was placed in a plasma chamber

(Advanced Plasma Systems, with a SEREN IPS R 300 13.56 MHz power supply, St. Petersburg, USA) and exposed to oxygen plasma (50 W or 100 W) for 5 min.

Also in order to decrease the curing temperature, DDM was added as chain stopping agent (2% relative to the amount of MMA) to the liquid part of chosen composition or NH_4NO_3 (0.125 g for 1 g PMMA) was added to the powder part of the cement formulations. In some formulations; zeolite (0.075 g for 1 g PMMA) was added to enhance the mechanical strength. Moreover, for in vivo experiments bone cement formulations without oxygen plasma application were prepared with addition of chitosan (0.05 g for CH1 group or 0.1 g for CH2 group chitosan per gram of PMMA), mechanical and curing properties of resultant bone cements were measured and compared with all compositions. All amounts of additives were chosen appropriately to keep the optimum handling properties.

2.1.5 Characterization of Acrylic Bone Cements

Mechanical properties of the prepared bone cement samples were examined with tension and compression tests. Mechanical tests were performed by using LLoyd® LRX 5K (LLoyd Instruments Limited, Fareham, Hampshire, UK) testing machine with a cell load of 5000 Newton at room temperature. The maximum curing temperatures of the prepared bone cements were measured by using thermocouples.

2.1.5.1 Mechanical Analysis

2.1.5.1.1 Tension Tests

In order to prepare tension test samples, the cement dough was rolled on a polyethylene surface, cut with dog bone shape mold ($5 \times 0.5 \times 0.5 \text{ cm}^3$) and allowed to cure for 1 h at room temperature. Then the specimens were kept in physiological saline solution in a temperature-controlled water bath for 24 h at $37 \pm 1^\circ\text{C}$ prior to mechanical tests. The samples were taken out from the water bath, their thickness and width were measured and load applied areas were calculated. Tension force was applied with a cross-head speed of $1 \text{ mm}\cdot\text{min}^{-1}$ at room temperature. Young's modulus and ultimate tensile strength values were calculated from load versus displacement curves. For each sample at least five specimens were tested and the average values were obtained. Tension test samples and test set up is shown in Figure 2.2.

2.1.5.1.2 Compression Tests

For the compression tests, samples were prepared by pressing the soft dough in a stainless steel mold which complies with ASTM standard F451-95 (Standard specification for acrylic bone cement). The mold was composed of three cylindrical plates which have 84 mm diameter and 12 mm height and one of the plates had 52 holes each having 6 mm diameter. The prepared dough was placed in the mould and pressed with the help of two clamps. The dough was allowed to cure for one hour and then the specimens were removed from the mould, kept in a saline solution in a temperature-controlled water bath for 24 h at $37 \pm 1^\circ\text{C}$. Then they were subjected to the compression test. Prior to test, the diameter and gauge lengths of specimens were measured and the load applied areas were calculated. Tests were performed with a cross-head speed of $25 \text{ mm}\cdot\text{min}^{-1}$ at room temperature. For each sample at least eight specimens were tested and their average values were obtained. Compression mold and test set up is shown in Figure 2.3.

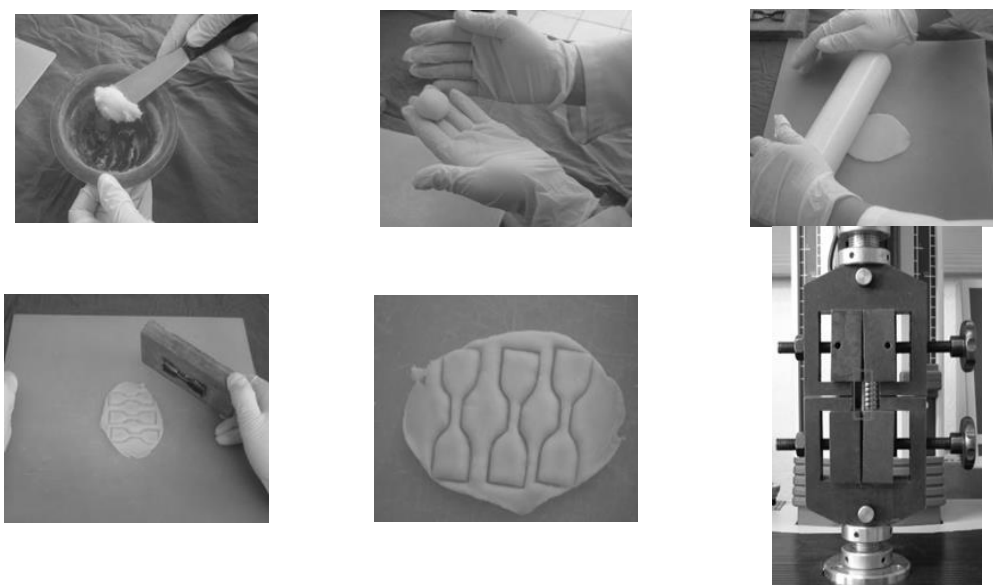


Figure 2.2 Tension test samples and test set up

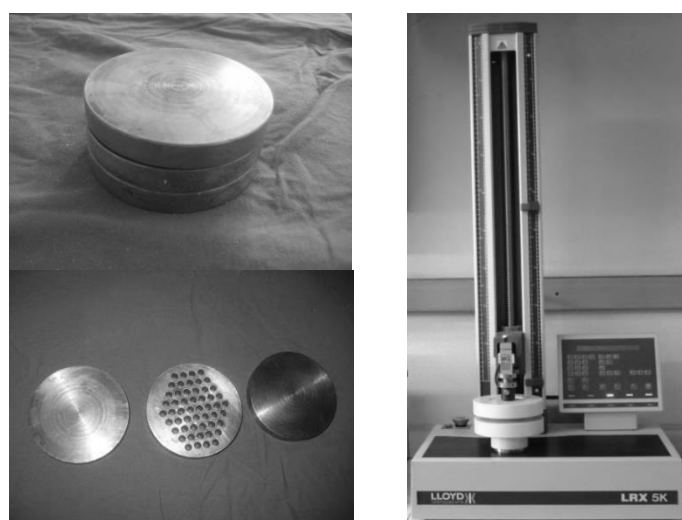


Figure 2.3 Compression mold and test set up

2.1.5.2 Thermal Analysis

The maximum curing temperatures of bone cements were measured by a “Thermocouple Input Module” (SuperLogics, Boston, USA). J-type thermocouples working in the temperature range of -210°C – 760°C were used. The positive conductor of the thermocouple is made of iron and the negative conductor is made of constantan. Thermocouples were cut into pieces with 5 cm in length and removed from isolators. Then they were rolled with Teflon band and one end of the thermocouple was electrically welded.

The temperature measurement experiments were performed at $23 \pm 2^{\circ}\text{C}$. The cement dough was prepared and rounded to give a spherical shape with a radius of ~ 15 mm. Then the welded end of the

thermocouple was placed in the centre of the dough. The temperature was recorded for 1200 seconds with a 1 data per second record rate.

Peak temperature was the maximum temperature reached during the polymerization process. Setting time of bone cement was defined as the time when the temperature rise was at halfway point between the maximum temperature and the ambient temperature (T_{amb}) (Li and Mason 2004). Setting temperature can be calculated by using the following equation:

$$T_{set} = (T_{amb} + T_{max}) / 2$$

A typical temperature versus time graph showing the exothermic temperature changes occurring in acrylic cements during the setting process of the cement is given in Figure 2.4.

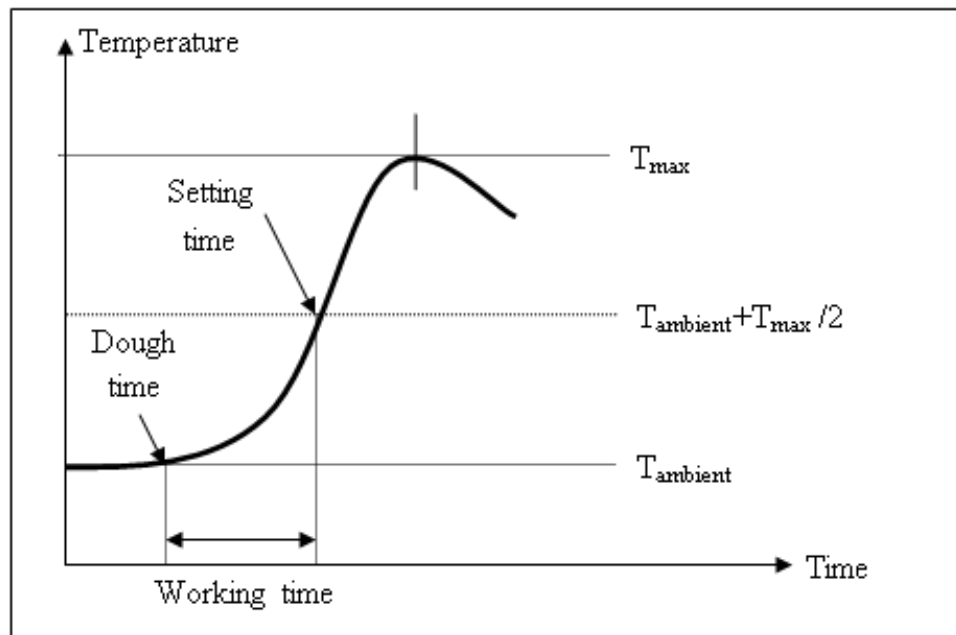


Figure 2.4 Typical temperature versus time graph of setting of acrylic cements

2.1.5.3 In Vivo Tests

BC1 and BC1-CH1 group (0.05 g chitosan per gram of PMMA) bone cements were chosen for in vivo tests and applied to rats with commercially available CMW1 cements. The obtained results were compared. In vivo tests were performed in Yeditepe University by Dr. Tahsin Beyzadeoğlu after getting ethics committee approval from Yeditepe University Institute of Experimental Medicine. Biocompatibility of the prepared bone cements was evaluated by using a rat model. Rats were anesthetized by intramuscular injection of Ketamine/xylazine. The skin of the animal was shaved and cleaned with Betadine. Defects were formed on both knees of the rats by anterior longitudinal incision. Powder and liquid parts of bone cements were mixed and the dough was immediately placed into the defect on the right knees while left knees were left unfilled as control groups as shown in Figure 2.5.

The cements were allowed to set in vivo after implantation and then the incisions were closed with a suture. Prophylactic antibiotic was applied to each animal in order to prevent postoperative infections. Animals were sacrificed at 4 weeks after surgery. Histological examinations were

performed on excised tissue which was fixed in 10% buffered formalin, decalcified and embedded in paraffin. Excised tissues having 5 μm thickness were stained with hematoxylin and eosin (H&E) and examined under light microscope (Olympus, Tokyo, Japan).



Figure 2.5 Illustration of bone cement application

2.2 Results and Discussion

2.2.1 Fourier Transform Infrared Spectroscopy Results

FTIR analysis is beneficial in the characterization of the functional groups present in the polymer. The FTIR spectrum of the prepared PMMA microspheres is shown in Figure 2.6. The sharp intense peak seen at 1731 cm^{-1} can be identified as C=O stretching vibrations in the pendant group ($-\text{COOCH}_3$) of PMMA. The bands at 2996 and 2952 cm^{-1} correspond to the C–H stretching of the methyl group (CH_3) while the bands at 1450 and 1388 cm^{-1} are associated with C–H asymmetric and symmetric stretching modes, respectively. The 1243 cm^{-1} band is assigned to torsion of the methylene group (CH_2) and the 1148 cm^{-1} band corresponds to vibration of the ester group C–O, while C–C stretching bands are at 990 and 840 cm^{-1} . The absence of the peak at 1650 cm^{-1} which belongs to methylene group of MMA monomer indicates complete polymerization of MMA monomer. It can be concluded that the prepared PMMA microspheres demonstrated the characteristic peaks of pure PMMA.

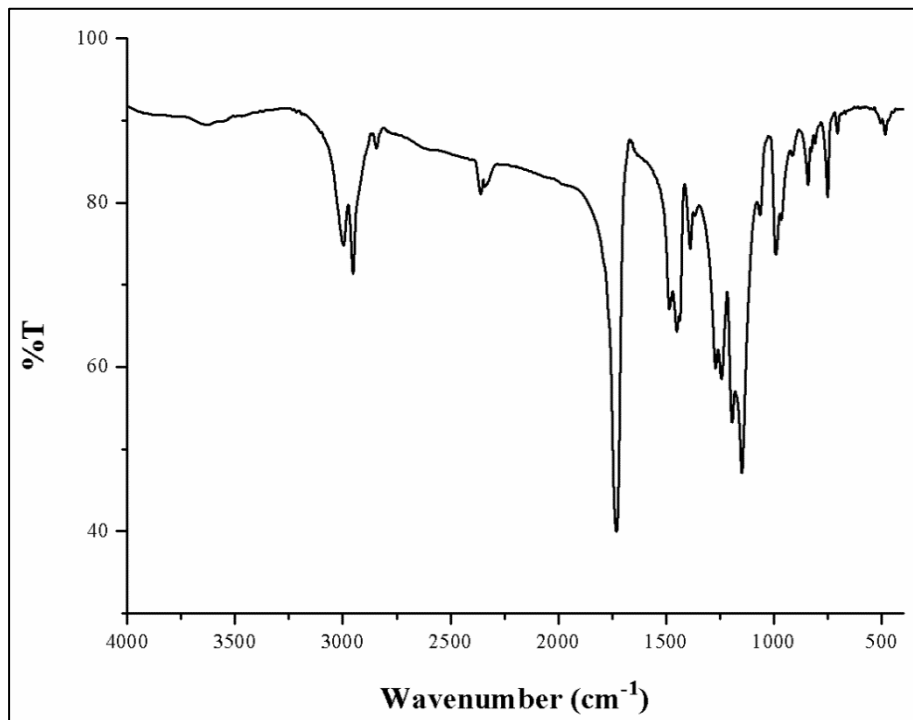


Figure 2.6 FTIR spectrum of PMMA microspheres

2.2.2 Morphological Analysis Results of PMMA Particles

Scanning electron micrographs of the PMMA particles used in the preparation of bone cement formulations are given in Figure 2.7. The particles prepared by grinding and sieving had irregular shapes and nonhomogenous particle surface and they were used in the preparation of BC1 and BC2 group bone cement formulations. The use of blades during grinding caused microparticles with random edges. The particles synthesized by suspension polymerization were very homogenous and monodisperse with perfect spherical shape and with size of approximately 1 μm . These small size particles were used in the preparation of BC3 group bone cement formulations.

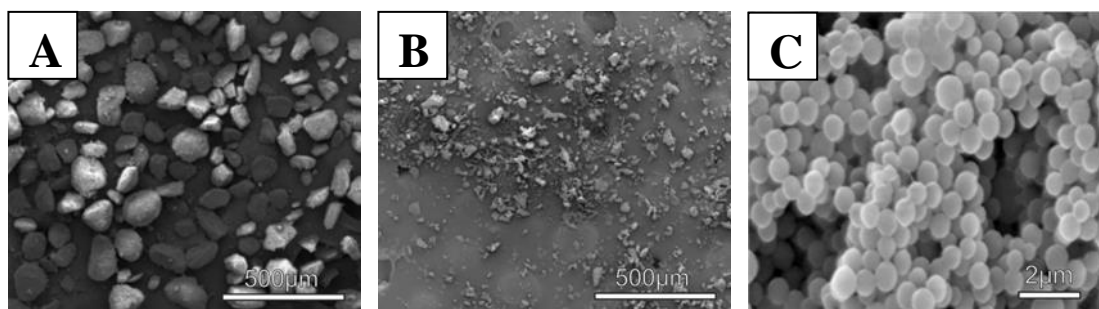


Figure 2.7 SEM micrographs of PMMA particles A) 50–150 μm , B) 0–50 μm , C) 1 μm

2.2.3 Particle Size Analysis Results

The volume weighted average particle sizes of PMMA, HAp and BaSO₄ particles used in these experiments were examined by using Malvern Mastersizer. Distilled water was used as dispersant for all particles. Average particle sizes of ground PMMA particles used in the preparation of bone cements were found as 76.84 μm and 21.14 μm for BC1 and BC2 groups, respectively. Particle size of PMMA particles ranged from 0.5 μm to 220 μm and from 0.5 μm to 115 μm for BC1 and BC2 group, respectively. Approximately 28% of the particles used for BC1 group were in the 1–50 μm range, while for BC1 group 92% of particles used were in the 1–50 μm range. The particle size distribution curves of PMMA particles are given in Figure 2.8.

Average diameters of the HAp and BaSO₄ were found to be 10.85 μm and 7.37 μm , respectively. The particle size distribution curves of HAp and BaSO₄ are given in Figure 2.9 and Figure 2.10, respectively.

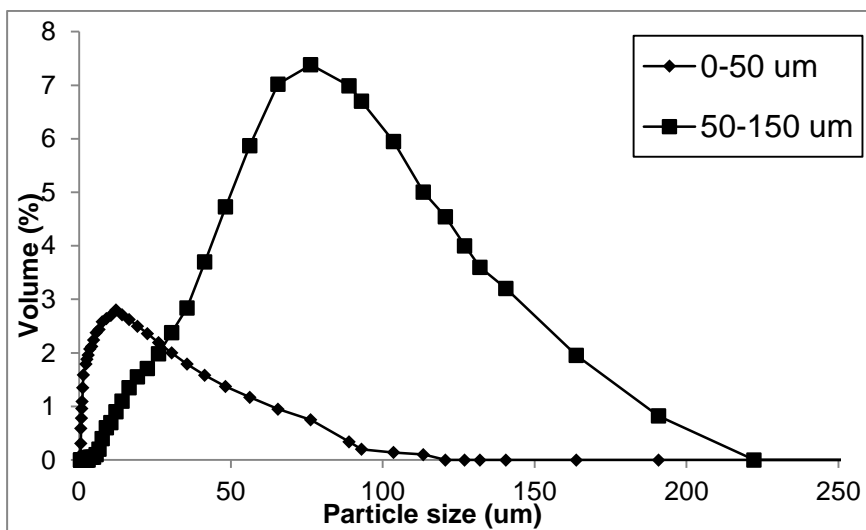


Figure 2.8 Particle size distributions of PMMA particles

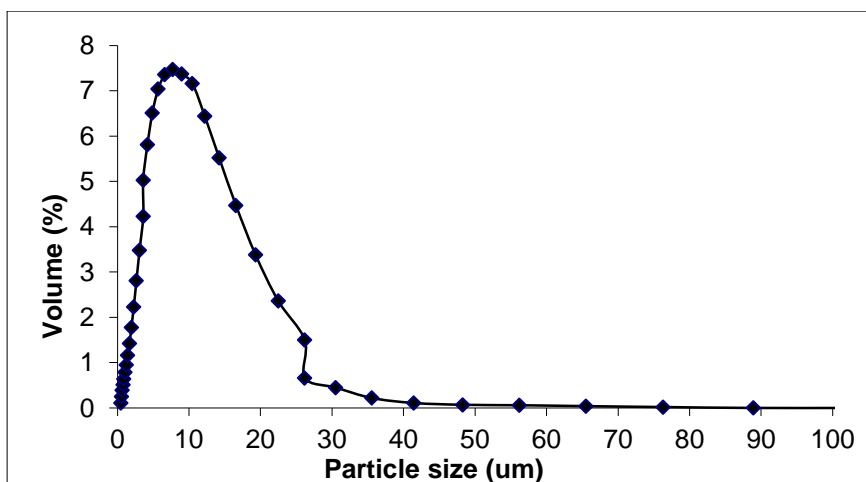


Figure 2.9 Particle size distribution of HAp particles

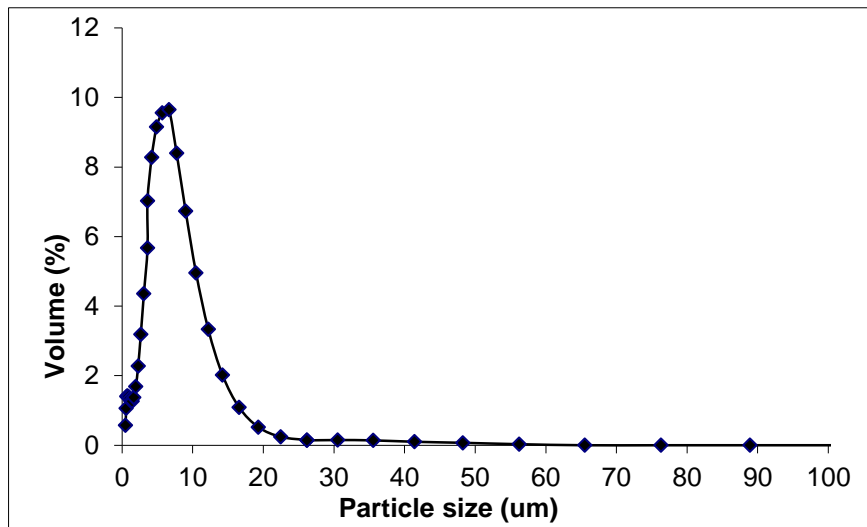


Figure 2.10 Particle size distribution of BaSO₄ particles

For the synthesized microspheres, since the average particle size was about 1 μm, precise size distribution curve could not be obtained by Malvern Instrument. Therefore, the particle size distribution curve of PMMA microspheres was examined by Zeta Sizer. During the experiments distilled water was used as a dispersant and the average particle size was found to be 1.01 μm. The size distribution is given in Figure 2.11. Particle size of the approximately 25% of the particles are below 1 μm.

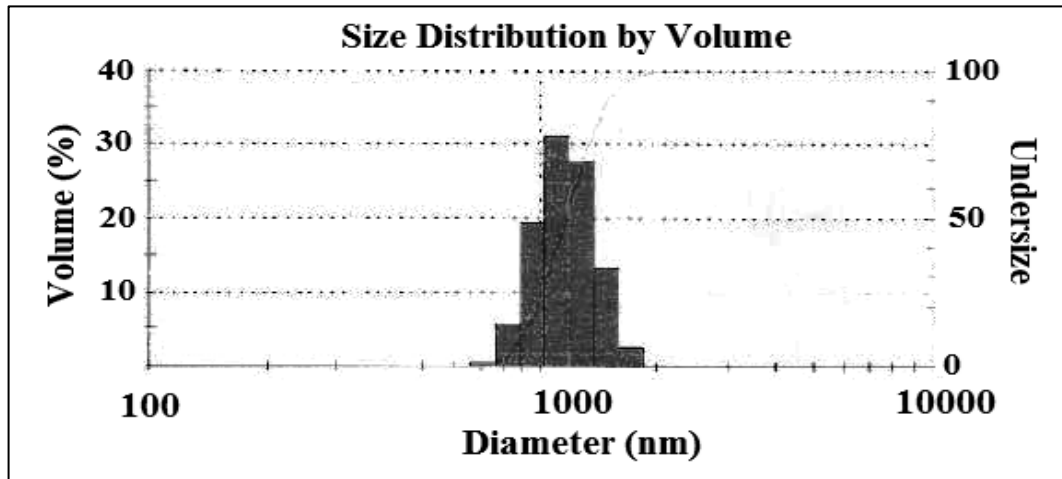


Figure 2.11 Particle size distribution of PMMA microspheres

2.2.4 Modification of Acrylic Bone Cements with Oxygen Plasma

Three set of acrylic bone cement formulations were prepared by using PMMA powders having three different particle size which are ground and sieved polymer particles with 0–50 μm (BC2 group) and 50–150 μm size (BC1 group) and microspheres with 1 μm size (BC3 group). Powder part composed of PMMA polymer, benzoyl peroxide initiator, barium sulphate radioopaque agent and HAp

bioactivator was mixed with liquid part consisting of methyl methacrylate (MMA) monomer and N,N-dimethyl-p-toluidine (DMPT) accelerator. Different modifications were applied to these three sets of bone cements. These modifications are oxygen plasma application, addition of various additives such as 1-dodecyl mercaptan, ammonium nitrate, zeolite and chitosan. Then effects of modifications on mechanical and curing properties were investigated. In order to examine mechanical properties; tension and compression tests were applied to the prepared bone cement formulations while for curing properties maximum curing temperatures and setting times were studied.

2.2.4.1 Effect of Oxygen Plasma on Mechanical Properties

It is known that the weak interfaces between the inorganic fillers and the organic matrix reduce the mechanical strength of bone cement (Pourdeyhimi *et al.* 1989, Dandurand *et al.* 1990). The interfacial adhesion strength can be increased by the plasma treatment, which is generally due to the improved wettability and possibly to the chemical bonds between the filler and the resin (Ladizesky *et al.* 1995, Hild *et al.* 1993). Plasma treatment introduces polar or excited groups that can form strong covalent bonds between the filler and the matrix, and sometimes roughens the surface of fillers to increase mechanical interlock between the filler and the matrix (Jang and Yang 2000). Kim and Yasuda improved the fatigue properties of PMMA bone cement by treating the radiopaque agent and reinforcing carbon fibers with hexamethyldisiloxane plasma followed by oxygen plasma posttreatment compared to untreated samples (Kim and Yasuda 1999). Therefore it was proposed in this thesis that mechanical strength acrylic bone cements may be improved by plasma treatment with improved chemical bonds between additives. In order to enhance the mechanical properties, two different powers (50 W and 100 W) of oxygen plasma were applied for 5 min to the powder part of bone cement formulations prior to mixing of powder and liquid parts. Tensile and compressive test results of oxygen plasma applied BC1, BC2 and BC3 group bone cement formulations are given in Table 2.4 and Figure 2.12.

Table 2.4 Mechanical properties of bone cements before and after O₂ plasma

BC	Tensile Properties		Compressive Properties	
	UTS (MPa)	E _T (GPa)	UCS (MPa)	E _C (GPa)
BC1	19.65 ± 2.70	0.39 ± 0.05	81.51 ± 3.43	0.57 ± 0.04
BC1-P50	26.52 ± 2.89	0.47 ± 0.07	90.59 ± 3.16	0.57 ± 0.04
BC1-P100	24.65 ± 2.64	0.44 ± 0.03	88.33 ± 1.99	0.59 ± 0.05
BC2	19.77 ± 1.78	0.39 ± 0.04	75.37 ± 7.47	0.48 ± 0.05
BC2-P50	24.67 ± 5.22	0.46 ± 0.05	86.38 ± 3.76	0.54 ± 0.04
BC2-P100	24.74 ± 2.66	0.43 ± 0.04	89.19 ± 4.92	0.55 ± 0.06
BC3	18.27 ± 5.14	0.38 ± 0.04	75.96 ± 2.21	0.53 ± 0.03
BC3-P50	27.70 ± 3.08	0.47 ± 0.06	89.39 ± 7.64	0.53 ± 0.08
BC3-P100	24.01 ± 3.06	0.43 ± 0.02	81.14 ± 5.28	0.53 ± 0.05

The oxygen plasma treatment enhanced tensile properties of each group formulations regardless of the PMMA particle size. It is known that free radical formation occur with plasma treatment and peroxides may be formed in the atmospheric or oxygen environment because of the oxidation of free radicals (Hsiue and Wang 1993). The presence of peroxy radicals on the surface of the oxygen plasma treated PMMA films was shown by ESR analysis and the intensity of these radicals increased

with increasing plasma power (Ozgen 2011). The peroxides may create free radicals by the reaction with DMPT activator in the bone cement which can initiate the MMA polymerization. Through this graft polymerization process, the interfacial bond strength between the filler particles and the MMA matrix may be enhanced, resulting in efficient stress transfer from the matrix to the fillers. With 5 minute 50 W oxygen plasma application the ultimate tensile strength (UTS) values increased from 19.65 MPa to 26.52 MPa, from 19.77 MPa to 24.67 MPa, from 18.27 MPa to 27.70 MPa for BC1-P50, BC2-P50 and BC3-P50 bone cement formulations, respectively. While tensile elastic modulus (E_T) values increased 21%, 18% and 24% for BC1-P50, BC2-P50 and BC3-P50 bone cement groups, respectively. The increase in the plasma power to 100 W did not cause further increase in tensile properties compared to 50 W oxygen plasma applied samples.

The ultimate compressive strength (UCS) values increased from 81.51 MPa to 90.59 MPa, from 75.37 MPa to 86.38 MPa, from 75.96 MPa to 89.39 MPa for BC1-P50, BC2-P50 and BC3-P50 group bone cements, respectively with 5 minute 50 W oxygen plasma application. 13% increase was observed for the compressive elastic modulus of BC2-P50 while compressive elastic modulus of other groups remained almost the same. It was reported that the compressive strength of bone cement usually varies from 44 MPa to 103 MPa (Saha and Pal 1984). For example compressive strength of Palacos R bone cement was found as 90 MPa (He *et al.* 2002) while it was 105 MPa for Osteobond (Nien *et al.* 2013).

100 W plasma application did not lead to further increase in ultimate compressive strength values except BC2-P100 group. When tensile and compressive properties of the bone cement samples treated with 50 W and 100 W plasma are considered it was observed that, the increase in tensile and compressive strengths was not significant compared to the samples treated with 50 W plasma. When bone cement formulations prepared with different PMMA particles are considered, it was seen that particle size of polymer did not make a significant difference in the mechanical properties of prepared bone cements. All bone cements prepared with plasma application satisfied the minimum compressive strength (70 MPa) required by ASTM F451 standard.

2.2.4.2 Effect of Oxygen Plasma on Curing Properties

The curing of bone cements is accompanied by a temperature rise in the cement due to release of polymerization heat. Setting time of bone cement was defined as the time when the temperature rise was at halfway point between the maximum temperature and the ambient temperature. At setting time, the cement gets harden and would no longer plastically deform under hand pressure.

Maximum curing temperatures and setting times of oxygen plasma treated bone cement formulations are given in Table 2.5 and Figure 2.12. Application of oxygen plasma increased the maximum curing temperatures in all bone cement groups. With application of 100 W plasma, the maximum curing temperatures increased from 71.60°C (BC1) to 91.48°C (BC1-P100), from 83.48°C (BC2) to 107.04°C (BC2-P100) and from 116.24°C (BC3) to 120.66°C (BC3-P100). This can be explained as the free oxygen radicals resulted from plasma treatment acted as additional initiator for polymerization of MMA and caused temperature rise by accelerating the polymerization rate. As a result, the oxygen plasma treatment showed a positive effect on mechanical strength, but an adverse effect causing an increase in the maximum curing temperature. The maximum curing temperature was lower in group BC1 than the group BC2 and BC3 with or without oxygen plasma application. This may be due to absorption of the released heat by the larger particles of PMMA in group BC1. It was stated in literature that PMMA particles larger than 50–60 μm could absorb the produced heat during the setting process and smaller than 20 μm undergo complete dissolution in the polymerizing MMA medium therefore it may cause an increase in the viscosity and curing temperature of the cement (Pascual *et al.* 1996). For BC3 group where microspheres with 1 μm size were used, there are two factors affecting the results. Polymer-to-monomer ratio is lower and the particle size is smaller which may lead complete dissolution of the particles in its monomer. Both factors cause higher curing temperatures increasing the polymerization rate and decreasing the absorption of

released heat by particles. Therefore, quite high curing temperatures ($\sim 116^{\circ}\text{C}$) was observed for BC3 group. The plasma treated samples in this group also showed the same trend in terms of mechanical and curing properties as other samples in BC2 and BC1 groups did. They showed no significant difference with respect to mechanical values, but the maximum polymerization temperature was higher compared to the other two groups.

When setting times were considered, it was observed that with 50 W plasma application, setting time shortened from 312 s to 302 s and from 190 s to 178 s, for BC1-P50 and BC2-P50 groups, respectively (Table 2.5). The number of free radicals increased after plasma application and so did the polymerization rate which caused faster setting time for bone cements. However; 50 W plasma application extended the setting time from 406 s to 472 s in BC3-P50 group. Setting time of BC3 group was higher compared to BC2 and BC1 groups, higher monomer amount in formulation allowed more time for the liquid and powder parts to be mixed giving rise to a longer time for the surgeon handling and application. But the curing temperatures higher than 100°C are the adverse effects of this group of cements. Setting time of bone cement should be in the range of 3 min to 15 min according to ISO5833 (Mori *et al.* 2003) and BC1 and BC3 group bone cements comply it. In literature there are varying values for setting time and maximum curing temperature of prepared bone cements because of different chemical compositions, preparation techniques such as mixing type, particle size and shape of powder components. For instance, setting time of ketoprofen loaded Osteobond was found as 286 s while maximum curing temperature was 69°C (Nien *et al.* 2013). Fukuda *et al.* prepared titania containing acrylic bone cement and found the setting time as 612 s and while setting time of Simplex commercial bone cement was 619 s (Fukuda *et al.* 2011).

Table 2.5 Curing properties of bone cements before and after O_2 plasma

BC	Curing Properties	
	T_{max} ($^{\circ}\text{C}$)	t_{set} (s)
BC1	71.60 ± 9.31	312 ± 17
BC1-P50	75.56 ± 6.46	302 ± 14
BC1-P100	91.48 ± 4.04	279 ± 18
BC2	83.48 ± 7.35	190 ± 20
BC2-P50	96.50 ± 4.52	178 ± 28
BC2-P100	107.04 ± 6.36	156 ± 20
BC3	116.24 ± 4.94	406 ± 8
BC3-P50	121.34 ± 2.80	472 ± 16
BC3-P100	120.66 ± 3.78	456 ± 18

Tensile, compressive and curing temperatures and setting times of bone cements before and after oxygen plasma application are summarized in Figure 2.12. It was observed that after plasma application both tensile and compressive properties of all bone cement groups improved. However, 100 W oxygen plasma application did not cause a significant improvement in mechanical strength compared to 50 W oxygen plasma application, but caused a significant increase in the maximum curing temperature.

For further modification of bone cement formulations, 5 min 50 W oxygen plasma applied bone cement compositions (BC-P50) were chosen as optimum with regard to their handling, mechanical and curing properties. Ingredients such as dodecyl mercaptane, ammonium nitrate, zeolite were

added into BC-P50 compositions and their effects on mechanical and curing properties were examined.

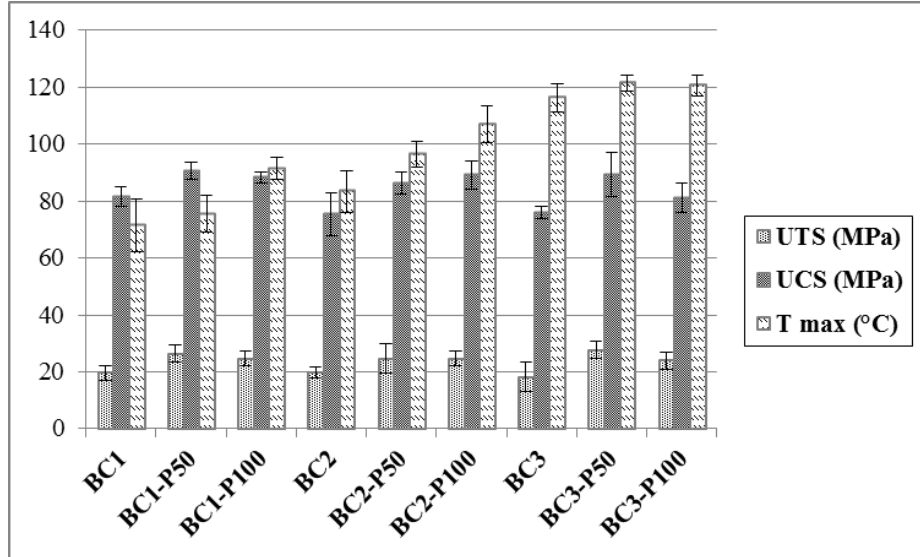


Figure 2.12 UTS, UCS and T_{max} values of O_2 plasma applied bone cements

2.2.5 Modification of Acrylic Bone Cements with DDM and AN

As mentioned before, plasma application enhanced the compatibility of components of the cement and had a positive effect on mechanical properties while increased the maximum curing temperature. To overcome negative effect of plasma on curing properties, further modifications were done by adding 1-dodecyl mercaptan (DDM) chain stopping agent or ammonium nitrate (AN) heat absorber. Acute toxicity value (LD50) of ammonium nitrate is reported as 2.217 g/kg for rats (<http://www.sciencelab.com/msds.php?msdsId=9927336>). In a 30 g bone cement package total amount of ammonium nitrate will be 3.75 g therefore dose of 0.054 g/kg for an average human will be lower than that of LD50 value of rats.

2.2.5.1 Effect of DDM and AN Addition on Mechanical Properties

Tensile and compressive test results of bone cement formulations before and after DDM or AN are given in Table 2.6 and Figure 2.13. Elastic tensile modulus values showed 11%, 11% and 6% decline for BC1-P50-DDM, BC2-P50-DDM and BC3-P50-DDM group, respectively. DDM addition caused drastic decrease in tensile properties in all bone cement groups. Similar type of decreases was also obtained for compressive strength values. DDM is a chain stopping agent; it controls the polymerization reaction and prevents formation of long chains and high molecular weight polymers. It decreases chain lengths of PMMA chains in the matrix, and this may lead to a decrease in mechanical properties of bone cements.

Table 2.6 Mechanical properties of DDM or AN containing bone cements

BC	Tensile Properties		Compressive Properties	
	UTS (MPa)	E _T (GPa)	UCS (MPa)	E _c (GPa)
BC1-P50	26.52 ± 2.89	0.47 ± 0.07	90.59 ± 3.16	0.57 ± 0.04
BC1-P50-DDM	13.85 ± 0.52	0.42 ± 0.02	60.79 ± 2.12	0.48 ± 0.06
BC1-P50-AN	13.79 ± 1.27	0.47 ± 0.05	72.22 ± 6.96	0.46 ± 0.08
BC2-P50	24.67 ± 5.22	0.46 ± 0.05	86.38 ± 3.76	0.54 ± 0.04
BC2-P50-DDM	16.73 ± 1.02	0.41 ± 0.04	65.59 ± 2.95	0.45 ± 0.08
BC2-P50-AN	15.92 ± 1.97	0.43 ± 0.03	68.10 ± 5.99	0.46 ± 0.04
BC3-P50	27.70 ± 3.08	0.47 ± 0.06	89.39 ± 7.64	0.53 ± 0.08
BC3-P50-DDM	12.67 ± 0.51	0.44 ± 0.03	69.04 ± 13.26	0.46 ± 0.06
BC3-P50-AN	16.13 ± 3.18	0.41 ± 0.08	64.57 ± 4.95	0.40 ± 0.05

Same trend was observed when ammonium nitrate was added, tensile properties in all bone cement groups were significantly decreased. Elastic tensile modulus value of BC1-P50-AN group bone cement remained same while 7% and 13% decrease was observed for BC2-P50-AN and BC3-P50-AN groups, respectively. Ammonium nitrate is added as solid powder, and it is possible that it created a different phase separation and decreased mechanical properties.

Addition of DDM and AN also decreased the compressive properties of all bone cement groups same as in tensile properties. Elastic compressive modulus values showed 16%, 17% and 13% decrease for BC1-P50-DDM, BC2-P50-DDM and BC3-P50-DDM group bone cements, respectively. 19%, 15%, 25% decline was observed in elastic compressive modulus values of BC1-P50-AN, BC2-P50-AN and BC3-P50-AN group bone cements, respectively. There are various ingredients added in order to give specific properties to bone cements. For instance drugs are loaded into bone cements to prevent and treat implant related infection. Commercial bone cement Osteobond was modified with ketoprofen and its compressive strength was found as 76 MPa while the compressive strength of plain Osteobond was 105 MPa (Nien *et al.* 2013). Compressive strength of Palacos R bone cement was reported as 90 MPa however it decreased to 74 MPa with gentamicin addition (He *et al.* 2002). May-Pat *et al.* found ultimate compressive strength of prepared acrylic bone cements containing barium sulphate radiopacifiers as 102 MPa and observed that the addition of monomers containing amine groups to liquid part of bone cement reduced the compressive strength down to 76 MPa depending on the concentration (May-Pat *et al.* 2012). Incorporation of some ingredients may improve one property while worsen other, therefore it is important to adjust proper amount.

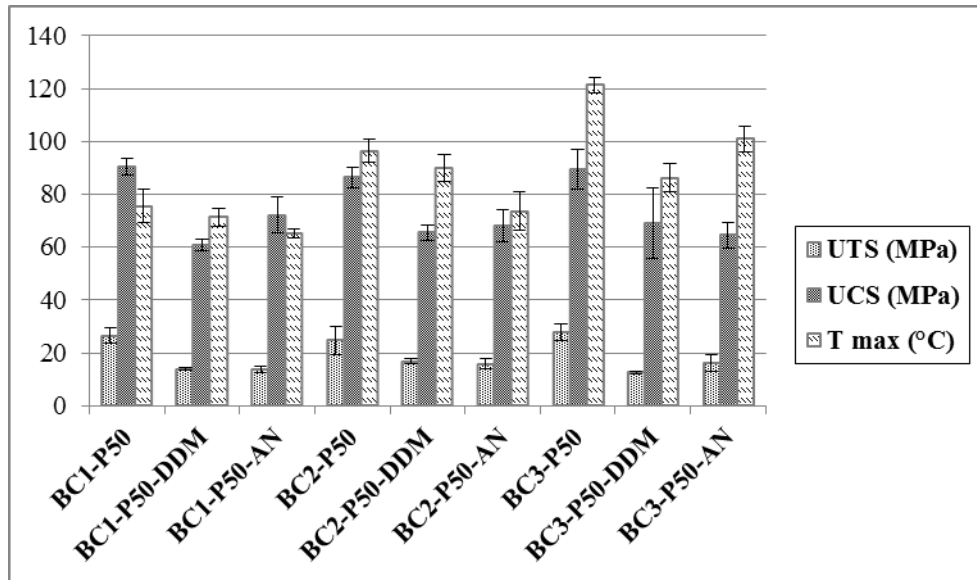
2.2.5.2 Effect of DDM and AN Addition on Curing Properties

Maximum curing temperatures and setting times of DDM and ammonium nitrate containing bone cement groups are given in Table 2.7 and Figure 2.13. Addition of DDM decreased the maximum curing temperatures in all groups. With DDM addition, the maximum curing temperatures decreased from 75.56°C (BC1-P50) to 71.31°C (BC1-P50-DDM), from 96.50°C (BC2-P50) to 90.12°C (BC2-P50-DDM) and from 121.34°C (BC3-P50) to 116.18°C (BC3-P50-DDM). DDM controls the polymerization reaction and prevents the highly exothermic reaction.

Table 2.7 Curing properties of DDM or AN containing bone cements

BC	Curing Properties	
	T_{max} (°C)	t_{set} (s)
BC1-P50	75.56 ± 6.46	302 ± 14
BC1-P50-DDM	71.31 ± 3.32	206 ± 9
BC1-P50-AN	65.22 ± 1.89	129 ± 33
BC2-P50	96.50 ± 4.52	178 ± 28
BC2-P50-DDM	90.12 ± 5.14	152 ± 11
BC2-P50-AN	73.64 ± 7.38	139 ± 7
BC3-P50	121.34 ± 2.80	472 ± 16
BC3-P50-DDM	116.18 ± 5.40	412 ± 31
BC3-P50-AN	101.04 ± 4.89	182 ± 16

Similarly, AN incorporation also caused a decrease in the T_{max} values from 75.56°C (BC1-P50) to 65.22°C (BC1-P50-AN), from 96.50°C (BC2-P50) to 73.64°C (BC2-P50-AN) and from 121.34°C (BC3-P50) to 101.04°C (BC3-P50-AN). Ammonium nitrate gives endothermic reactions with water and expected to absorb heat formed during polymerization of MMA monomer in a humid media as natural tissue. The lowest temperature rise was observed in group BC1 due to absorption of the released heat by the larger particles of PMMA in this group. When setting times were considered, it was observed that DDM or AN addition shortened setting times in all groups.

**Figure 2.13** UTS, UCS and T_{max} values of DDM or AN containing bone cements

2.2.6 Modification of Acrylic Bone Cements with Zeolite

Oxygen plasma was applied to the powder part of bone cement formulations in order to increase the mechanical properties by increasing the interaction between PMMA powder particles and MMA monomer molecules. However beside mechanical properties, maximum curing temperature was also increased. Therefore, in order to decrease maximum curing temperature, formulations were modified with DDM chain stopping agent and ammonium nitrate. As a result both mechanical properties and curing temperature values were reduced, even ultimate compressive strength values obtained with DDM and AN addition was not in the range of acceptance ($UCS > 70$ MPa). Then the powder part of bone cement formulations was modified by zeolite addition with the purpose of increasing the mechanical properties.

2.2.6.1 Effect of Zeolite Addition on Mechanical Properties

Tensile and compressive test results are given in Table 2.8 and Figure 2.14. Addition of zeolite to DDM and AN containing bone cement formulations increased the tensile properties of all groups. Elastic tensile modulus values showed 19% increase for BC2-P50-AN-Z group and there was no significant increase for BC1-P50-AN-Z and BC3-P50-AN-Z groups, respectively.

Table 2.8 Mechanical properties of zeolite containing bone cements

BC	Tensile Properties		Compressive Properties	
	UTS (MPa)	E_T (GPa)	UCS (MPa)	E_C (GPa)
BC1-P50-DDM	13.85 ± 0.52	0.42 ± 0.02	60.79 ± 2.12	0.48 ± 0.06
BC1-P50-DDM-Z	16.56 ± 3.53	0.52 ± 0.09	98.20 ± 9.15	0.58 ± 0.05
BC1-P50-AN	13.79 ± 1.27	0.47 ± 0.05	72.22 ± 6.96	0.46 ± 0.08
BC1-P50-AN-Z	17.06 ± 3.01	0.48 ± 0.06	87.30 ± 5.42	0.51 ± 0.06
BC2-P50-DDM	16.73 ± 1.02	0.41 ± 0.04	65.59 ± 2.95	0.45 ± 0.08
BC2-P50-DDM-Z	20.59 ± 3.02	0.59 ± 0.12	86.19 ± 7.73	0.54 ± 0.06
BC2-P50-AN	15.92 ± 1.97	0.43 ± 0.03	68.10 ± 5.99	0.46 ± 0.04
BC2-P50-AN-Z	20.87 ± 3.45	0.51 ± 0.05	90.21 ± 6.81	0.56 ± 0.02
BC3-P50-DDM	12.67 ± 0.51	0.44 ± 0.03	69.04 ± 13.26	0.46 ± 0.06
BC3-P50-DDM-Z	18.11 ± 4.49	0.46 ± 0.08	80.95 ± 13.53	0.58 ± 0.03
BC3-P50-AN	16.13 ± 3.18	0.41 ± 0.08	64.57 ± 4.95	0.40 ± 0.05
BC3-P50-AN-Z	19.21 ± 1.99	0.42 ± 0.06	80.20 ± 4.62	0.52 ± 0.04

Similarly significant improvement was observed in the compressive properties with addition of zeolite in all groups. Zeolite acted as a load carrier and improved both tensile and compressive properties. It was stated that zeolite can be used as an ingredient in a dental cement composition (Saghiri *et al.* 2012). Several polymer-zeolite composites were prepared and it was stated that composites exhibited an improved interfacial adhesion and mechanical performance due to good interaction and reinforcing behavior of zeolite fillers (Kumar *et al.* 2010, Yuzay *et al.* 2010). It can be said that reinforcing effect depends on the type and amount of fillers incorporated. Zeolites are porous particles; methyl methacrylate monomer might have diffused into pores of zeolites during

mixing of powder and liquid part of bone cement and PMMA polymer formation occurred inside the pores. In literature XRD and ESR studies proved the presence of methyl methacrylate, various vinyl monomers within the pores of zeolites (Möller *et al.* 1998, Spange *et al.* 2001, Nakayama *et al.* 2003). The incorporation of some polymer chains within the pores of zeolite particles might provide better mechanical interlock between organic-inorganic composites and therefore improved mechanical properties of prepared bone cements.

2.2.6.2 Effect of Zeolite Addition on Curing Properties

Maximum curing temperatures and setting times of zeolite containing groups are given in Table 2.9 and Figure 2.14. Addition of zeolite decreased the maximum curing temperatures in the range of 1–7 degrees in all bone cements groups.

Zeolite particles might act as heat sink and absorbed the released heat during exothermic polymerization reaction. Setting times extended in BC2 and BC1 group bone cements with zeolite addition while unexpectedly decreased in BC3 group. Maximum curing temperature of PMMA based bone cements was decreased from 95°C to 75°C with magnetite addition (Li *et al.* 2012) while 10°C decline was observed with nano-sized titania fibers (Khaled *et al.* 2011) due to the absorption of the released heat by ingredients.

Table 2.9 Curing properties of zeolite containing bone cements

BC	Curing Properties	
	T _{max} (°C)	t _{set} (s)
BC1-P50-DDM	71.31 ± 3.32	206 ± 9
BC1-P50-DDM-Z	65.03 ± 3.46	256 ± 23
BC1-P50-AN	65.22 ± 1.89	129 ± 33
BC1-P50-AN-Z	62.46 ± 2.64	126 ± 25
BC2-P50-DDM	90.12 ± 5.14	152 ± 11
BC2-P50-DDM-Z	86.90 ± 7.27	221 ± 10
BC2-P50-AN	73.64 ± 7.38	139 ± 7
BC2-P50-AN-Z	72.66 ± 2.38	336 ± 8
BC3-P50-DDM	116.18 ± 5.40	412 ± 31
BC3-P50-DDM-Z	112.88 ± 6.52	300 ± 40
BC3-P50-AN	101.04 ± 4.89	182 ± 16
BC3-P50-AN-Z	94.68 ± 9.69	100 ± 14

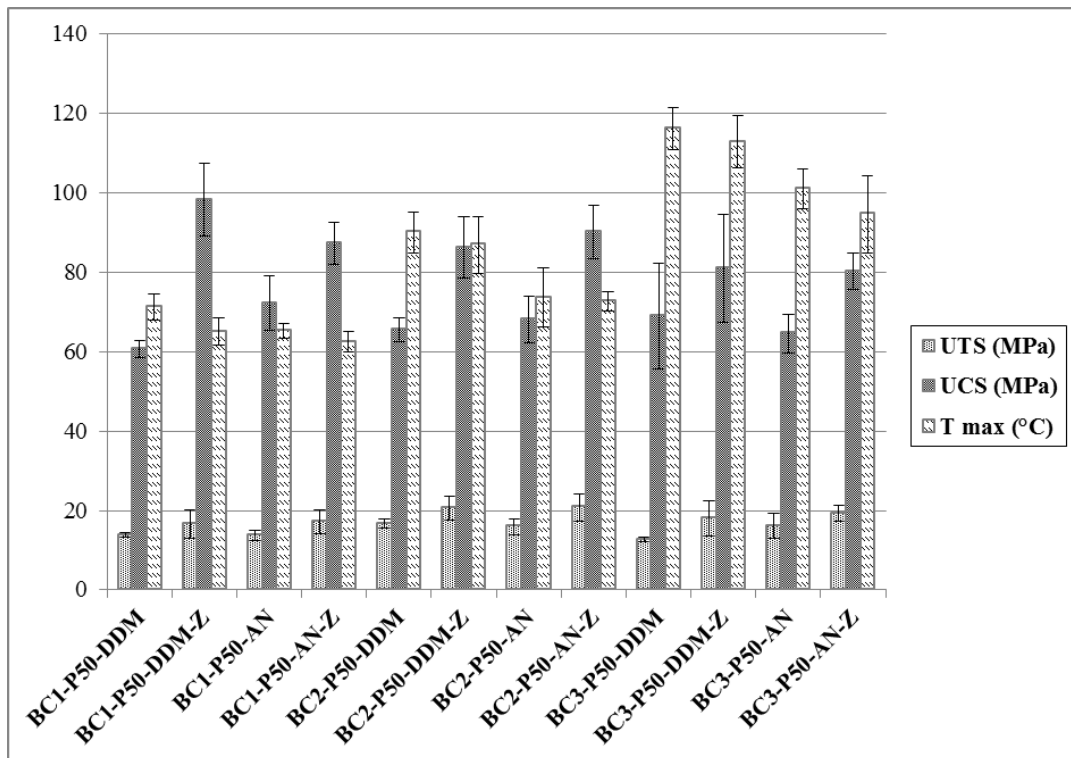


Figure 2.14 UTS, UCS and T_{max} values of zeolite containing bone cements

2.2.7 Modification of Acrylic Bone Cements with Chitosan

Chitosan is a co-polymer of glucosamine (deacetylated unit) and N-acetylglucosamine (acetylated unit). It has become an attractive natural polymer for biomedical applications since it is biocompatible, biodegradable and antimicrobial. It was reported that chitosan improves osseous healing and stimulates cell proliferation. The effect of incorporation of natural biodegradable polymers into bone cements was investigated in some studies (Zou *et al.* 2008, Xu *et al.* 2008). It was proposed that as natural biodegradable polymer degraded in the body by enzymatic fragmentation, new bone tissue was expected to fill the spaces formed due to absorption of chitosan and created a strong link between bone and cement. In this thesis bone cement formulations were modified by incorporation of chitosan into the powder part of the cement and effects of this natural polymer on mechanical and curing properties were investigated.

2.2.7.1 Effect of Chitosan Addition on Mechanical Properties

Tensile and compressive test results are given in Table 2.10 and Figure 2.15. Ultimate tensile strength of BC1 and BC2 group bone cements almost remained the same as the pristine controls. The highest increase in UTS value was observed for BC3 group as from 18.27 MPa to 22.72 MPa with the addition of 0.4 g chitosan. The compression strength values increased from 81.51 MPa to 96.62 MPa, from 75.37 MPa to 89.29 MPa, from 75.96 MPa to 81.64 MPa for BC1, BC2 and BC3, respectively, when 0.4 g chitosan was added to powder part of the formulation. It may be said that chitosan acted as a load carrier and improved compressive properties in all bone cement groups. Several studies reported in the literature that chitosan increased the mechanical properties of its composites (Korach *et al.* 2011, Zhang *et al.* 2005). Hansen and Jensen reported the typical range of values of compressive strength of bone cements and chitosan containing bone cements are within the

range of 80–105 MPa (Hansen and Jensen 1992). The mechanical properties of commercially available bone cement CMW1 were also examined. It was found that tensile strength and compressive strength of CMW1 was 20.05 MPa and 100.20 MPa, respectively. Tensile strength values are similar with the prepared cement formulations while compressive strength value of CMW1 is about 6.6% higher than the UCS value of BC1-CH1 group but compressive strength values of all prepared cement formulations are in acceptable range according to ASTM standards.

Table 2.10 Mechanical properties of chitosan containing and CMW1 bone cements

BC*	Tensile Properties		Compressive Properties	
	UTS (MPa)	E _T (GPa)	UCS (MPa)	E _C (GPa)
BC1	19.65 ± 2.70	0.39 ± 0.05	81.51 ± 3.43	0.57 ± 0.04
BC1-CH1	20.16 ± 2.58	0.46 ± 0.02	94.04 ± 3.77	0.57 ± 0.03
BC1-CH2	18.72 ± 4.17	0.46 ± 0.07	96.62 ± 4.70	0.58 ± 0.04
BC2	19.77 ± 1.78	0.39 ± 0.04	75.37 ± 7.47	0.48 ± 0.05
BC2-CH1	17.53 ± 0.81	0.41 ± 0.04	98.40 ± 6.02	0.55 ± 0.06
BC2-CH2	19.66 ± 3.11	0.42 ± 0.07	89.29 ± 7.89	0.57 ± 0.02
BC3	18.27 ± 5.14	0.38 ± 0.04	75.96 ± 2.21	0.53 ± 0.03
BC3-CH1	23.53 ± 3.25	0.43 ± 0.06	80.26 ± 6.07	0.59 ± 0.02
BC3-CH2	22.72 ± 4.20	0.42 ± 0.05	81.64 ± 7.14	0.63 ± 0.02
CMW1	20.05 ± 2.98	0.51 ± 0.06	100.20 ± 5.49	0.56 ± 0.04

* CH1: 0.05 g chitosan per gram of PMMA, CH2: 0.1 g chitosan per gram of PMMA

2.2.7.2 Effect of Chitosan Addition on Curing Properties

It is expected that chitosan would cause a decrease in the curing temperature by absorbing some of the heat released by exothermic polymerization reaction. But the addition of chitosan caused a decrease in curing temperature only in BC1 group from 71.60°C to 59.04°C. This can be attributed to the presence of chitosan as well as size of PMMA particles which both acted as a heat sink and absorbed the released heat (Table 2.11 and Figure 2.15). On the other hand, for BC2 and BC3 groups chitosan caused an increase in curing temperature. This can be explained by the formation of extra intermolecular attractions between chitosan molecules as well as chitosan-acrylate attractions. It is clear that, less damage in the surrounding bone tissue occurs during in situ applications when the maximum curing temperature is lower. On the other hand, when setting times were compared, it was observed that the setting times of BC1-CH1 and BC2-CH1 samples were shorter than BC1 and BC2 samples. When liquid to solid parts ratio is considered, the amount of MMA monomer in chitosan containing bone cements became lower with addition of chitosan to the solid part. It was stated that polymerization time gets longer as the amount of MMA monomer increases (Kawashita et al. 2010). As a result, the decrease in the monomer to powder ratio might be the reason for the shorter setting time of BC1-CH1 and BC2-CH1 samples compared with BC1 and BC2 samples. When the amount of chitosan increased setting time of samples elongated. This might be because of inhibition effect of the increased chitosan amount on the polymerization reaction of MMA monomer. In literature similar trend was reported for different kind of additive. It was reported that addition of magnetite particles shortened the setting time but then increased with increasing magnetite particle

concentration. They explained this behavior as the inhibition effect of particles on the polymerization reaction of MMA became significant with increased amount of magnetite particles (Kawashita et al. 2010). When BC1, BC2 and BC3 groups are compared, setting time values of BC3 group were longer because of the higher amount of MMA monomer compared to polymeric PMMA particles, requiring more time for polymerization. Maximum curing temperature of CMW1 bone cement was found as 96.03°C which is higher than the BC1 group bone cement formulations.

Table 2.11 Curing properties of chitosan containing and CMW1 bone cements

BC	Curing Properties	
	T _{max} (°C)	t _{set} (s)
BC1	71.60 ± 9.31	312 ± 17
BC1-CH1	68.58 ± 8.92	253 ± 28
BC1-CH2	59.04 ± 9.59	274 ± 19
BC2	83.48 ± 7.35	190 ± 20
BC2-CH1	94.42 ± 8.02	174 ± 7
BC2-CH2	86.78 ± 3.73	180 ± 11
BC3	116.24 ± 4.94	406 ± 8
BC3-CH1	123.12 ± 4.16	456 ± 34
BC3-CH2	116.32 ± 5.14	395 ± 32
CMW1	96.03 ± 0.9	405 ± 10

BC1-CH1 bone cement formulation was chosen as optimum formulation for in vivo applications considering its handling, mechanical and curing properties. The chosen cement composition was used in in vivo experiments with rats and compared with commercial CMW1 bone cement. As a result, incorporation of the PMMA cement with chitosan powder had a positive effect on prepared cement formulation and could improve the bone bonding ability and the bioactivity of the modified bone cements.

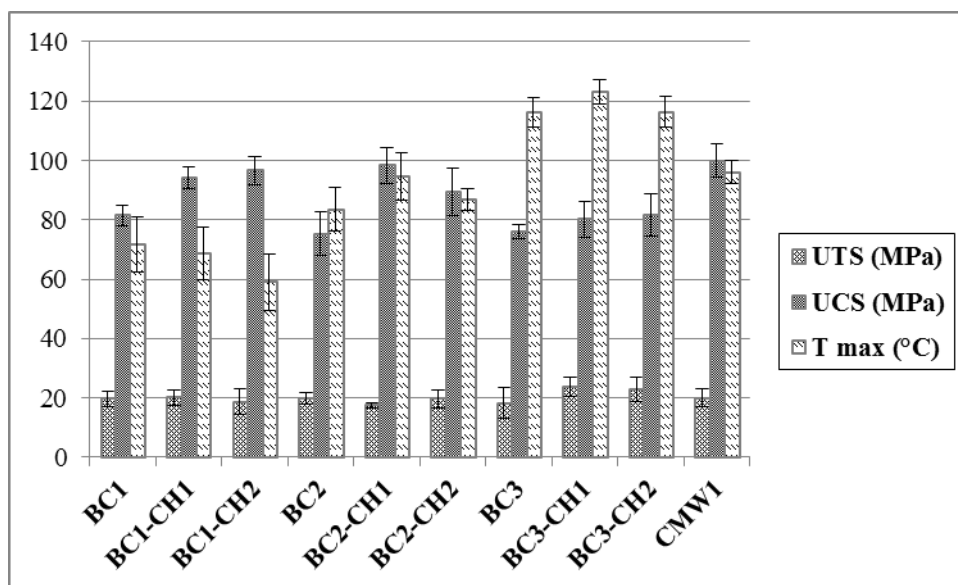


Figure 2.15 UTS, UCS and T_{max} values of chitosan containing bone cements

2.2.8 In Vivo Tests

In bone cement preparation the amount of additives and the particle size of the powder highly affect the quality and the handling of the resulting dough. It was observed that bone cement composed of PMMA with particle size between 50–150 μm (BC1) seems to be more favorable for mechanical, curing and handling properties. Therefore, BC1 group chitosan containing bone cement formulation was chosen as optimum for in vivo tests.

For in vivo tests, bone cements with and without chitosan (CH) incorporation (BC1 and BC1-CH1 groups) were applied to the defects formed on the rat knee. After 4 weeks post operation, histological examination was done on excised tissue sections and interface region between the cement and the cancellous bone was examined for fibrous tissue and new bone formation between the osseous tissue and the bone cement were examined. Hematoxylin and eosin staining was used, in which hematoxylin colors nuclei of cells blue and eosin colors cytoplasm and extracellular matrix pink or red. Microscopic images of neighboring tissue 4 weeks after the implantation of bone cements are given in Figure 2.16. In histological analysis, osteoid is the unmineralized, organic portion of the bone matrix that occurs before the development of bone tissue. At the beginning of bone tissue formation, osteoblasts secrete several specific proteins and form osteoid. At the end of bone tissue formation, osteoid becomes mineralized.

In the control group of this study where the defect was left unfilled; normal empty space (white part) was observed and there was no osteoid formation (Figure 2.16A). Empty space was surrounded with a thin fibrous tissue as a red line between bone cement and bone tissue.

BC1 cement sample was surrounded with few focal osteoid formation (Figure 2.16B). However, more new bone formations were observed in the chitosan modified bone cement samples (BC1-CH1) (Figure 2.16C) than in BC1 cement samples. New osteoid formation is shown with black arrows. The absence of fibrous tissue interface between the host bone and the bone cement material is an indication of good integration of the chitosan modified cement sample with the bone tissue. In the case of CMW1 cement sample, new bone formation was observed in many areas around the bone cement as was also seen with the BC1-CH1 sample (Figure 2.16D). New osteoid formation was

observed only in 40% of the samples treated with BC1 bone cements while all the BC1-CH1 and commercial CMW1 bone cement samples showed new osteoid formation after four weeks of application in the defect area.

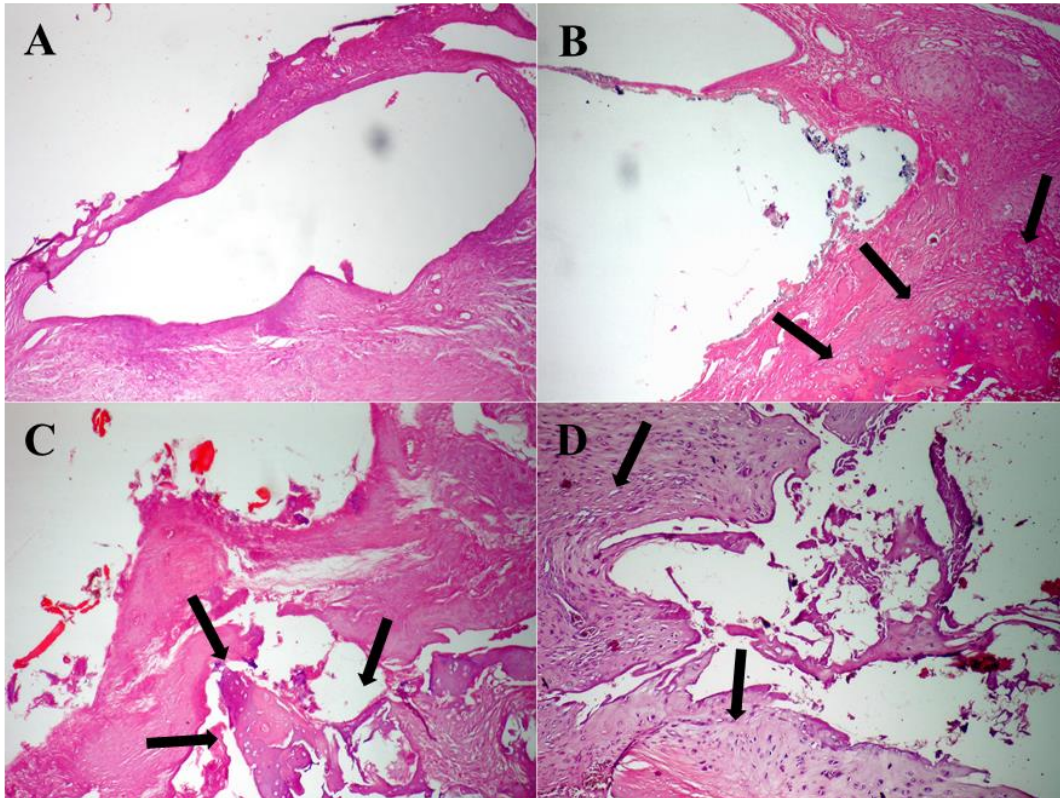


Figure 2.16 Microscopic images of neighboring tissue 4 weeks after the implantation of bone cements. Arrows show newly formed osteoid. A) Control, B) BC1, C) BC1-CH1, D) CMW1.

Chitosan and various calcium phosphates have been extensively used together in composite materials to combine the advantages of the two. The favorable contributions of chitosan when used in composites have been reported in many investigations (Bao *et al.* 2011, Tanase *et al.* 2012). Its positive contributions were also shown when used as a coating material for titanium implants. Park *et al.* investigated the effect of surface chemistry on response of human MG63 osteoblast-like cells and found that chitosan coated microstructured titanium surfaces induced a greater osteoblast specific protein production compared to the uncoated ones. Chitosan with its positive charged (NH_3^+) surface induced a greater osteocalcin and osteoprotegerin production than other coating components suggesting that surface chemical composition and charge plays a role in controlling osteoblast differentiation (Park *et al.* 2012). Travan *et al.* coated methacrylate thermosets used for orthopedic and dental applications with bioactive chitosan-derivative in order to enhance osseointegration. It was shown that chitosan induced osteoblast proliferation and increased alkaline phosphatase activity (Travan *et al.* 2012). Therefore, the positive contribution of chitosan in this study was not surprising.

2.2.9 Morphological Analysis Results of Crosssections of Bone Cements

SEM micrographs of cross-sections of bone cement samples after tensile tests are given in Figure 2.17. Pores can be observed at the fracture surfaces of all bone cement groups. Acrylic bone cements are prepared by hand-mixing and pores can be formed because of the entrapment of air during mixing. In addition, exothermic polymerization reaction may also cause fast evaporation of MMA monomer, and as a consequence, lead to porosity. Mechanical strength of bone cement is adversely affected by the presence of pores.

In the BC3 group cements in which the smallest PMMA microspheres were used with higher amount of monomer in the preparation of cements it was observed that porosity was increased. This may be because of the higher amount of monomer and higher maximum curing temperature of BC3 group when compared to BC2 and BC1 groups.

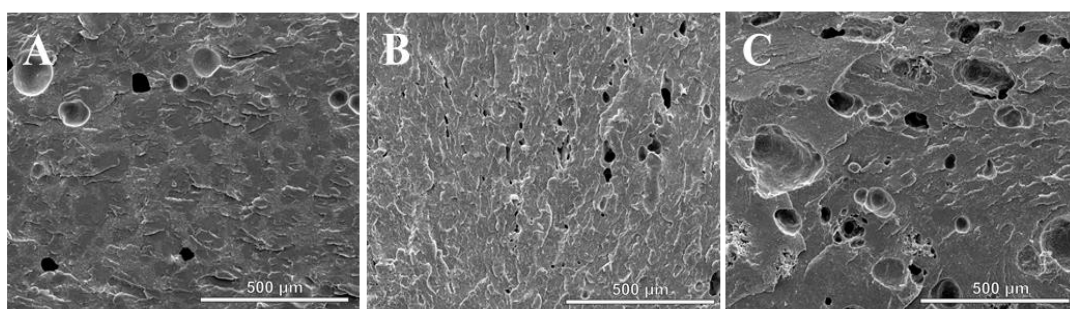


Figure 2.17 SEM micrographs of cross-sections of bone cements. A) BC1; B) BC2; C) BC3

In this part of the thesis three main groups of bone cement formulations were prepared by using ground and sieved PMMA particles with particle size in the range of 1–50 μm (Group 1, BC2), 50–150 μm (Group 2, BC1) and synthesized PMMA microspheres by suspension polymerization with average particle size of 1 μm (Group 3, BC3). In the first and second group bone cement formulations polymer/monomer ratio was kept as 2/1 (w/w). However, for BC3 group the average particle size of the synthesized PMMA microspheres was about 1 μm and the surface to volume ratio of these small microspheres was much higher more monomer was needed to wet all powder particles. Therefore, powder to monomer ratio was used as 2/3. All prepared compositions contained HAp as inorganic load carrying substance and barium sulphate (BaSO_4) as radioopaque agent.

In order to improve mechanical strength by increasing the compatibility and interaction between particles, 50 W or 100 W oxygen plasma was applied for 5 min to the powder part of bone cement compositions prior to mixing with liquid part. Plasma application had positive effects on mechanical properties of all groups while caused an increase in maximum curing temperature which is undesirable for bone cements. There was no significant difference in bone cement strength when the applied plasma power was 50 W or 100 W. Therefore, not to cause further increase in maximum curing temperature, 5 min 50 W oxygen plasma application was chosen as optimum. Maximum curing temperatures of group 3 bone cements (BC3) were always higher than other groups because of higher amount of monomer used.

Moreover, 1-dodecyl mercaptan (DDM) chain stopping agent and ammonium nitrate were added to compositions in order to decrease the curing temperature. Although decreases in curing temperatures of bone cements were observed, there were undesirable reductions in mechanical strengths. However, zeolite addition had positive effect on mechanical properties and compressive strength values were in the acceptable range. In addition zeolite incorporation in ammonium nitrate containing bone cement formulations caused 10°C decrease in maximum curing temperature.

Furthermore biocompatible, biodegradable, high mechanical strength natural polymer chitosan containing bone cement formulations were prepared. Chitosan did not have significant effect on tensile properties while caused positive effect on compressive strength. Moreover, it reduced maximum curing temperature when added to BC1 group bone cement. Chitosan is expected to degrade in vivo over time as the new bone tissue forms leading to stronger attachment between bone and bone cement and extend the survival of implant.

Among three bone cement groups, compositions prepared with PMMA particles having 50–150 μm particle size had better handling properties and lower maximum curing temperature. This is because as the particle size increases the surface area decreases, so fewer particles are solved in the monomer and therefore acted as heat sink.

Bone cement formulations containing chitosan prepared with larger PMMA particles (BC1-CH1) selected as optimum for in vivo applications in rats. According to results when new osteoid formation compared there was no significant difference between commercial bone cement and our optimum chosen formulation.

As a conclusion PMMA particles having particle size in the range of 50–150 μm can be more appropriate to be used in bone cement preparation due to handling and setting properties. Plasma technique, in the literature which is one of the methods used to form stronger chemical interaction and hence compatibility between materials, can be employed to increase the mechanical strength of bone cements but cause an undesirable increase in curing temperature. Small amount of zeolite incorporation can improve the mechanical strength of bone cement. 1-dodecyl mercaptan and ammonium nitrate addition may reduce maximum curing temperature but cause undesirable decrease in mechanical strength. However amounts of these additives are vital, the amounts added should not have intolerable effects on some properties while improving the other properties. In addition, incorporation of biocompatible, biodegradable, antibacterial natural polymer chitosan had positive effect on mechanical and curing properties of bone cements. As a result, a novel composition containing chitosan was used in in vivo experiments on rats and the new bone formation was compared with commercially available CMW1 bone cement. There was no significant difference between chitosan containing bone cement and the commercial bone cement.

It should be known that, there is a delicate balance between all the ingredients present in the bone cement formulations. A small change in all ingredients may enhance one property but may cause an undesirable effect on another property. Therefore, scientists need to search all parameters before any application.

CHAPTER 3

BONE TISSUE ENGINEERING SCAFFOLDS

Bone tissue engineering is an alternative approach to restore functionality of damaged hard tissue. Scaffolds are one of the essential components to be used as a temporary support material in tissue engineering. They allow the cells to adhere, proliferate and differentiate to form a healthy tissue for restoring the functionality. There are many different processing techniques for the preparation of scaffolds. In this part of the thesis, scaffolds prepared for bone tissue engineering as 2D and 3D structures with three different techniques are discussed. As preparation techniques, microfabrication, freeze drying and electrospinning were used. In the preparation of scaffolds chitosan and poly(lactic acid-co-glycolic acid) (PLGA) as the biodegradable biopolymeric component and HAp as the mineral component were used. Resultant polymeric matrices were characterized to determine their chemical, curing and mechanical properties as well as their suitability as a tissue engineering scaffold.

3.1 Membranes Prepared by Microfabrication

Different materials and fabrication techniques are employed to produce scaffolds that can support cell adhesion, migration and proliferation for tissue engineering purposes. In particular, rapid prototyping techniques are widely investigated because they permit the design and the production of highly ordered, three dimensional (3D) scaffolds. Rapid prototyping can be achieved with different techniques such as fused deposition modelling (FDM), three dimensional printing (3DP), selective laser sintering (SLS) and stereolithography (SLA).

Some in-house systems working on similar principles have also been used to fabricate scaffolds with highly ordered structures and reproducibility. In this part of the thesis in-house microfabrication system which was developed and optimized in Prof. Claudio Migliaresi's laboratory at Trento University (Italy) was used to produce chitosan and PLGA polymeric membranes with micrometric designed porosity. Polymeric membrane preparation and characterization experiments were conducted in collaboration with Dr. Eleonara Carletti by using facilities in Department of Materials Engineering and Industrial Technologies in Trento University. In this in-house microfabrication system a polymer solution placed in a microsyringe was injected onto a base, which can move in x-y-z directions. Successive layers of polymer solution were deposited on top of each other with a predetermined order to obtain homogeneously porous scaffolds. Resultant membranes were characterized by chemical, thermal, mechanical and preliminary cell culture tests.

3.1.1 Experimental

3.1.1.1 Materials

Chitosan (low viscosity, 75–85% deacetylated) and acetic acid were purchased from Fluka (Osaka, Japan) and sodium hydroxide (NaOH) from J.T. Baker (Deventer, Holland). Poly(D,L-lactic acid-co-glycolic acid) (PLGA, type RESOMER[®] 503, 50:50 molar ratio D,L-lactic acid:glycolic acid, MW: 39 kDa) was purchased from Boehringer Ingelheim (Ingelheim, Germany). Dichloromethane (DCM) and dimethylformamide (DMF) were obtained from BDH Chemicals (Poole, Dorset, UK) and J.T.Baker (Deventer, Holland), respectively.

3.1.1.2 Microfabrication System

The microfabrication instrument was composed of computer controlled three independent slides (National Instrument, Austin, Texas, USA), which have a micro-resolution and a travel range of 100 mm. Each slide was connected to a DC motor which can enforce a 15 mm/s maximum velocity. These slides could move a base on which the polymer solution is injected and scaffold is fabricated. There was an automatic pumping system (11 Plus, Harvard Apparatus, Massachusetts, USA) from which a proper flow rate could be adjusted. The system contained a glass syringe, which was fixed on the automatic pumping device. The syringe was mounted on the z-axis of a three-axis micro-positioning system. A metal micro-needle (Hamilton™, 34 gauge) with inner diameter of 60 μm and the length of 1 cm, was connected to the glass syringe and the connection mechanism was the luer lock having fitting connector with locking mechanism. The polymer solution or melt was deposited from the needle of a syringe by a constant flow rate on the support, which was a polyethylene terephthalate (PET) sheet. Scaffold was built by layer over layer in the vertical direction and each layer was orthogonal to the following one. After the first layer has been deposited, subsequent layers were deposited by moving the support down along the z-axis by an amount corresponding to the height of each layer. The dimensions of the deposited structures depend on the pressure applied to the syringe, the viscosity of the solution, the motor speed and the dimensions of the needle. Slide velocity and acceleration, the distance between fibers, the number of layers and the vertical displacement of the support between the depositions of two subsequent layers are the process parameters that can be controlled through the LabView programme. All of the process parameters were set using the LabView programme except the flow rate which was controlled directly from the automatic pumping system. The photograph of the microfabrication instrument used in the experiments is given in Figure 3.1.

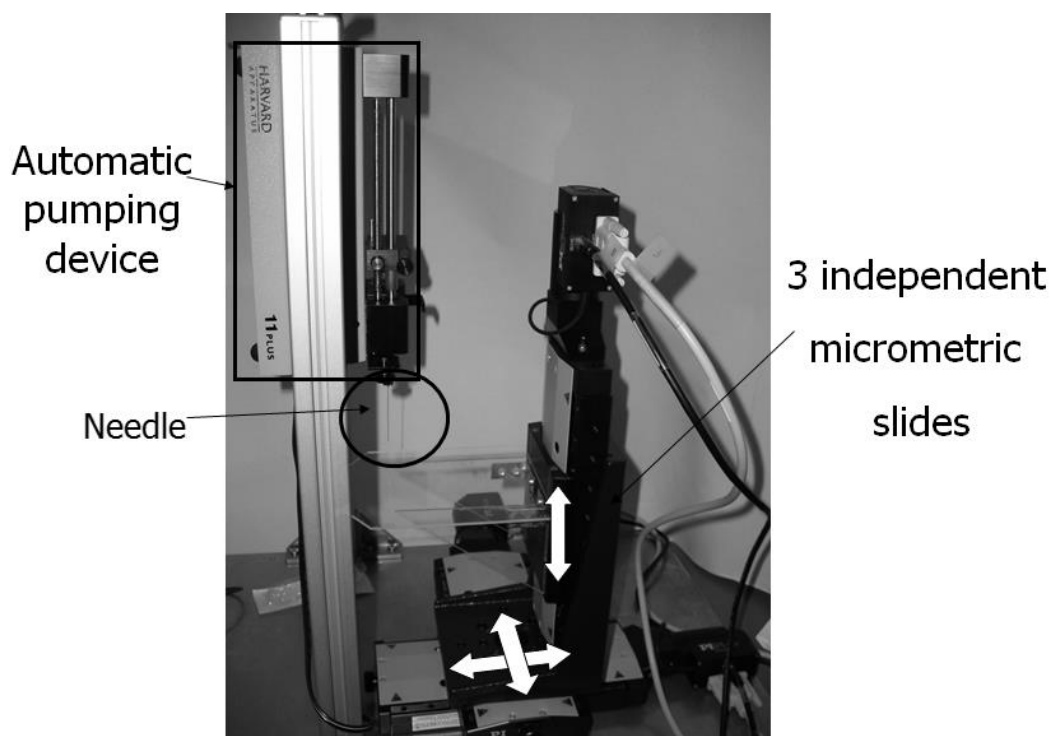


Figure 3.1 The photograph of microfabrication device

LabView software controlled and moved the slides, consequently permitting the deposition of the extruded polymer solution filament forming the desired geometry scaffold. From the front panel it

was possible to set the proper process parameters such as the slide velocity and acceleration and the grid dimensions, which represent the scaffold dimensions (distance between rows and layers and number of rows and layers). The microfabrication system was covered with a protective glass box in order to minimize environmental effects such as temperature and humidity.

3.1.1.3 Preparation of Microfabricated Membranes

Chitosan solution (3%, w/v) was prepared by dissolving chitosan in aqueous acetic acid solution (5%, v/v) and filtered through Millipore Nylon Net filter with a 20 μm pore size. The filtrate was placed in a glass syringe with a stainless steel capillary needle. Syringe pump was used to create a proper flow rate and the membrane was build up on a polyethylene terephthalate (PET) sheet. The process was computer controlled and proper process parameters were set by using LabView software. Every membrane was generated by overlapping orthogonal square layers following an array sequence representing the final geometry of membrane. Flow rate, slide velocity and distance between layers were set as 1 $\mu\text{L}\cdot\text{min}^{-1}$, 4.5 $\text{mm}\cdot\text{s}^{-1}$ and 25 μm , respectively. After the microfabrication process, chitosan membranes were treated with 1 M NaOH for 1 h to neutralize the acetic acid and then washed with distilled water to remove NaOH. Membranes were 1cm x 1cm, 80 layers and approximately 100 μm thickness. Cast films used as control.

PLGA (50:50) was dissolved in DCM:DMF (70:30, v/v) to prepare a 25% (w/v) polymer solution. PLGA solution was magnetically stirred overnight and then filtered with Millipore Nylon Net filters with a 20 μm pore size. By extrusion of solution filaments through the syringe needle, membranes with 1cm x 1cm dimension, 30 layers and approximately 350 μm thickness were prepared.

3.1.1.4 Characterization of Microfabricated Membranes

3.1.1.4.1 Rheological Tests

Flow behavior of the polymer solutions was determined by rheological tests to optimize the working conditions. A rotational rheometer (Advanced Rheometric Expansion System-ARES-TA Instrument, New Castle, DE-USA) with a cone-plate configuration (50 mm plate diameter, 0.04 rad cone angle, 0.050 mm initial gap between cone and plate) was used and a dynamic frequency sweep test mode (strain control, 3% strain, 0.1 $\text{rad}\cdot\text{s}^{-1}$ initial frequency, 22°C working temperature) was chosen. To prevent solvent evaporation during the tests, a humidity chamber lined with a solvent soaked sponge was used to enclose the cone-plate apparatus. Complex viscosity over shear rate was measured and efficiency of humidity chamber was tested by sequentially running the rheometric measurements on the same sample.

3.1.1.4.2 Morphological Investigations

Morphology of the microfabricated structures was examined with light microscope (ZEISS Axiovert 25, Göttingen, Germany), Scanning Electron Microscopy (SEM, Stereoscan 200, Cambridge, UK). Prior to SEM imaging the samples were sputter coated (SEM Coating Unit PS3, Assing S.p.A., Rome, Italy) with a thin layer of gold for imaging in argon atmosphere (20 mA at 5×10^{-7} Pa for 30 s).

3.1.1.4.3 Fourier Transform Infrared Spectroscopy

Fourier Transform Infrared-Attenuated Total Reflectance (FTIR-ATR) spectroscopy analysis (Spectrum One Spectrometer, Perkin Elmer, Maryland, USA) was used to evaluate possible modifications of the chemical structure of the polymers during processing and to determine the remaining solvent inside the membranes. All the spectra were analyzed after baseline correction.

3.1.1.4.4 Differential Scanning Calorimetry

Differential scanning calorimetry (DSC, 30 Mettler-Toledo, Giessen, Germany) was used to investigate possible modifications due to the fabrication process. Samples (5-10 mg) were placed into aluminum DSC pans and each sample was exposed to two heating scans; for chitosan samples the first scan was from 0°C to 200°C and the second scan was from 0°C to 300°C at a rate of 10°C/min while for PLGA samples heating scans were from -20°C to 120°C. The cooling rate under nitrogen flux (10 mL/min) was very rapid (100°C/min).

3.1.1.4.5 Dynamic Mechanical Thermal Analysis

Dynamic mechanical thermal analysis (DMTA, Mk II of Polymer Laboratories Scientific Firm, Piscataway, NJ, USA) was performed in tensile mode. The dynamic mechanical spectra were recorded by adjusting the frequency constant (1 Hz) and changing the temperature with a heating rate of 3°C.min⁻¹ from -60°C to 100°C for PLGA samples, and from -60°C to 200°C for chitosan samples. Cast films of chitosan and PLGA were used as controls. Storage modulus (E') and loss factor ($\tan \delta$) versus temperature graphs were obtained.

3.1.1.4.6 Preliminary Cell Culture Tests

MG63 cells human osteosarcoma derived osteoblasts and human embryonal lung origin fibroblast MRC5 cells were seeded on the fabricated membranes. Cells were incubated at 37°C in a 5% CO₂ incubator, harvested when reached confluence by trypsinization followed by the addition of fresh culture medium. Minimum essential medium (MEM, Gibco, Italy) supplemented with 10% Fetal Bovine Serum (FBS), 1% penicillin, 1% Glutamax, 1% Vitamin, 1% non-essential amino acids was used for MG63 cell line. For MRC5 cell line in addition to these 1% sodium pyruvate was added. All the membrane samples were sterilized by immersion in 70% ethanol followed by washing with distilled water before cell seeding. Each membrane was seeded with a cell suspension of 2.5x10⁵ cell/mL concentration, 0.5 mL of media was added to each well. Medium was changed in every 2 days. At predetermined times, membranes were removed, cells were fixed with glutaraldehyde solution (2.5% glutaraldehyde in cacodylic buffer solution 0.1 M, pH 7.2) to preserve the structure of the cells. The samples were dehydrated by immersing in 30%, 50%, 70%, and 90% ethanol solutions for 10 min, respectively, and then 20 min in 100% and then air dried in the hood. The morphologies of the cells were examined with SEM.

3.1.2 Results and Discussion

3.1.2.1 Microfabricated Chitosan Membranes

3.1.2.1.1 Morphological Analysis Results

In this step, the main aim was preparation of chitosan scaffolds in the form of three dimensional solid matrix by microfabrication. However, the microfabricated fibrous layers strongly attached to the neighboring layers and fused forming porous chitosan membranes with predetermined pore organization and size. Microfabrication of chitosan membranes with 80 layers from 3% (w/v) chitosan solution was attempted. SEM micrographs and light micrographs (Figure 3.2) showed that the microfabricated porous membranes have a very ordered structure with evenly distributed and very regular square holes; the distance between fibers was approximately 100 μm thus they created pores of 100 μm x 100 μm. The obtained porous membranes were very flexible.

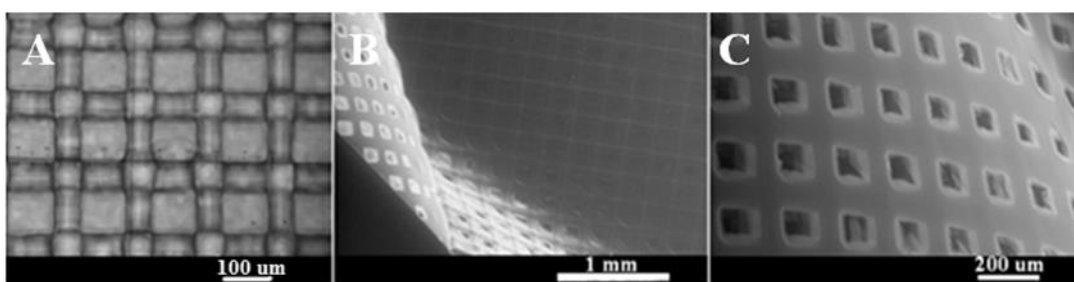


Figure 3.2 Images of chitosan membranes A) Light micrograph, B) and C) SEM micrographs

At the beginning of the study, the chitosan solution was directly microfabricated into a sodium hydroxide-ethanol solution (7:3, v/v) which served as a coagulation medium to obtain chitosan fibers. However, micron sized chitosan fibers could not attach to each other and maintain their final shape. Chitosan structures having regular pores could be prepared by deposition on a PET sheet and then treatment with 1 M NaOH for 1 h to neutralize the acetic acid. The product was washed with distilled water. The resultant membrane, after solvent evaporation, was very thin (100 μm) due to the low concentration of the starting chitosan solution.

After preparation, the chitosan membranes were kept in 1 M NaOH solution to neutralize the acetic acid and then washed with distilled water. After the neutralization step membranes maintained their shape. They were characterized by chemical, thermal, mechanical and biological tests for their suitability for tissue engineering applications.

3.1.2.1.2 Rheological Test Results

Complex viscosities of chitosan solution, after three successive runs is reported in Figure 3.3. Chitosan solution showed a complex viscosity that slightly changed over the selected frequency range 1–100 $\text{rad}\cdot\text{s}^{-1}$. Complex viscosity decreased from 1.28 Pa.s to 0.74 Pa.s at 22°C when test frequency was increased from 1 $\text{rad}\cdot\text{s}^{-1}$ to 100 $\text{rad}\cdot\text{s}^{-1}$ which is the typical non-newtonian with a shear-thinning behavior of polymer solutions. For chitosan solution, a significant evaporation is not expected since the boiling points of water (100°C) and acetic acid (118°C) are quite high. Therefore, viscosity does not significantly change during successive experiments and the used chitosan solution was stable during microfabrication process. Since the viscosity of the solution was found to be almost constant during the three successive runs, homogeneous flow of the solution was obtained through the process, and therefore, the film thickness was almost the same for each layer.

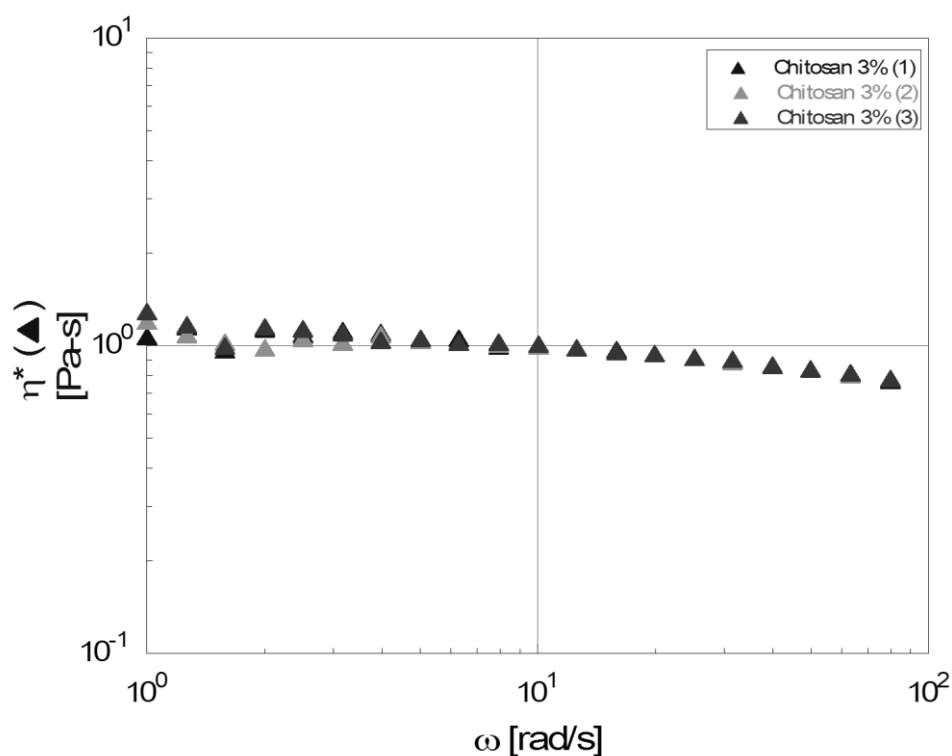


Figure 3.3 Rheological test results of chitosan solution

3.1.2.1.3 Fourier Transform Infrared Spectroscopy Results

The FTIR-ATR spectra of chitosan powder, cast chitosan film and microfabricated chitosan membrane are given in Figure 3.4. The absorption bands observed at 1580 and 1645 cm^{-1} are due to the N-H bending vibration in the amine groups and the stretching vibration of C=O of the amide bond, respectively. The absorption at about 1645 cm^{-1} is typical of unmodified N-acetyl bonds of chitosan. The peak at 2860 cm^{-1} may be attributed to C-H stretching vibrations and -H stretching linked to cyclic ring. The broad band at 3300 cm^{-1} is due to OH linked to polymer. It was observed that all spectra show the characteristic peaks of chitosan and it was concluded that there was no modification in chitosan structure after microfabrication process as expected.

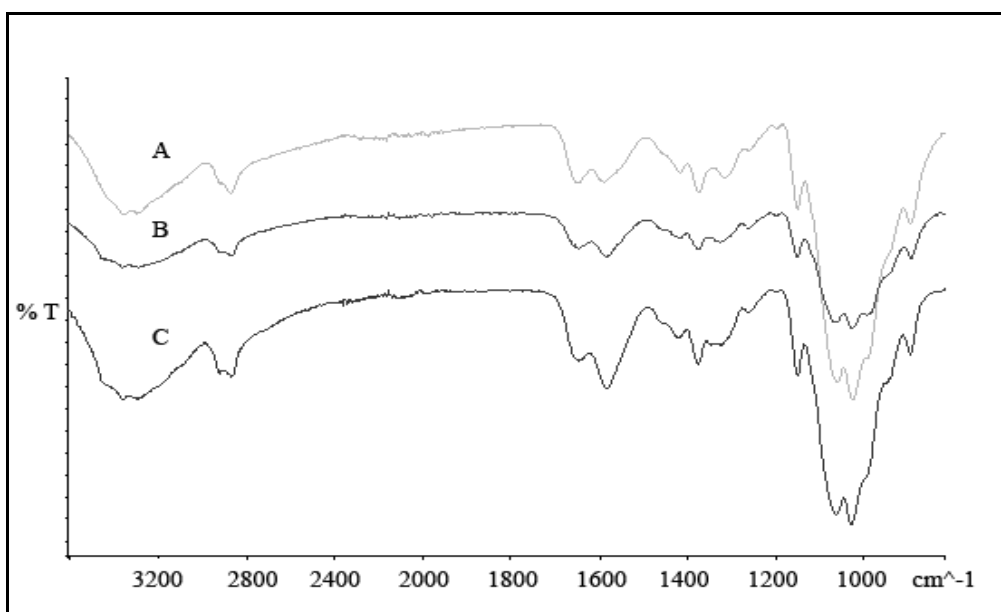


Figure 3.4 FTIR-ATR spectra of chitosan A) powder, B) film, C) membrane

3.1.2.1.4 Differential Scanning Calorimetry Results

DSC thermograms of chitosan powder, film and microfabricated membranes are given in Figure 3.5. In each case, the broad endothermic peak centered at about 100°C with an onset at around 50°C can be ascribed to water evaporation in the first run. The disappearance of this peak in the second run shows that water evaporation occurred during the first DSC scan. The exothermic peak at approximately 300°C, that is present in all the samples analyzed, is mostly due to the degradation of the chitosan. It was stated that the exothermic peak resulted from crosslinking reactions of chitosan. In literature, when FTIR spectrum of thermal degradation of chitosan were examined, a decrease in amine group absorption and an increase in absorption of N-acetylated groups were observed and these results interpreted as thermal destruction of the pyranose ring, possible thermal crosslinking of various macroradicals of the chain following the destruction of amino groups (Wanjun *et al.* 2005). Glass transition temperature (T_g) of chitosan is still a subject of controversy. Being a natural polymer some properties like crystallinity, molecular weight, deacetylation degree can show large variations according to the source and/or to the method of extraction and these properties influence the T_g . A weak signal related to T_g was observed at around 200°C. The slope is more evident in chitosan film sample compared to the powder or membrane forms.

Degradation of chitosan powder started at 290°C while film and membrane started to degrade at lower temperatures, at 261°C and 266°C, respectively. Since film and membrane had similar degradation onset temperatures, it can be stated that there was no significant degradation associated with the microfabrication process.

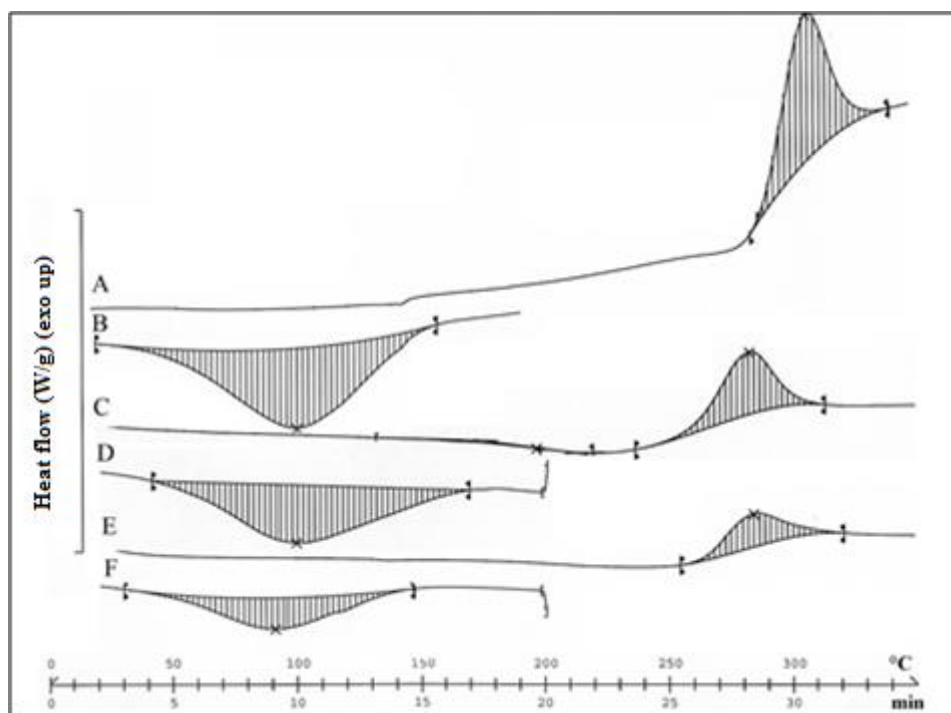


Figure 3.5 DSC thermograms of chitosan powder (A. 2nd run and B. 1st run); film (C. 2nd run and D. 1st run); and membrane (E. 2nd run and F. 1st run)

3.1.2.1.5 Dynamic Mechanical Thermal Analysis Results

Dynamic mechanical thermal analysis is one of the most sensitive techniques to example all kinds of relaxation. In a DMTA spectra loss factor which is the ratio of loss modulus and storage modulus can show few peaks which are attributed to the the mainly α and β relaxation processes. The β process has been assigned to the local mode of relaxation in the amorphous phase while α relaxation related to the glass transition of the amorphous phase and controlled by intra- and intermolecular interactions. It is accompanied by a distinct decrease of the storage modulus E' with increasing temperature. Storage modulus (E') and loss factor ($\tan \delta$) versus temperature graph of chitosan film and membrane are given in Figure 3.6. In particular, the transition at about -18°C may be attributed to β relaxation, which occurs due to the local motions of the side groups in chitosan. In literature, broad relaxation peak of pure polysaccharides such as cellulose, starch and dextran, observed at -120 to -5°C temperature range is recognized as due to orientational motions of local segments via the glycosidic bonds. The molecular similarity between these polysaccharides and chitosan and the presence of the glycosidic linkage in their polymer backbone allows expecting the same behavior. Storage modulus had the lowest value at 40°C . The peak at this temperature can be explained as a structural reorganization or packing of chitosan molecules due to an increase in residual water mobility, volume expansion and change of hydrogen bond strength. Thus after initial strong decrease of E' an increase at about 50°C is observed. Finally, the peak around 150°C is related to α relaxation, which is interpreted as T_g of chitosan.

It is difficult to observe the T_g of chitosan due to hygroscopicity, semicrystalline structure of polymer and different sample preparation techniques. There are various methods in order to find glass transition temperature such as DSC, DMTA, dilatometry. Different values in the range 150°C – 200°C are reported for T_g of chitosan which were determined with different methods (Sakurai *et al.*

2000, Dong *et al.* 2004). In this study, Tg of chitosan film was found to be around 150°C by DMTA and at 200°C by DSC.

DMTA analysis usually shows Tg transitions much more evident when compared to DSC analysis due to drop of E' . Furthermore, lower heating rate ($3^{\circ}\text{C}\cdot\text{min}^{-1}$) during DMTA analysis causes a lower Tg. When heating rate is higher there is not enough time for the polymer to dissipate heat along the polymer chains, so Tg is observed at a higher temperature.

As expected, in the case of chitosan membrane, the modulus was lower than that of the film since the membrane had a porous and weaker structure and the trend of the curves was almost the same. The peak at about -10°C was due to β transition and the Tg was around 170°C .

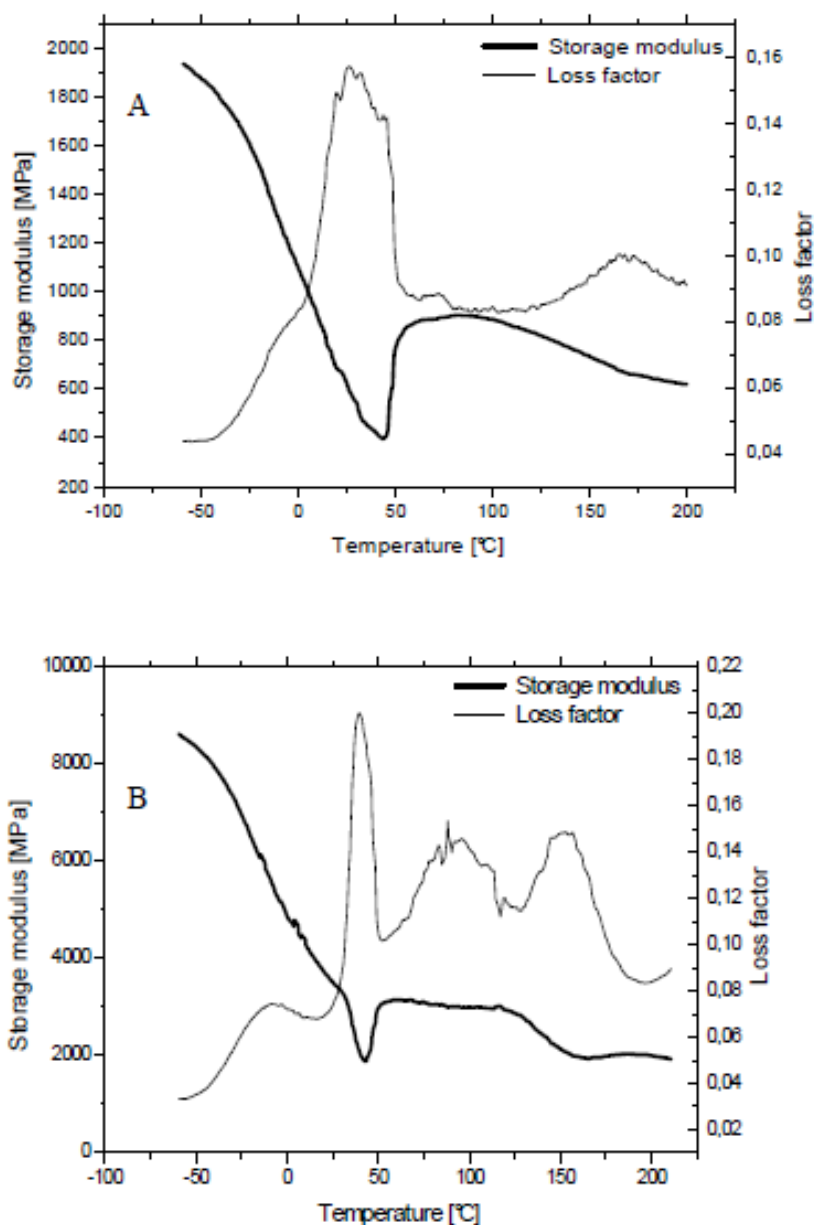


Figure 3.6 Storage Modulus and $\tan \delta$ curves of chitosan. A) membrane, B) film

3.1.2.1.6 Preliminary Cell Culture Test Results

Osteoblast (MG63) and fibroblast (MRC5) cell lines were seeded on chitosan membranes to study the suitability of the membrane to serve as scaffolds. The chitosan membranes examined after cell seeding broke into fragments and no cells could be observed to be adhered on the membranes. This was most probably caused by the remaining acetic acid in the material, and therefore, makes the material acidic and unsuitable for the cells. After this observation, from this point on the membranes neutralized with NaOH and washed extensively. These samples demonstrated enhanced stability in the cell culture medium.

SEM micrographs of these NaOH neutralized chitosan membranes after 4 days and 10 days of seeding with MG63 and MRC5 cells are given in Figure 3.7 and Figure 3.8, respectively. The membranes appeared to have maintained their original shape during these cell culture tests. Adhesion and spreading of the cells were observed on the membranes and the pores were invaded by cells. The result confirms the compatibility of the material with these types of cells. Cell growth in the pores points to the suitability of the pore size of the material.

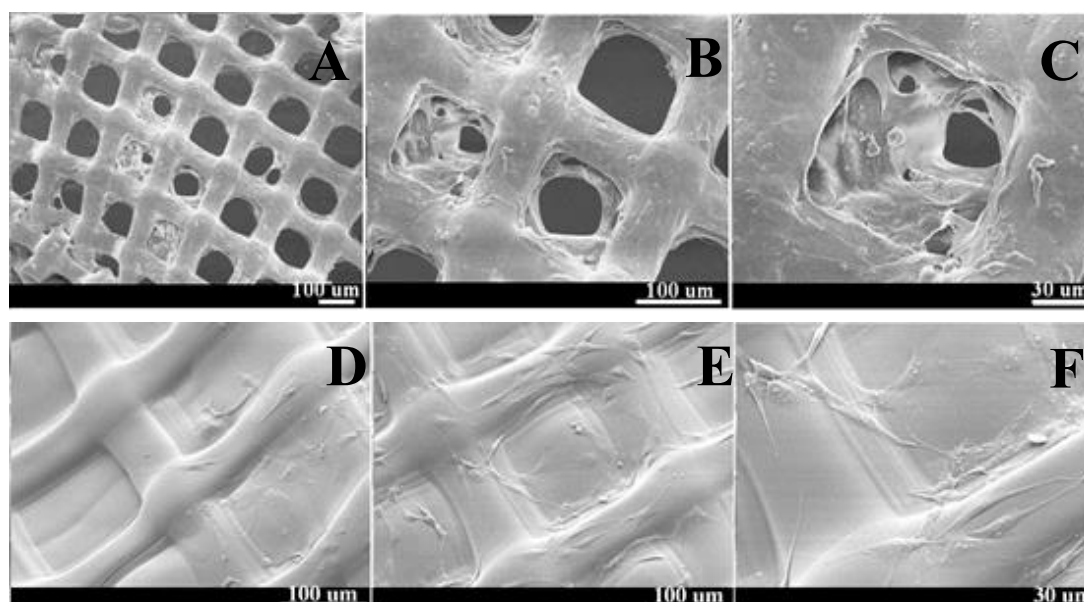


Figure 3.7 SEM micrographs of chitosan membranes after MG63 cell seeding. A, B, C after 4 days, D, E, F after 10 days

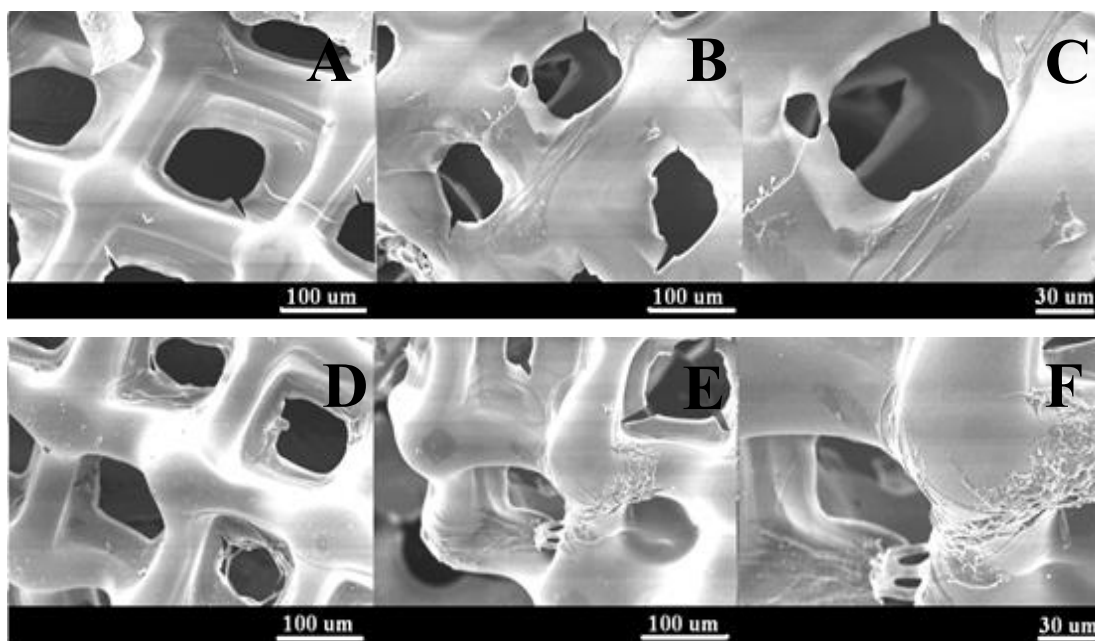


Figure 3.8 SEM micrographs of chitosan membranes after MRC5 cell seeding. A, B, C after 4 days, D, E, F after 10 days

3.1.2.2 Microfabricated PLGA Membranes

3.1.2.2.1 Morphological Analysis Results

PLGA membranes with predetermined pore size and shape were prepared by a in-house microfabrication technique. In the preparation of the well-ordered scaffold structures, proper adjustment of the process parameters is very important. Incorrect parameters combined with improper concentration of polymer solution produce defects in the resultant scaffolds.

The choice of the solvent or combination of solvents and concentration of polymer solution is supposed to assure a continuous flow of the material out of the needle with a proper solvent evaporation rate. It was observed that, when low-boiling temperature solvents such as chloroform, dichloromethane were used, they evaporated too fast, even on the needle tip, causing discontinuous flow of the polymer solution and stick at the tip of the needle. Similar results were observed when the solution concentration was too high. Therefore, non-continuous flow created defects such as large droplets and broken fibers in different layers of PLGA membranes (Figure 3.9 A and B). High boiling temperature solvents such as dimethyl formamide, on the contrary, were difficult to remove from the material, so that the polymer would spread on the collector plate and following the layers collapsed over each other (Figure 3.9 C and D). The same effect could be observed when the polymer concentration was too low.

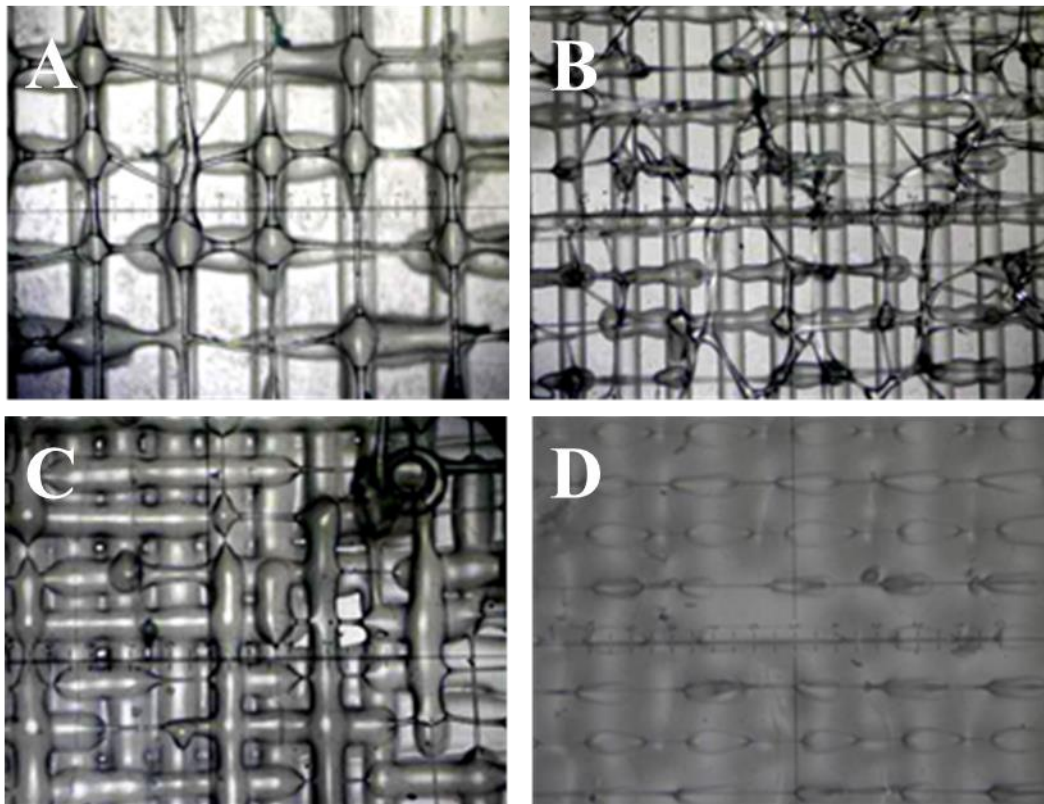


Figure 3.9 Light micrographs of PLGA membranes microfabricated from PLGA solution prepared in A, B) DCM, C, D) DMF

Proper solution concentration was the most important process parameter in the PLGA microfabrication. At low polymer concentrations (15%, w/v, in DCM:DMF), the solution flowed out easily from the needle, the solvent evaporated too slowly and the microfabricated structure spread and collapsed. At 30% w/v PLGA concentration, concentration was high and solution behaved as a gel. 25% (w/v) PLGA solution was found to be the optimum concentration for ease of processing and the quality of the resultant membranes. Microfabricated PLGA membranes with 25 overlapping layers, with 100 μm fiber thickness were prepared and examined with light microscope and SEM (Figure 3.10).

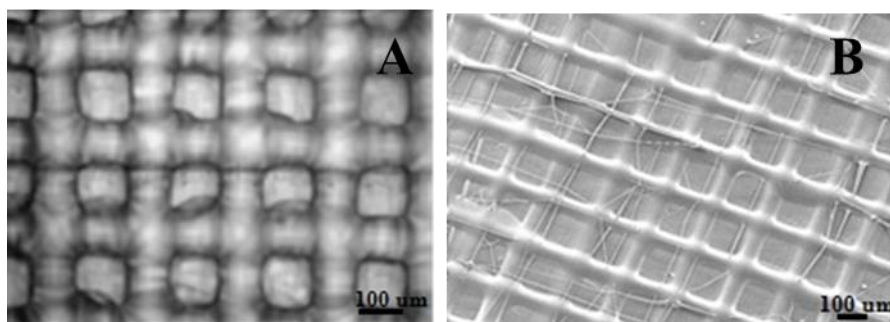


Figure 3.10 Images of PLGA membrane A) light microscopy, B) SEM

3.1.2.2.2 Rheological Test Results

Rheological test on the PLGA solution was performed in order to evaluate in which viscosity range the solution was extruded during the microfabrication process. Viscosity of 25% PLGA solution prepared in DCM:DMF solvent couple was tested with a rotational rheometer by a dynamic frequency sweep test over a frequency range between 1 and 100 $\text{rad}\cdot\text{s}^{-1}$ at 22°C. At 1 $\text{rad}\cdot\text{s}^{-1}$ frequency viscosity was 1.30 Pa.s while it decreased to 1.00 Pa.s at 100 $\text{rad}\cdot\text{s}^{-1}$ frequency which is due to typical non-newtonian behavior of polymer solution. In addition, the effect of evaporation phenomena was evaluated by performing three measurements on the same sample successively. An increase in viscosity values was observed after each run at the same frequency. In the second run for 1 $\text{rad}\cdot\text{s}^{-1}$ frequency viscosity increased from 1.30 Pa.s to 3.23 Pa.s, while it was 10.38 Pa.s in the third run proving the evaporation effect of solvents. It can be concluded that, PLGA solution was not as stable as chitosan solution. Due to the fast evaporation of solvent during microfabrication process, some defects were observed like broken fibers on PLGA membranes.

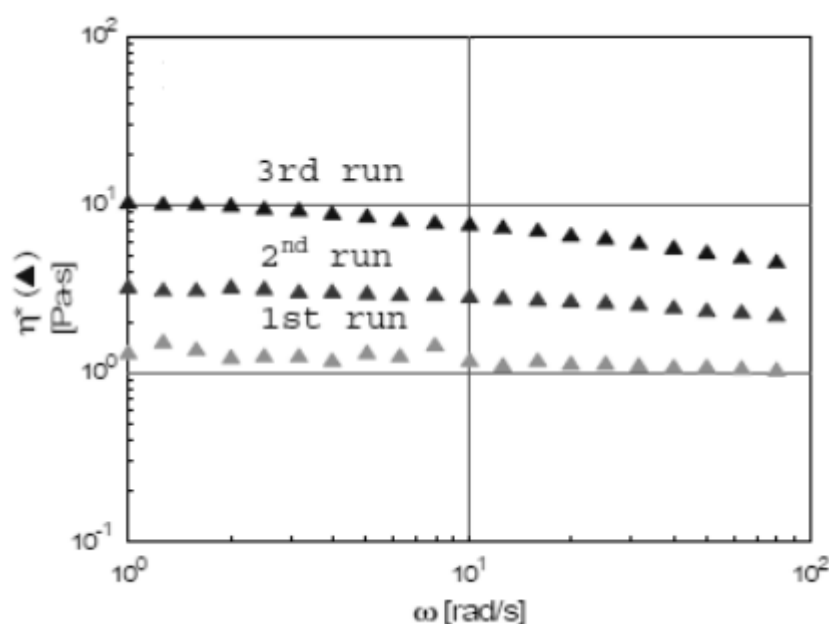


Figure 3.11 Rheological test results of PLGA solution

3.1.2.2.3 Fourier Transform Infrared Spectroscopy Results

FTIR-ATR spectra of PLGA powder, film and membrane are given in Figure 3.12. The peak at 1745 cm^{-1} is attributed to the carbonyl stretching of the ester. The peaks at about 2950 cm^{-1} may be attributed to $-\text{CH}$ stretching. The presence of a peak at 1452 cm^{-1} is due to $-\text{CH}_3$ bending and a peak at 1130 cm^{-1} is due to the $\text{C}-\text{O}$ stretching of the ester groups. All PLGA samples showed characteristic peaks of PLGA except one peak at 1670 cm^{-1} . Absorption peak near 1670 cm^{-1} , typical for Amide I stretching vibration and characteristic for DMF solvent, reveals the presence of trapped solvent (DMF) inside the microfabricated PLGA membranes and cast film as confirmed by thermal analysis.

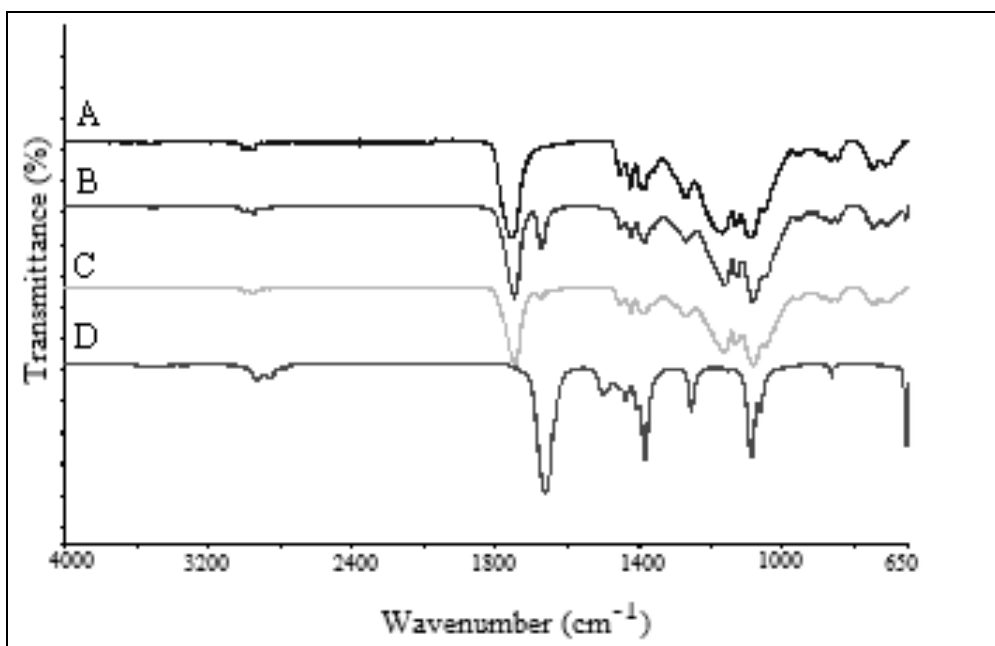


Figure 3.12 FTIR-ATR spectra of PLGA A) powder, B) film, C) membrane, D) DMF

3.1.2.2.4 Differential Scanning Calorimetry Results

DSC test results showed that the PLGA powder before microfabrication process presents a Tg that decreases from the first scan to the second scan. In the first scan it is also possible to notice an aging peak at about 60°C that followed Tg (Figure 3.13). Tg of PLGA film was observed at 26.59°C at the first scan (Figure 3.14). Tg of PLGA film was lower than Tg of PLGA powder since residual solvent acted as a plasticizer in the polymer and lowered the Tg. There was an endothermic peak at 83.02°C in the first scan because of the evaporation of residual solvent. In the second heating scan Tg increased by 10 degrees up to 36.45°C. Residual DMF acted as a plasticizer in the microfabricated membrane and caused a decrease in the glass transition temperature value to 21°C. In the second scan Tg increased to 42°C because of evaporation of solvent during first heating (Figure 3.15).

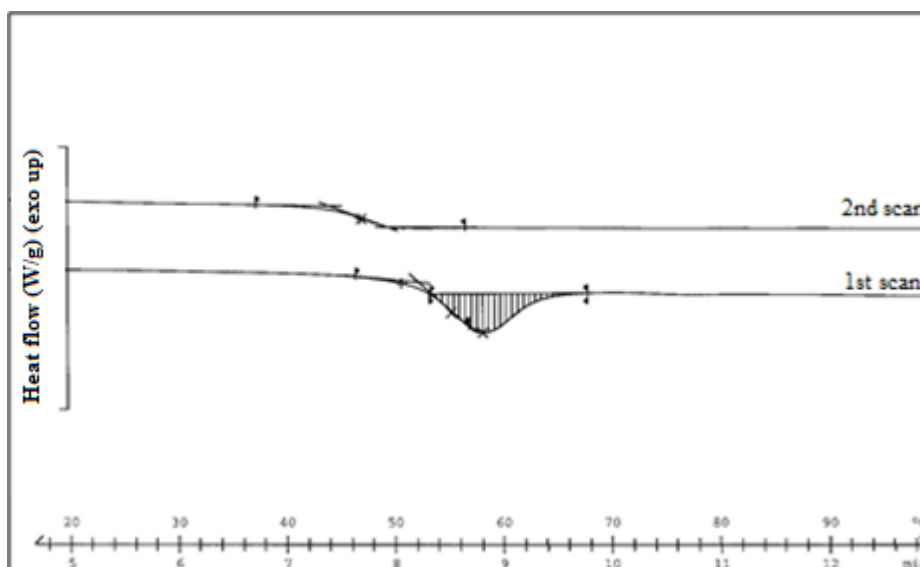


Figure 3.13 DSC thermogram of PLGA powder

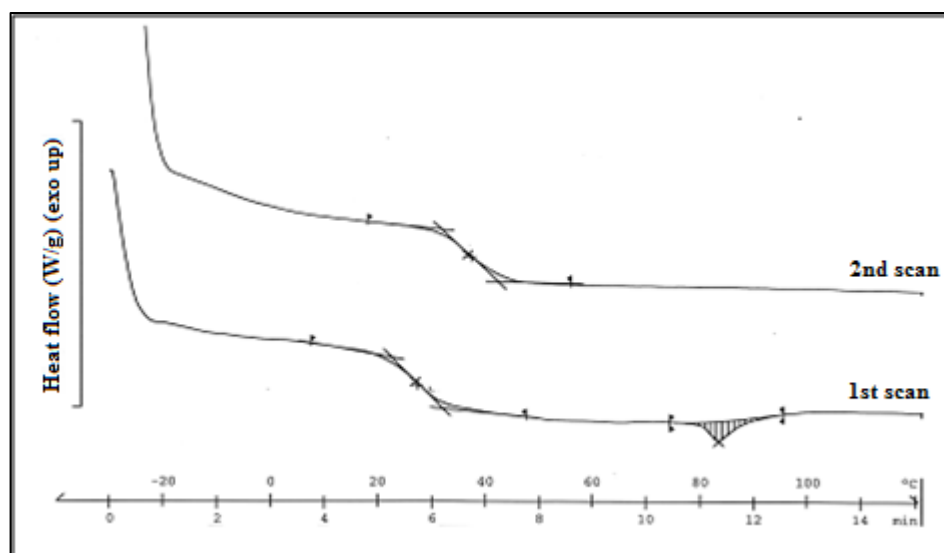


Figure 3.14 DSC thermogram of PLGA film

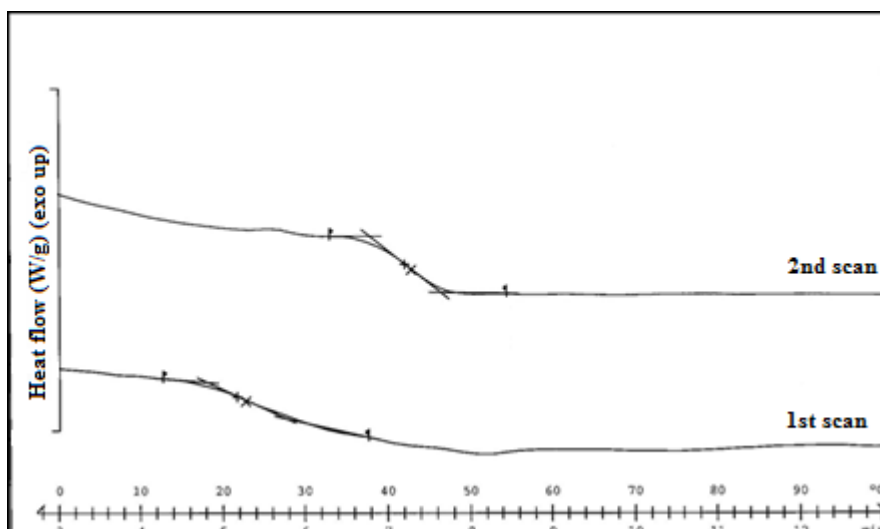


Figure 3.15 DSC thermogram of PLGA membrane

3.1.2.2.5 Dynamic Mechanical Thermal Analysis Results

Storage modulus and loss factor as a function of temperature for PLGA film and membrane is given in Figure 3.16. Storage modulus value of PLGA membrane is approximately 6 MPa while it is 100 MPa for film at 25°C. Storage modulus for PLGA membrane is too low when compared to PLGA film because porous structure lowers the resistance of membrane against applied force. Decreasing of the storage modulus, which corresponds to a peak in the loss factor curve, indicates the glass transition temperature of the amorphous polymers. The T_g value is low because of the residual solvent still present inside the polymer which acts as a plasticizer. T_g value of PLGA film was found to be around 40°C by DSC while it was observed around 30°C by DMTA because of lower heating rate during DMTA analysis.

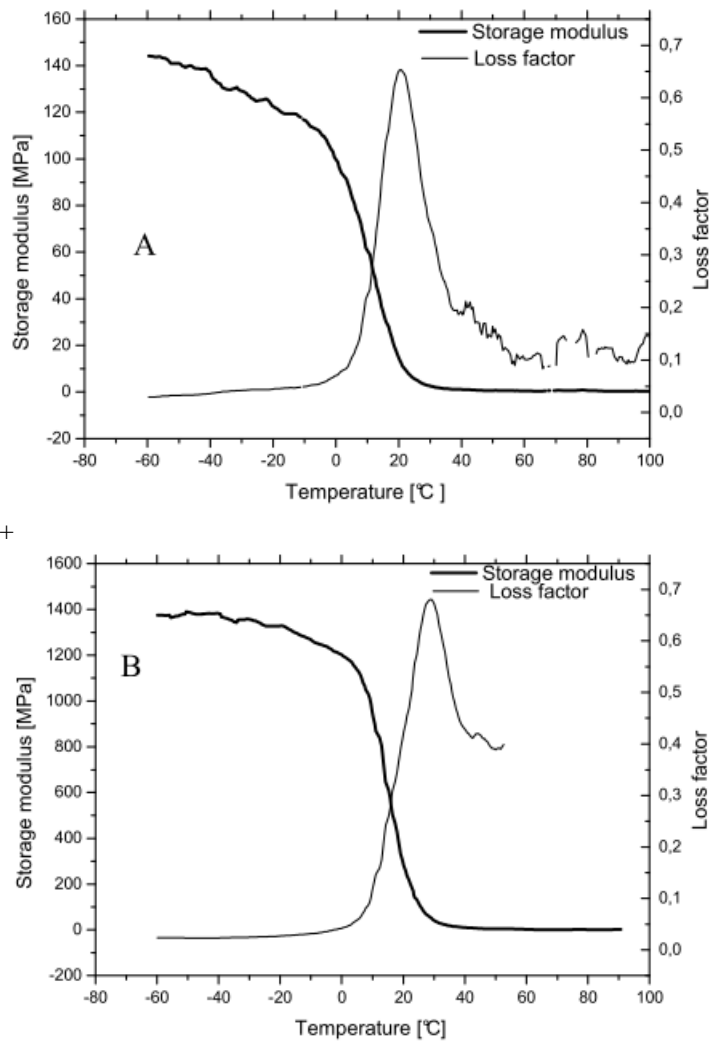


Figure 3.16 Storage Modulus and $\tan \delta$ curves of PLGA. A) membrane, B) film

3.1.2.2.6 Preliminary Cell Culture Test Results

MG63 and MRC5 cell lines were seeded on PLGA membranes and SEM images were taken after 4 and 10 days of cell culture (Figure 3.17 and Figure 3.18). PLGA membranes were fully covered by a cell layer that was quite denser in the case of osteoblasts after 10 days cell culture when compared to MRC5 cells. Cell penetration into the structure could not be detected because of the compact structure of PLGA membranes.

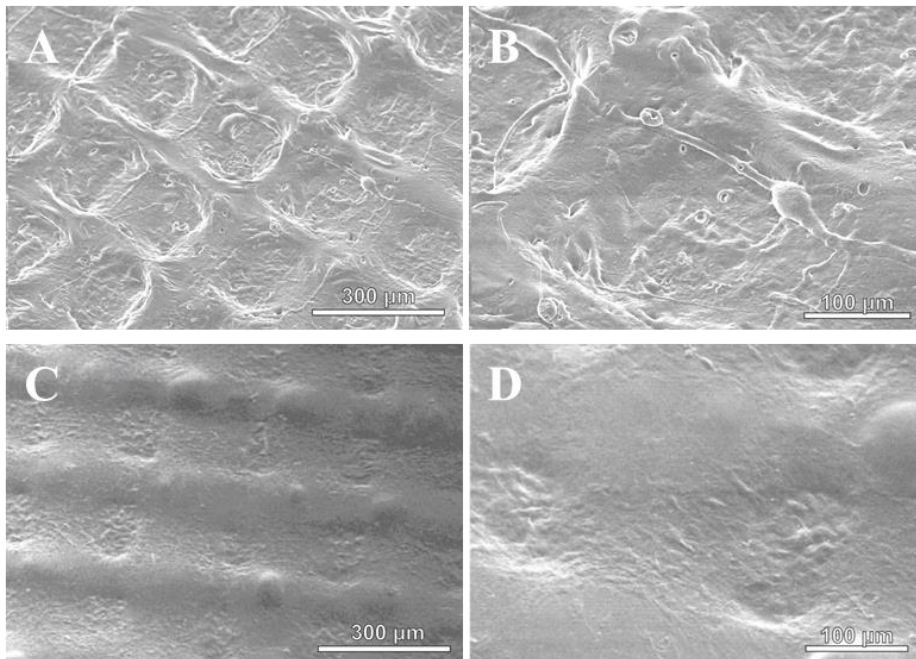


Figure 3.17 SEM micrographs of PLGA membranes after MG63 cell seeding. A, B) 4 days, C, D) 10 days in the culture

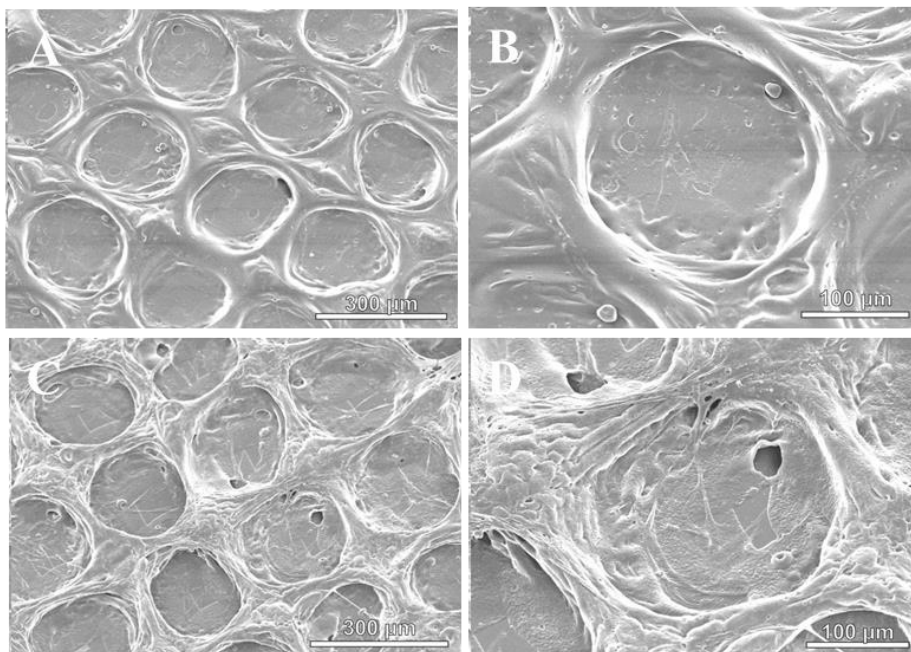


Figure 3.18 SEM micrographs of PLGA membranes after MRC5 cell seeding. A, B) 4 days, C, D) 10 days in the culture

Among the widely used techniques for tissue engineering scaffold preparation, microfabrication has the potential to produce matrices with high resolution, controlled geometry and porosity at a micro scale. In this study “in house” microfabrication device was used to manufacture chitosan and PLGA

porous membranes. The use of low polymer concentration solutions caused collapsing of the layers, leading to the fabrication of thin membranes with regular square holes at micron level although the initial aim was to produce 3D structures for scaffolds. These microfabricated membranes may still be used in tissue regeneration especially for skin, dental and wound dressing applications due to their regular porous structure, which will promote cell adhesion and migration and moisture transport.

3.2 Scaffolds Prepared by Freeze Drying

Bone is an organic/inorganic composite material composed of collagen and minerals. This natural composite material has a good balance between strength and toughness, better than either of its individual components. Generally one polymer does not fulfil all of the requirements for bone tissue engineering and it can be advantageous to use composite scaffolds. HAp is chemically similar to the mineral component of the bone. Studies have shown that polymer-hydroxyapatite composite matrices had improved bioactivity and osteoblast cell differentiation (Yaylaoglu *et al.* 1999, Bong-Soon *et al.* 2000, Opara *et al.* 2003, Woodard *et al.* 2007, Zou *et al.* 2008, Danilchenko *et al.* 2011, Isikli *et al.* 2012, Karadas *et al.* 2012).

Freeze drying, also known as lyophilization, is a conventional technique used to produce scaffolds from both natural and synthetic polymers. It is conducted by freezing a polymer solution and then reducing the pressure by applying vacuum and allowing the frozen solvent in the material to sublime directly from the solid phase to the gas phase leaving behind a porous foam. In this part of the thesis, polymer/hydroxyapatite composite scaffolds were prepared by freeze drying in order to mimic the organic/inorganic nature of the bone. Chitosan and PLGA were used as the polymer components and HAp as the inorganic component. Chitosan (CH) and chitosan-hydroxyapatite (CH-HAp) scaffolds could be prepared by this approach, however, the PLGA foams produced had low porosity (20%) and low mechanical strength. They did not maintain their shape. Therefore, PLGA was incorporated into CH and CH-HAp scaffolds. Morphology, porosity, degradation, water uptake, mechanical and thermal properties of the resultant scaffolds was studied. In addition, they were tested in vitro using SaOs-2 osteoblast cells.

3.2.1 Experimental

3.2.1.1 Materials

Poly(lactic acid-co-glycolic acid) (PLGA, type RESOMER® 503, 50:50 molar ratio D,L-lactic acid:glycolic acid, MW: 39 kDa) was purchased from Boehringer Ingelheim (Ingelheim, Germany). Chitosan (low viscosity, 75–85% deacetylated) was purchased from Fluka (Osaka, Japan). The polymers were used without further purification. Acetic acid was obtained from Sigma Aldrich (St. Louis, USA). Dioxane was purchased from Scharlau (Barcelona, Spain). N-decane was obtained from Fluka (Steinheim, Germany). HAp particles used in the preparation of freeze dried scaffolds were synthesized in the laboratory. Calcium nitrate and ammonium phosphate were used in HAp synthesis and were purchased from Merck (Darmstadt, Germany). Sodium hydroxide was obtained from J.T. Baker (Deventer, Holland). 25% ammonium hydroxide solution was purchased from Carlo Erba. Lysozyme from chicken egg white (activity of 96831 U.mg⁻¹) was bought from Fluka (Bornem, Belgium). Sodium azide was obtained from Scharlau (Barcelona, Spain). Roswell Park Memorial Institute (RPMI) Medium, fetal bovine serum (FBS) and penicillin/streptomycin (Pen/Strep) solution were obtained from Hyclone (Logan, UT, USA). Trypsin-EDTA (0.25%) was provided from Sigma (Utah, USA). Glutaraldehyde and cacodylic acid (sodium salt) were obtained from Sigma (Saint Louis, USA). Alamar Blue cell proliferation assay kit was from Biosource (Frederick, MD, USA).

3.2.1.2 Synthesis of Hydroxyapatite

In the preparation of HAp, 0.5 M Ca(NO₃)₂·4H₂O and 0.3 M (NH₄)₂HPO₄ solutions were prepared in deionized water separately and stirred vigorously. pH values of calcium and phosphate solutions adjusted to pH=11–12 by addition of NH₄OH with continuous stirring. After initial pH adjustment, calcium containing solution was added drop wise to phosphate solution. Throughout this addition the pH of the solution was kept constant in the range of pH=11–12 by ammonia addition. After adding all the components and adjusting the pH value to 11–12, the final solution was stirred for extra 2 h. Then, the solution was heated to 90°C on a hot plate and stirred for 1 h at this temperature. Then the

solution was cooled down to room temperature and stirred overnight. The solution was filtered and washed with water to remove excess ammonia. The filtered cake was dried at 80°C overnight and calcined at 1000°C for 3 h. The chemical reaction for hydroxyapatite synthesis is given below:



3.2.1.3 Characterization of Hydroxyapatite

The crystal structure of the synthesized and ground non-sintered and sintered HAp samples (nsHAp and sHAp) were characterized by X-ray diffraction (XRD). The patterns were recorded with X-Ray diffractometer (Rigaku model Ultima D/MAX 2200/PC, Tokyo, Japan) using CuK α radiation generated at 40 kV and the scan speed was 2°·min⁻¹. Morphology of synthesized HAp powders was examined by SEM. The samples were sputter-coated with Au-Pd prior to examinations. FTIR spectrum was obtained by Perkin Elmer FTIR Spectrometer (Maryland, USA).

3.2.1.4 Preparation of Freeze Dried Scaffolds

Chitosan solution with a concentration of 3% (w/w) was prepared in 5% (v/v) aqueous acetic acid and transferred to a 24 well plate, frozen at -20°C overnight and lyophilized in a freeze dryer (Labconco Freeze Dry, Model 78680, Missouri, USA). To prepare chitosan-hydroxyapatite (CH-HAp) scaffolds, 0.3 g HAp was weighed and then 47.5 mL deionized water was added. The mixture was stirred at room temperature for 4 h to disperse HAp powder in deionized water. Then 1.2 g chitosan and 2.5 mL acetic acid were added under agitation. After stirring overnight, the mixture was transferred to a well plate, frozen at -20°C overnight and lyophilized. All scaffolds were neutralized by immersing in 1 M NaOH for 2 h followed by washing with distilled water until neutralized and then lyophilized again.

To prepare chitosan-PLGA (CH-PLGA) and chitosan-HAp-PLGA (CH-HAp-PLGA) scaffolds, first 5% (w/v) PLGA solution was prepared in dioxane. Then freeze dried CH and CH-HAp scaffolds were soaked into PLGA solution and kept under vacuum for 3 h so that PLGA would cover the pores of scaffolds. Then CH-PLGA and CH-HAp-PLGA scaffolds were frozen at -20°C and dried by lyophilization. Scaffolds were stored under vacuum until use.

3.2.1.5 Characterization of Freeze Dried Scaffolds

3.2.1.5.1 Morphological Investigations

Morphology of synthesized HAp powders and porous structures of scaffolds, cell behavior on constructs were investigated by scanning electron microscopy (SEM, Quanta 400F Field Emission, FEI, Eindhoven, Holland). The samples were sputter-coated with Au-Pd prior to examinations.

3.2.1.5.2 Fourier Transform Infrared Spectroscopy

Fourier Transform Infrared-Attenuated Total Reflectance (FTIR-ATR) spectroscopy analysis (Spectrum One Spectrometer, Perkin Elmer, Maryland, USA) was used to evaluate the chemical structure of the scaffolds. All the spectra were analyzed after baseline correction.

3.2.1.5.3 Differential Scanning Calorimetry

The thermal properties of the scaffolds were determined by differential scanning calorimetry (DSC, Perkin Elmer Diamond, Shelton, USA). Approximately 5–10 mg samples were placed in aluminum DSC pans. Samples underwent two heating scans under nitrogen atmosphere from 0°C to 200°C. Heating rate was kept as 10°C.min⁻¹ for all samples.

3.2.1.5.4 Porosity and Pore Size Distribution Determination

Scaffold porosity was determined using liquid displacement method using pycnometer. The pycnometer is a glass vessel with a close-fitting ground glass stopper with a capillary hole through it. First, the sample and the empty pycnometer with glass stopper was weighed and recorded as m_s and m_p , respectively. Then, the pycnometer was filled with n-decane (nonsolvent for the samples), weighed and recorded as m_{p+d} . Volume of n-decane that fills an empty pycnometer was calculated as follows:

$$V_1 = \frac{m_{p+d} - m_p}{\rho_d}$$

Where, ρ_d is density of n-decane. V_1 gives the volume of the pycnometer.

Then, the sample was immersed in decane and the total weight (pycnometer + n-decane + sample) was recorded as m_{p+d+s} . Mass of decane (m_d) was found by subtracting ($m_s + m_p$) from m_{p+d+s} . Volume of n-decane that added (V_d) was obtained by dividing its mass (m_d) by its density (0.73 g.cm⁻³). The volume of the sample (V_s) was found as:

$$V_s = V_1 - V_d$$

The percent porosity (P) of each scaffold was determined according to the following equation:

$$P(\%) = \frac{V_a - V_s}{V_a} \times 100$$

Where V_a is apparent volume of the sample calculated from simple formula for cylinders:

$$V_a = \pi r^2 h$$

Pore size distributions of the scaffolds were determined by mercury intrusion porosimeter (Quartachrome Corporation, Poremaster 60, Florida, USA).

3.2.1.5.5 Mechanical Tests

Compression moduli of dry and hydrated (1 h in 0.01M PBS at 37°C) scaffolds were determined by using Lloyd LRX 5K Mechanical Tester (Lloyd Instruments Limited, Fareham, Hampshire, UK), controlled by a computer running program (WindapR). The dimensions of the cylindrical scaffolds were approximately 10 mm in diameter and 5 mm in thickness. A constant extension rate of 1 mm.min⁻¹ was applied. For each type of sample, at least five experiments were carried out and the average values of Young's modulus were taken. The compression modulus of scaffolds was calculated from the initial linear slope of the stress-strain curve.

3.2.1.5.6 Water Uptake Capacity

Dry scaffolds were weighed (W_d) and immersed in phosphate buffered saline (PBS, 0.01 M, pH 7.4) at 37°C. Scaffolds were drawn at various times (0.5, 1, 1.5, 2, 3, 4, 24 and 48 h), water on the surface was removed by gentle contact with a filter paper and then weighed. Three repeats were carried out for each sample and the results averaged. The percent water uptake capacity was calculated from the equation:

$$\text{Water uptake capacity \%} = [(w_s - w_i) / w_i] \times 100$$

where w_i and w_s are the sample weights initially and after water absorption, respectively.

3.2.1.5.7 In vitro Degradation Tests

The weight loss of the scaffolds was evaluated by incubating the samples in aqueous media with the presence of enzyme lysozyme. For enzymatic degradation, scaffolds were placed into vials containing 5 mL of PBS (0.01 M, pH 7.4) with 0.5 mg.mL⁻¹ enzyme and 0.5 mg.mL⁻¹ of sodium azide to inhibit bacterial growth. Solutions were incubated at 37°C in a water bath. The solutions were changed every two days. Samples were removed periodically, washed with distilled water, freeze dried and weighed in order to determine the weight loss due to erosion of the samples. The weighed samples were then placed into fresh PBS medium containing the enzyme and sodium azide. Three parallel experiments were carried out for each type of scaffold and the data averaged. Weight loss was calculated as follows:

$$\text{Weight loss (\%)} = [(w_0 - w_1) / w_0] \times 100$$

where w_0 and w_1 are weight of dry samples before and after enzymatic degradation test, respectively.

3.2.1.5.8 Cell Culture Tests

Scaffolds were sterilized in 70% ethyl alcohol for 3 h, and then washed 3 times with PBS (pH 7.4, 0.01 M) to remove residual ethanol. Cell culture studies were conducted using human osteosarcoma cell line SaOs-2. SaOs-2 cell line has been widely used as a model system for human osteoblastic cells in biomaterial studies. Aliquots of 100 µL of cell suspension containing 10⁵ cells were seeded dropwise on the scaffolds. After incubation for 3 h, complete RPMI medium (1 mL) was added and cells were grown at 37°C in the CO₂ incubator. Medium was changed every two days.

Alamar Blue™ assay was used to determine cell numbers on the scaffolds after 1, 7, 14 days. The active ingredient of Alamar Blue (resazurin) is a nontoxic, cell permeable compound that is blue in color and virtually nonfluorescent. Upon entering cells, resazurin is reduced to resorufin, which produces very bright red fluorescence. Viable cells continuously convert resazurin to resorufin, thereby generating a quantitative measure of cell viability. After transferring of SaOs-2 seeded scaffolds into a new, sterile 24 well plate and washing with sterile PBS, 1 mL of Alamar Blue solution (10% in colorless medium) was added to each sample in the 24 well plate and incubated for 1 h at 37°C in the CO₂ incubator. All experiments were performed in triplicate. After 1 h incubation, 200 µL of solution from each well was transferred in triplicate to a new 96 well plate. Absorbance was measured at 570 nm and 595 nm using an Elisa Plate Reader (Molecular Devices, V max Microplate Reader, California, USA). The cell morphology was characterized by SEM. For SEM examination, samples were fixed in 1% glutaraldehyde solution, rinsed with cacodylate buffer and freeze dried. After drying, the samples were mounted on aluminum stubs, sputter-coated with gold-palladium and placed into the instrument for SEM examination.

3.2.2 Results and Discussion

3.2.2.1 XRD Results of HAp

HAp can be synthesized with several methods using a range of different reactants. Some of the production methods include wet chemical methods (precipitation), hydrothermal techniques, hydrolysis of other calcium phosphates and sol-gel method. In this thesis HAp was synthesized by wet chemical synthesis method which is the most common synthesis technique. The structural properties of HAp powder were characterized by X-ray diffraction (XRD). XRD spectra of non-sintered (nsHAp) and sintered hydroxyapatite (HAp) powders are shown in Figure 3.19. Characteristic peaks of HAp were at around 26.0° and 31.9° (JCPDS card no. 9-432). There was no carbonate impurity (no peaks at 37° and 54°) showing that the main inorganic phase of the synthesized powder was HAp. It was seen that the 1000°C heat treatment caused higher crystallinity with sharper apatite peaks. Therefore, final products with sintering process have high crystallinity while non-sintered HAp particles show less crystalline structure.

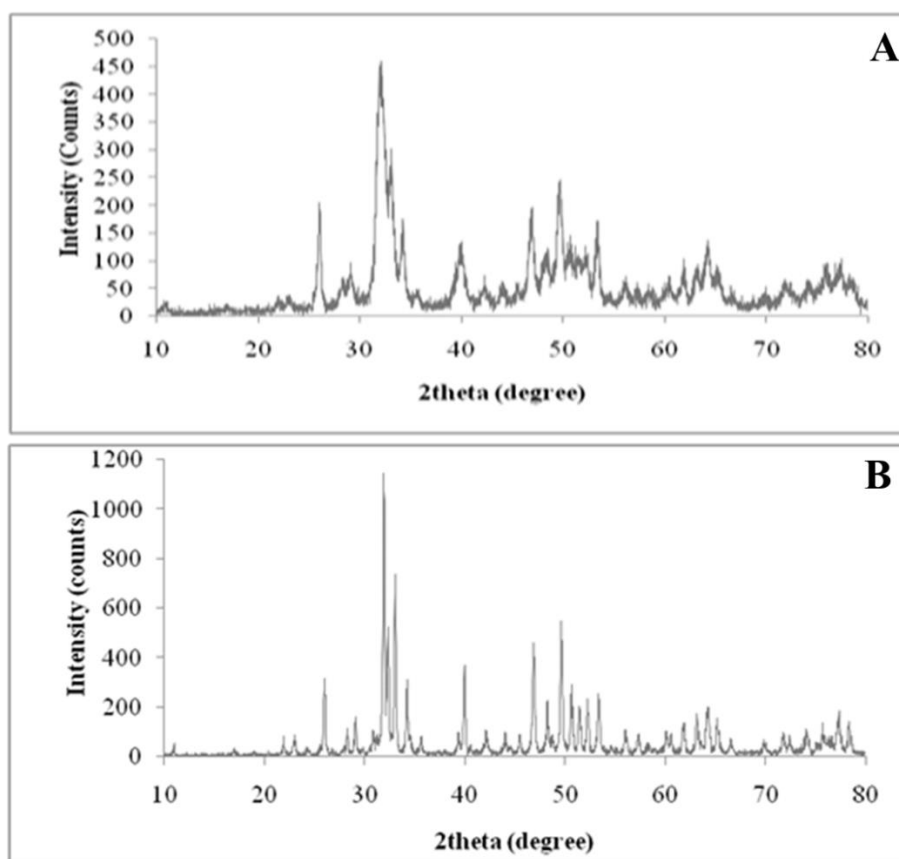


Figure 3.19 XRD patterns of A) nsHAp, B) sintered HAp powder

3.2.2.2 Morphological Analysis Results

SEM micrographs of HAp particles, both sintered at 1000°C and non-sintered HAp (nsHAp) are given in Figure 3.20. Aggregates of HAp particles sintered formed more crystalline, densely packed structures while non-sintered particles demonstrated amorphous structures with smaller flakes.

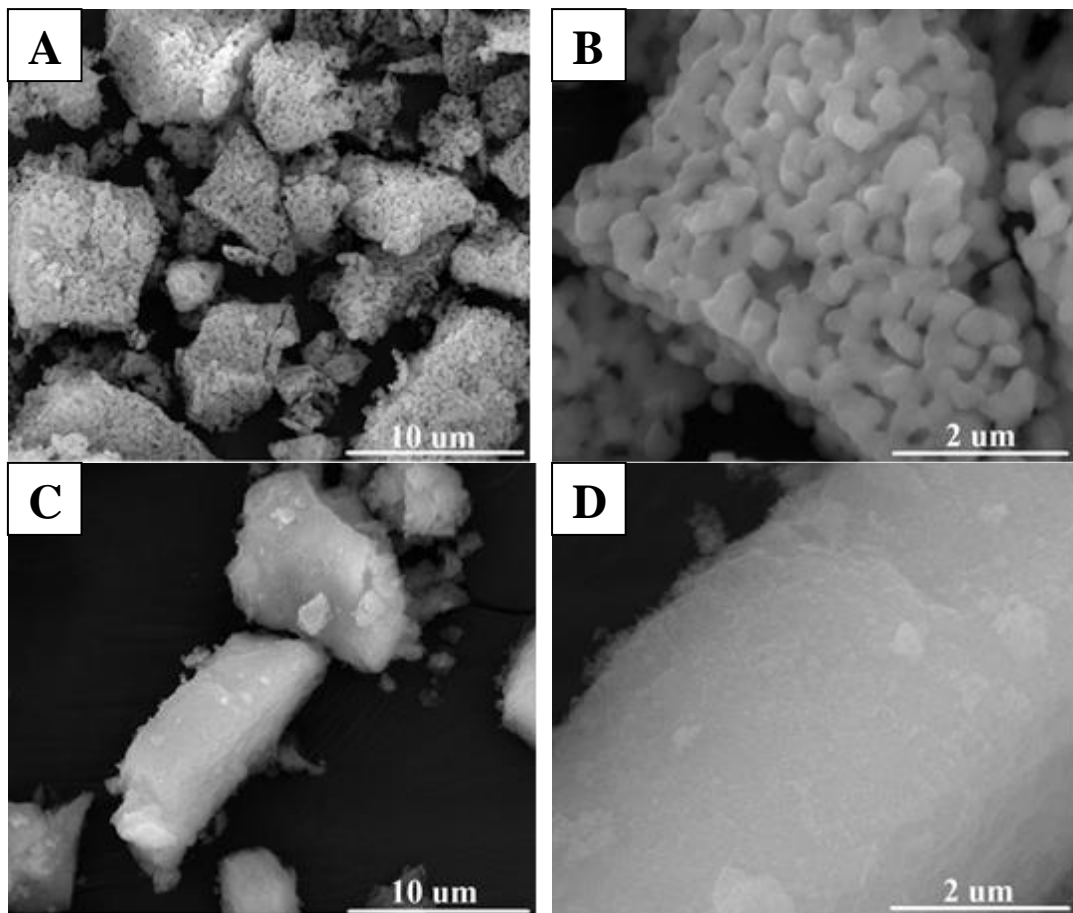


Figure 3.20 SEM micrographs of A, B) HAp, C, D) nsHAp powder

All of the scaffolds were soft, sponge-like, flexible and strong enough to handle in wet and dry conditions without deformation. The microstructure of scaffolds was observed by SEM (Figure 3.21, Figure 3.22). Macroporous structure with interconnected pores was observed on the surface of the scaffolds. All the scaffolds were highly porous with an approximate pore size ranging between 5 μm and 200 μm. In addition, homogenous dispersion of HAp particles in CH-HAp and CH-HAp-PLGA scaffolds was observed (Figure 3.21 E and F). Pore size is important in tissue engineering applications because if the pores are too small, cell penetration, extracellular matrix production and neovascularization of the inner parts of scaffold will be inhibited. The minimum requirement for pore size is considered to be around 100 μm (Karageorgiou and Kaplan 2005).

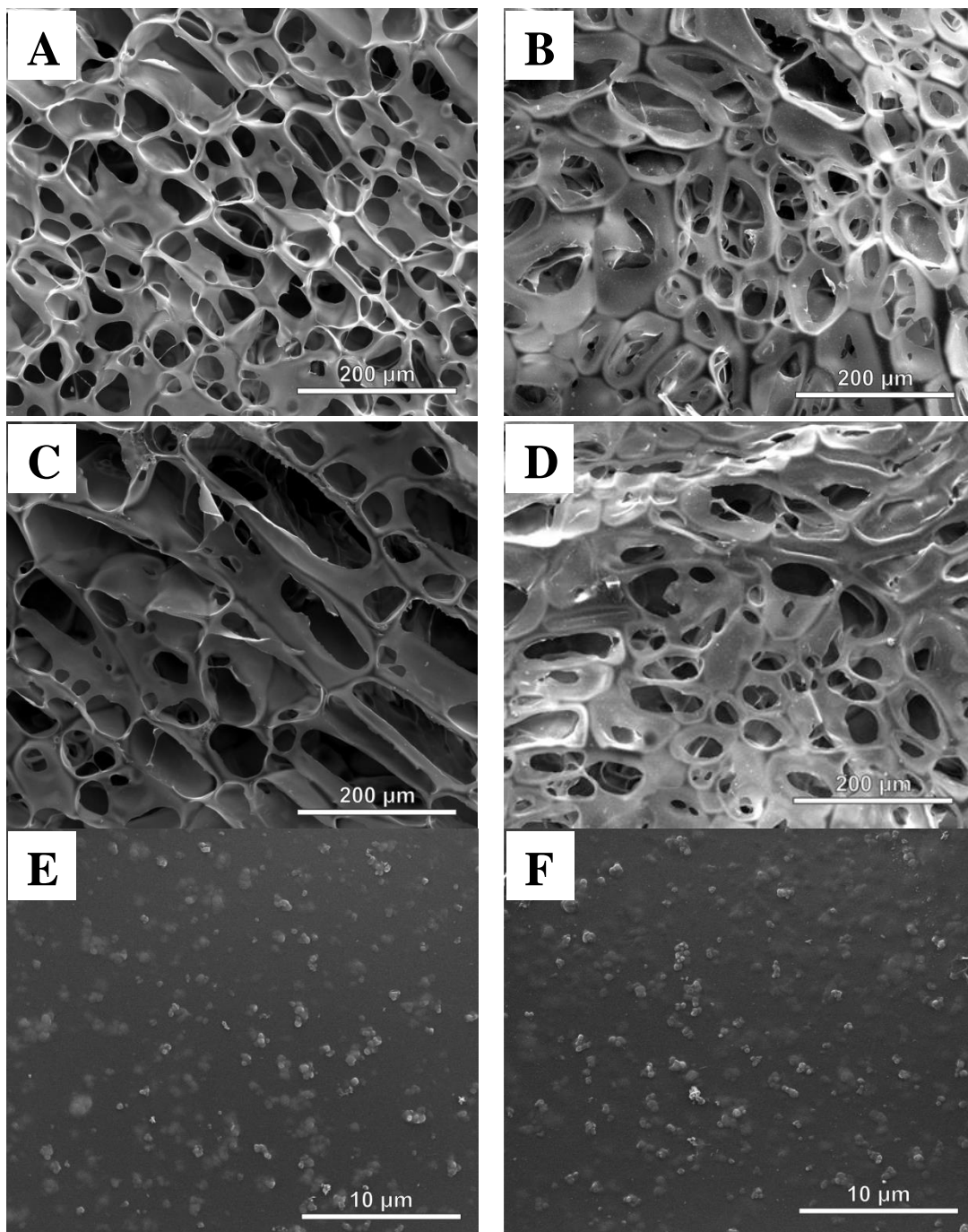


Figure 3.21 SEM micrographs of scaffolds A) CH; B) CH-HAp; C) CH-PLGA; D) CH-HAp-PLGA; E) CH-HAp; F) CH-HAp-PLGA at higher magnification

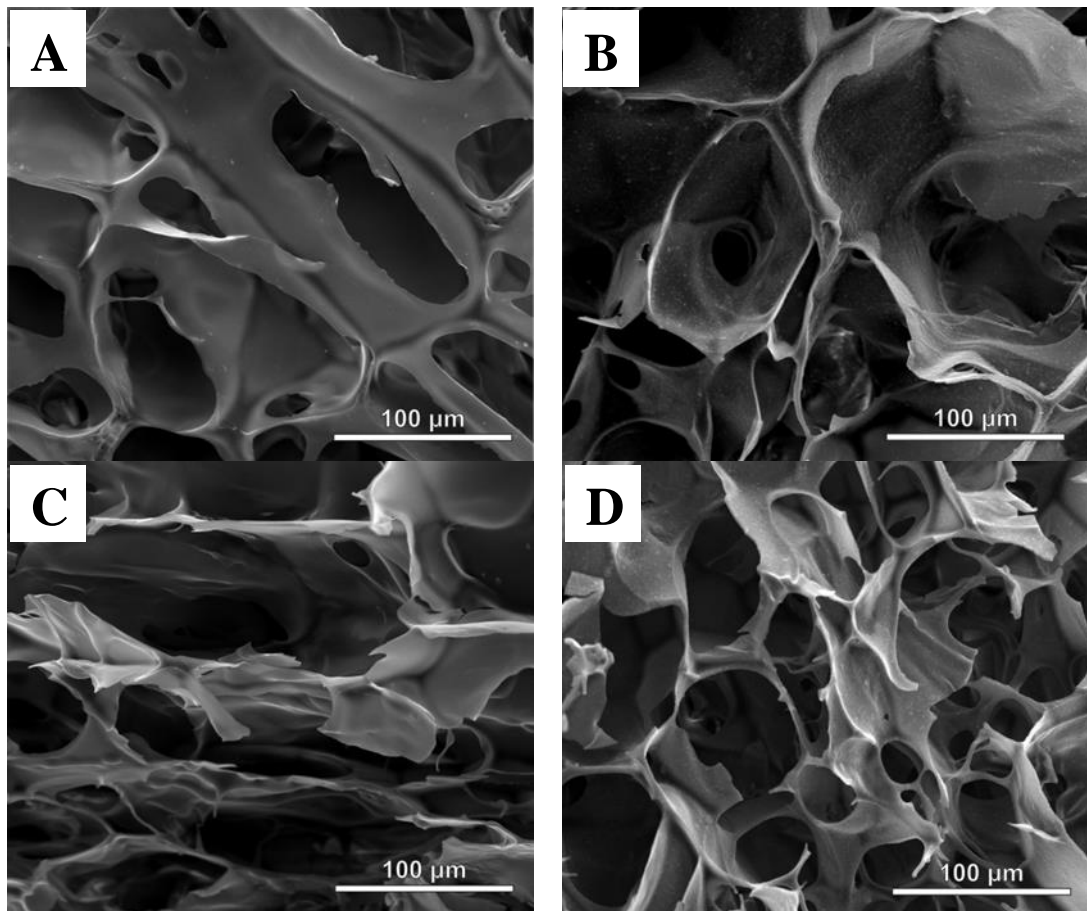


Figure 3.22 SEM micrographs of the crosssections of scaffolds A) CH; B) CH-HAp; C) CH-PLGA; D) CH-HAp-PLGA

It was shown that 100–200 μm pores showed significant bone ingrowth, 75–100 μm pores resulted in ingrowth of unmineralized osteoid tissue while 10–75 μm pores were penetrated only by fibrous tissue. Itala *et al.* (2001) tested bone formation in rabbit femoral defects under non-load-bearing conditions using titanium plates having four different pore sizes (50 μm , 75 μm , 100 μm and 125 μm). Bone ingrowth was similar in all the pore sizes, therefore 100 μm may not be the critical pore size for non-load-bearing conditions (Itala *et al.* 2001). Collagen matrices having pores ranging between 11–105 μm and 14–134 μm healed tibia defects in rats (Rocha *et al.* 2002). Hyaluronic acid based scaffolds having pores ranging from 100 to 600 μm prepared by salt leaching technique and used for delivery of BMP-2 in vitro and osteogenic differentiation of the murine pluripotent cell line C3H10T1/2 (Kim and Valentini 2002).

Elongated pores were seen in CH-PLGA scaffold. This kind of pore structure was observed in some chitosan scaffolds prepared with freeze drying technique (Nwe *et al.* 2009). It was stated that these pores might be formed because of highly parallel ice crystal growth between scaffold substrate layers, created by formation of hydrogen bonds between the long chains of polymers during the freeze drying process. An open pore structure was observed in the cross sections of all prepared scaffolds; the pores were separated from each other and they were interconnected (Figure 3.22). This interconnected porosity of freeze dried scaffolds will provide better cell attachment and migration, tissue ingrowth and transportation of nutrients.

3.2.2.3 Fourier Transform Infrared Spectroscopy Results

FTIR is an useful technique to characterize the functional groups present in the polymer. FTIR-ATR spectra of prepared scaffolds, PLGA powder and synthesized HAp powder is given in Figure 3.23.

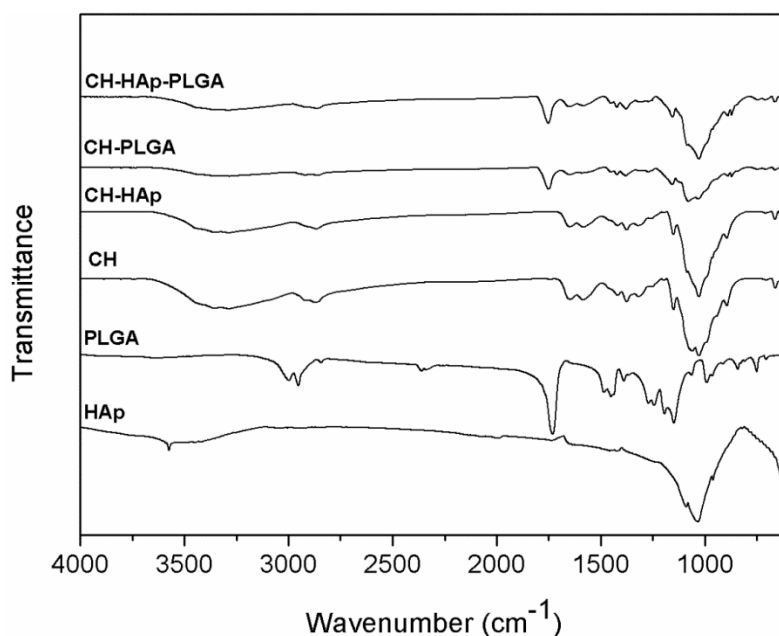


Figure 3.23 FTIR-ATR spectra of HAp, PLGA powder and scaffolds

In FTIR spectrum of HAp the peaks at 1095-1045 cm^{-1} , 975 cm^{-1} and 601 cm^{-1} correspond to different vibration modes of phosphate group. The peaks at 3570 cm^{-1} and 635 cm^{-1} correspond to stretching and bending vibration of hydroxyl group, respectively. For PLGA powder the strong characteristic absorption bands at about 1752 cm^{-1} is attributed to the stretching vibration of C=O bond. The bands at 1182 cm^{-1} are assigned to the C-O-C ether group stretching, the bands at 1130 cm^{-1} and 1452 cm^{-1} corresponds to C-O bond and methyl group C-H bond of PLGA, respectively. The FTIR-ATR spectrum of chitosan scaffold shows characteristic broad band around 3287 cm^{-1} corresponding to -OH linked to polymer, while 1647 cm^{-1} and 1586 cm^{-1} are the characteristic peaks of the stretching vibration of C=O amide bond and -NH bending vibration in amine groups, respectively. The peaks at 1420 cm^{-1} are assigned to the CH_3 symmetrical deformation mode while the peaks at 1150 cm^{-1} , 1060 cm^{-1} and 1029 cm^{-1} correspond to C-O stretching vibrations. When FTIR spectra of HAp powder, CH, CH-HAp and CH-HAp-PLGA scaffolds are compared, new absorption bands appeared at 631 cm^{-1} are due to bending vibration of O-H and at 601 cm^{-1} are due to phosphate group show the presence of HAp. A peak at 1750 cm^{-1} appeared in the spectra of CH-PLGA and CH-HAp-PLGA scaffolds because of carbonyl group present in PLGA polymer.

3.2.2.4 Differential Scanning Calorimetry Results

The DSC thermograms of scaffolds are given in Figure 3.24. All scaffolds exhibited an endothermic peak at around 90°C in the first scan (Table 3.1). This endothermic peak was attributed to the evaporation of absorbed water. In the second scan of CH-PLGA and CH-HAp-PLGA scaffolds, aging peak followed by T_g at 46°C was observed due to presence of PLGA polymer. Glass transition

temperatures of PLGA could not be observed clearly in the first scans, probably broad endothermic peak masked them.

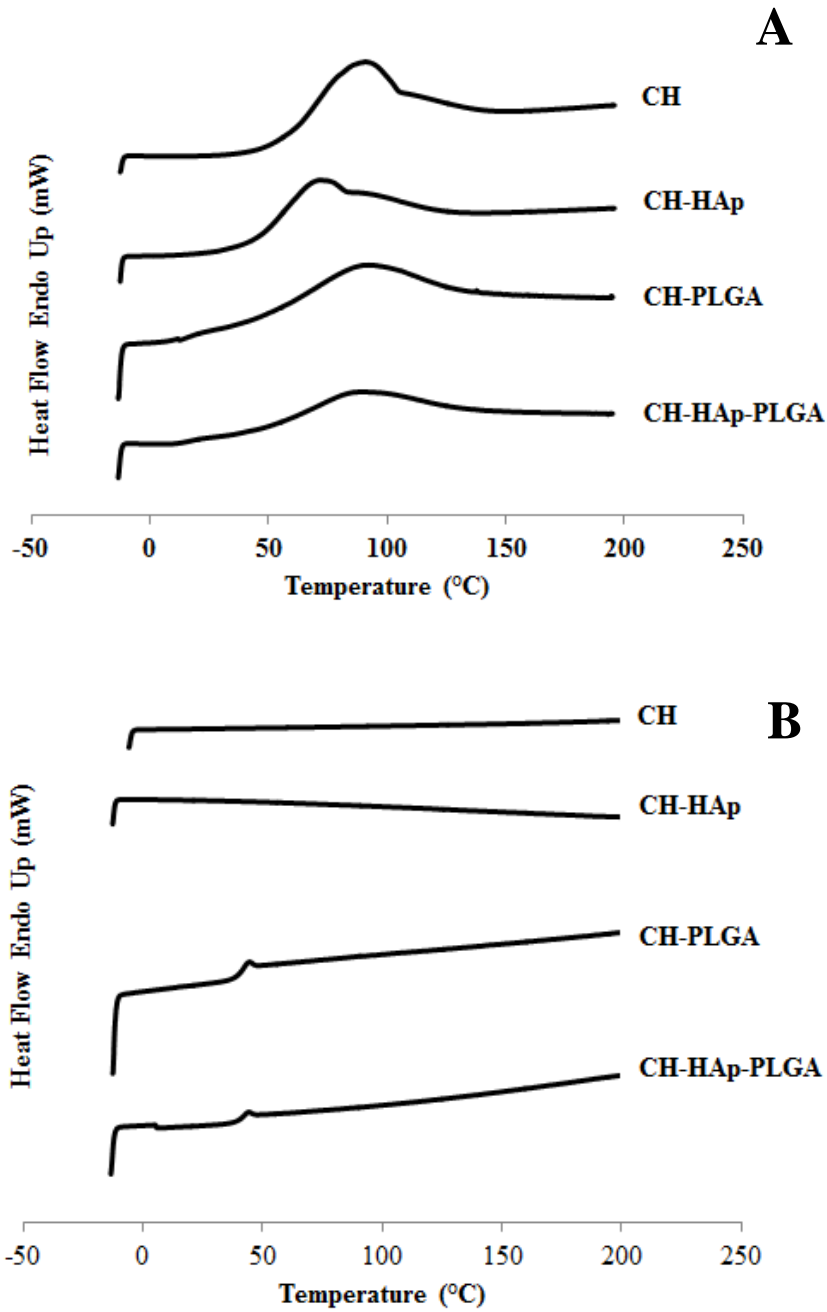


Figure 3.24 DSC thermograms of scaffolds A) 1st scan, B) 2nd scan

Table 3.1 Results of DSC analysis of scaffolds

	1st Scan	2nd Scan
	T _{peak} (°C)	T _g (°C)
CH	96.1	-
CH-HAp	76.8	-
CH-PLGA	94.9	46.1
CH-HAp-PLGA	94.9	46.5

3.2.2.5 Porosity and Pore Size Distribution Results

Scaffolds must have a porous structure with an interconnected geometry to provide a large surface area that will allow cell ingrowth, distribution, transfer of oxygen and nutrients. Scaffolds having varying porosities from 15 to 90% were prepared by using different techniques like sintering, salt leaching, freeze drying (Chen *et al.* 2001, Zhang *et al.* 2001, Kim and Valentini 2002, Itoh *et al.* 2004, Hsieh *et al.* 2007). Chitosan scaffolds having around 80% porosity were produced by a liquid hardening method (Hsieh *et al.* 2007). Collagen/hydroxyapatite scaffolds containing different amounts of HAp were prepared by freeze drying method and sponges with 49, 73 and 79% porosity and 50–300 µm pore size were obtained (Itoh *et al.* 2004).

Porosity of scaffolds was determined by using pycnometer and values are given in Table 3.2. The porosities of CH and CH-PLGA scaffolds were determined to be 88.8 and 81.8%, respectively. Porosity of chitosan scaffolds decreased by 6% when soaked with PLGA solution since the polymer concentration in the resultant scaffold (CH-PLGA) increased. It is stated in literature that porosity decreases with increase of polymer solution concentration (Hsieh *et al.* 2007). In addition, percent porosity of chitosan scaffolds was decreased with HAp incorporation. Similarly the porosity decrease was observed in the composite scaffold probably because of the possible chemical interaction between NH₂ group of chitosan and OH group of HAp (Pallela *et al.* 2012).

Table 3.2 Porosity of scaffolds

Sample	Porosity (%)
CH	88.8 ± 3.2
CH-HAp	82.3 ± 3.7
CH-PLGA	81.8 ± 5.2
CH-HAp-PLGA	77.4 ± 1.8

Pore size distribution and pore volume of scaffolds were determined by mercury intrusion porosimetry. Mercury porosimetry is the most common technique for porosimetry analysis; however it does not measure pore sizes over 200 µm. Figure 3.25 shows the pore size distribution of prepared scaffolds. It was observed that pores of scaffolds were inhomogenous and pores as small as six microns were present within scaffolds which are necessary to provide pore interconnections. Distributions of pore sizes of scaffolds were in the range of 5–200 µm. All scaffolds exhibited a similar pore size distribution with peak located around pores at 30 µm and 40 µm and a wide range of smaller pores. The volume fraction of pores between 30–100 µm was much closer to each other in

CH-HAp, CH-PLGA, CH-HAp-PLGA scaffolds when compared to CH, indicating existence of relatively more homogenous pore distribution.

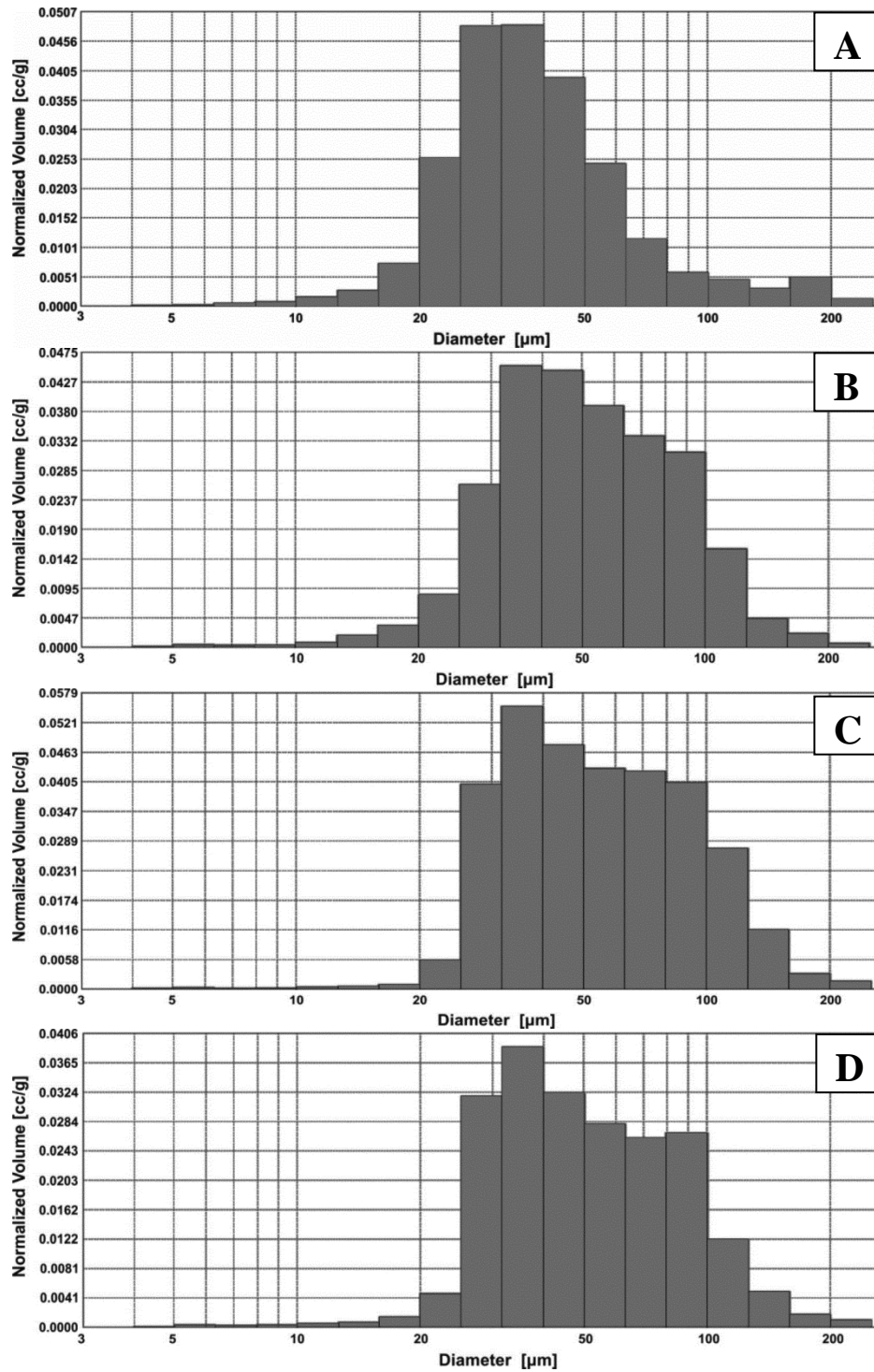


Figure 3.25 Pore size distributions of scaffolds A) CH; B) CH-HAp; C) CH-PLGA; D) CH-HAp-PLGA

3.2.2.6 Mechanical Test Results

Scaffolds must have enough mechanical strength to support tissue regeneration at the site of implantation and preserve sufficient integrity during cell growth. The mechanical strength depends on the target tissue but at least 100 kPa is reported to be necessary for cell culture and ultimate organ formation (Zhang *et al.* 2006). One of the main challenges in the preparation of scaffolds is the balance between adequate porosity and mechanical strength because porosity, pore volume, size, shape, orientation and connectivity are the major factors affecting the mechanical properties of scaffolds (Thein and Kitiyanant 2006, Dhandayuthapani *et al.* 2011). Compressive modulus and strength values of chitosan scaffold are reported to be in the range of 0.0038–2.56 MPa and 0.059–0.125 MPa, respectively (Li *et al.* 2005, Subramanian and Lin 2005, Hsieh *et al.* 2007).

The mechanical properties of scaffolds were examined under wet and dry conditions. Porous scaffolds exhibited compressive stress–strain curves with characteristics indicative of elastomeric cellular solids, including a linear elastic region, elastic collapse stress, elastic buckling region and densification (Kane and Roeder 2012). Compressive modulus is defined as the slope of the linear elastic region and calculated for both dry and hydrated scaffolds and given in Table 3.3. Representative compressive force–extension curves for scaffolds are given in Figure 3.26.

HAp containing scaffolds showed higher modulus when compared to CH and CH-PLGA scaffolds. The compressive modulus of chitosan was increased with the addition of HAp from 1.70 MPa to 3.73 MPa which is in accordance with literature. It has been reported that the incorporation of calcium phosphates into a polymer matrix improves the mechanical properties; this increase was attributed to the strong interaction between chitosan and HAp to form a chitosan-hydroxyapatite complex (Zhang and Ma 1999).

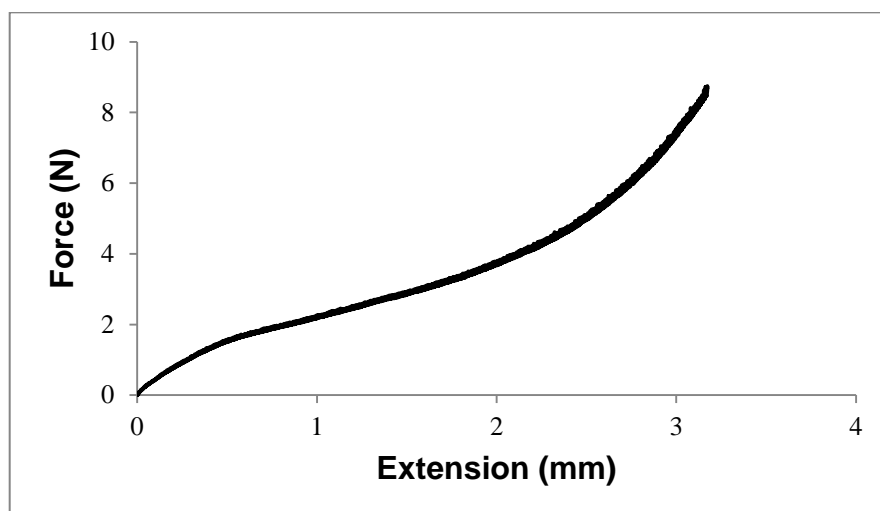


Figure 3.26 Representative force–extension curve for scaffolds

Compressive modulus of hydrated chitosan scaffolds was lowered to 0.035 MPa because of their high water uptake capacity. Water molecules that entered scaffolds may have acted as a plasticizer, and lowered mechanical strength. In addition, it is stated in literature that due to absorption of water the polymer chains became uncoiled and separated in swollen gel structure and hence the sliding friction between polymer chains decreased and reduced mechanical strength (Johnson *et al.* 2004). Incorporation of PLGA into chitosan scaffolds improved mechanical property in hydrated state compared to chitosan scaffolds. The modulus of hydrated CH-PLGA scaffold was approximately 10 times higher than the modulus of CH and CH-HAp scaffolds. CH-PLGA scaffolds did not absorb

water as much as chitosan scaffolds since PLGA is a hydrophobic polymer therefore in hydrated form it has the highest mechanical strength.

Compressive moduli for cancellous bone are given as 10–500 MPa depending on age, gender, porosity, density and mineralization (Nalwa 2004). It is seen that compressive moduli of all prepared scaffolds were lower than the values of natural cancellous bone. It can be concluded that scaffolds can be suitable for bone defects which are exposed to only low compressive strength.

Table 3.3 Compressive elastic modulus of dry and hydrated scaffolds

Samples	E_c (MPa)
Dry CH	1.70 ± 0.54
Dry CH-HAp	3.73 ± 0.80
Dry CH-PLGA	1.90 ± 0.60
Dry CH-HAp-PLGA	2.64 ± 0.63
Hydrated CH	0.04 ± 0.01
Hydrated CH-HAp	0.04 ± 0.01
Hydrated CH-PLGA	0.44 ± 0.11
Hydrated CH-HAp-PLGA	0.49 ± 0.05

3.2.2.7 Water Uptake Capacity Results

The water uptake capacity of scaffolds at different times was tested by keeping them in phosphate buffer at 37°C and the data is given in Figure 3.27. Water uptake of a scaffold is necessary for the absorption of physiological fluid and for the transfer of nutrients and metabolites through the scaffold (Thein and Misra 2009). The water uptake capacity of chitosan scaffolds was higher when compared to CH-HAp, CH-PLGA and CH-HAp-PLGA scaffolds since chitosan is a very hydrophilic polymer due to its hydroxyl and amino groups on the backbone. The addition of HAp particles to chitosan caused a decrease in water uptake of chitosan. Similar trend of decrease in water uptake with HAp addition has been previously reported (Thein and Misra 2009, Pallela *et al.* 2012, Venkatesan *et al.* 2012). The pore size, porosity and distribution pattern of pores in the scaffold affect the water absorption (Thein and Kitiyanant 2006). Among prepared scaffolds, chitosan scaffold had the highest porosity. This might be one of the reasons that the highest amount of water was absorbed by it. All of the scaffolds took up water more than their own weight since the water uptake values were greater than 100% and they still maintained their shape and stability. Scaffolds started swelling rapidly in the first hour showing good swelling characteristic. Hydrophobic nature of PLGA decreased the water uptake capacity of scaffolds significantly. Chitosan scaffolds were swelled approximately 12 fold while PLGA containing chitosan scaffolds swelled 2 fold.

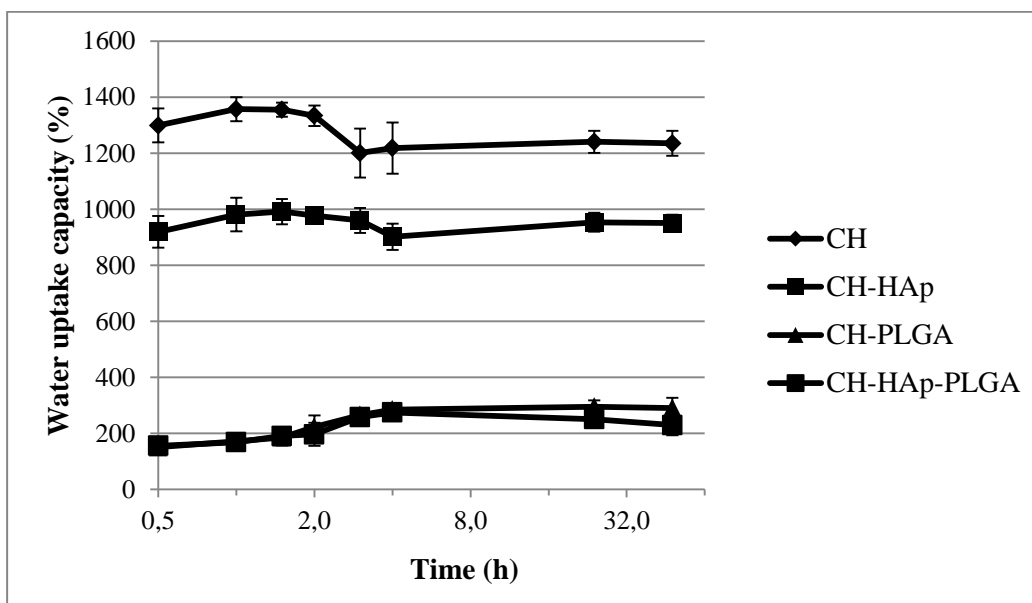


Figure 3.27 Water uptake capacity of the scaffolds

3.2.2.8 In vitro Degradation Results

Chitosan can be degraded by lysozyme. Lysozyme cleaves N-acetyl glucosamine sequences in the chitosan molecules, therefore, hydrolysis by lysozyme increases with increasing degree of N-acetylation in the polymer chain (Aiba 1992). It was reported that the chitosan with a high degree of N-acetylation crumbled into pieces after a few days of lysozyme treatment while chitosan with a low degree of N-acetylation remained relatively unchanged for a long time (Thein and Kitiyanant 2006, Ren *et al.* 2006). Thus, it is possible to adjust the degradation rate of chitosan. It has been reported that degradation of chitosan increases at acidic pH (Nordtveit *et al.* 1996). Therefore, a second polymer may be added to chitosan matrix that produces acidic byproducts during its own degradation. It can be possible to control the pH in the chitosan scaffold and further increase and control chitosan's degradation rate by controlling the second polymer's degradation rate. PLGA degrades with a chemical hydrolysis of the hydrolytically unstable ester bond into lactic acid and glycolic acid which are non-toxic. Therefore by incorporating PLGA into chitosan scaffolds it can be probable to control chitosan's degradation rate.

In previous studies we have observed that chitosan matrices did not show any significant weight loss in PBS or distilled water. Therefore, the degradation behavior was studied by incubating scaffolds in PBS in the presence of lysozyme and Figure 3.28 shows the degradation profile of scaffolds. In the degradation process of scaffolds by lysozyme, the enzyme must enter the scaffolds and react with the polymer. All of the scaffolds have porous structure about 5–200 μm pore sizes, which provide a large enough area for lysozyme to enter. Scaffolds retained a constant shape during degradation. The CH, CH-HAp and CH-HAp-PLGA scaffolds maintained 84%, 86% and 85% of their initial weight after 35 days of degradation, respectively. The CH-PLGA retained 75% of its initial weight, which showed a much faster rate of weight decrease than that of the other scaffolds. Probably because of acidic degradation products of PLGA, chitosan's degradation rate may have increased. However, when HAp was incorporated, degradation rate of CH-HAp-PLGA scaffolds was lower compared to CH-PLGA. Chitosan have cationic groups and HAp has calcium and phosphate ions. Therefore because of the probable interactions between amine group of chitosan and phosphate group of hydroxyapatite, HAp containing scaffolds may have an increased stability for enzymatic degradation.

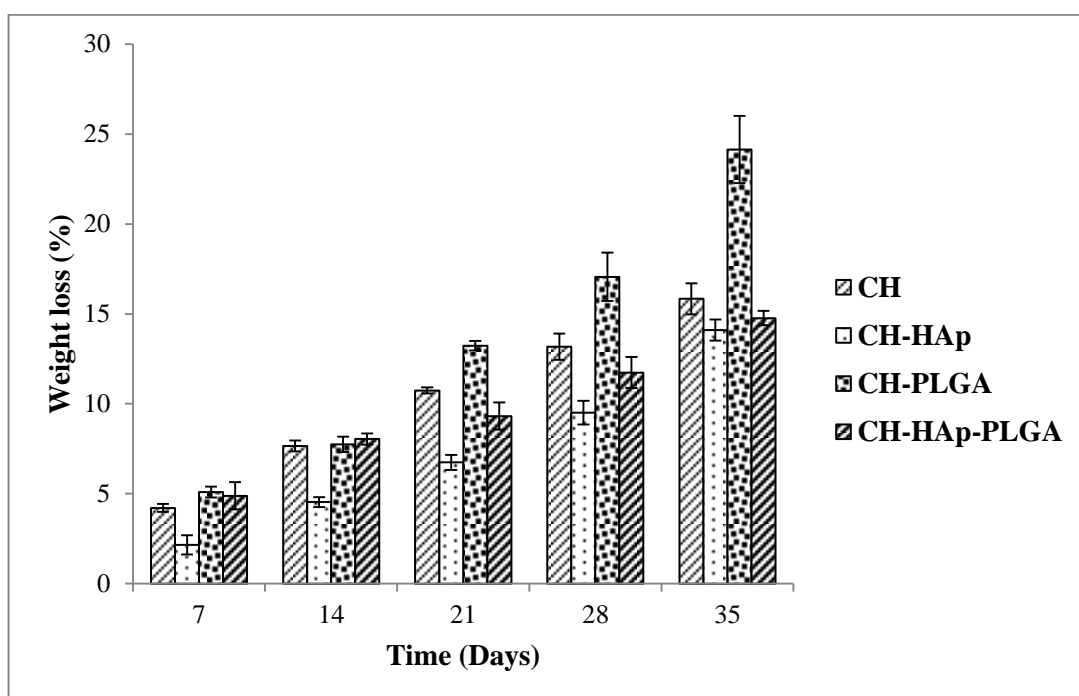


Figure 3.28 Degradation behavior of scaffolds in lysozyme containing PBS

3.2.2.9 Cell Culture Test Results

Cell adhesion and proliferation on a material are indicators of biocompatibility of the material and define the suitability of the material for tissue engineering applications. Chemistry, structure and morphology of the scaffolds, which are affected by the polymer, processing technique and sterilization conditions are some important factors that determine the biocompatibility of scaffolds. It is stated that adhesion and proliferation of cells on polymeric materials depends on the surface characteristics such as wettability, hydrophilicity/hydrophobicity ratio, bulk chemistry, surface charge and charge distribution, surface roughness and rigidity.

SaOs-2 cells were cultured on scaffolds and cell attachment and proliferation on these scaffolds was assessed by Alamar Blue assay. The cell proliferation of SaOs-2 cell line on scaffolds is given in Figure 3.29. It was observed that the initial cell attachment on all scaffolds (the day 1 values) were almost the same except the control, TCPS. It can be said that osteoblast cells could attach well on prepared scaffolds. Cell seeded scaffolds were incubated in RPMI medium at 37°C for 14 days. The number of cells on scaffolds increased with time. After 7 days, the cell numbers on all scaffolds were higher than those on day 1. On day 7 the cell number on CH-HAp scaffolds was higher than on CH scaffolds probably due to presence of HAp particles in the former. CH-PLGA scaffolds showed the highest cell number on days 7 and 14 among all the other scaffolds. However, CH-HAp-PLGA showed a lower cell number increase regardless of the presence of HAp which may be due to reduced porosity of this type of scaffold. Presence of PLGA did not have a significant influence in terms of attachment but positively affected proliferation of cells on CH-PLGA scaffolds. The scaffolds were stable in size and shape during the cell culture period; cell adhesion and proliferation on the scaffolds did not deform or shrink the surfaces. Cell number on TCPS control decreased between days 7 and 14 probably due to the confluence of the cells on the 2D control surfaces. Alamar results show that CH-PLGA scaffolds are suitable for osteoblast proliferation.

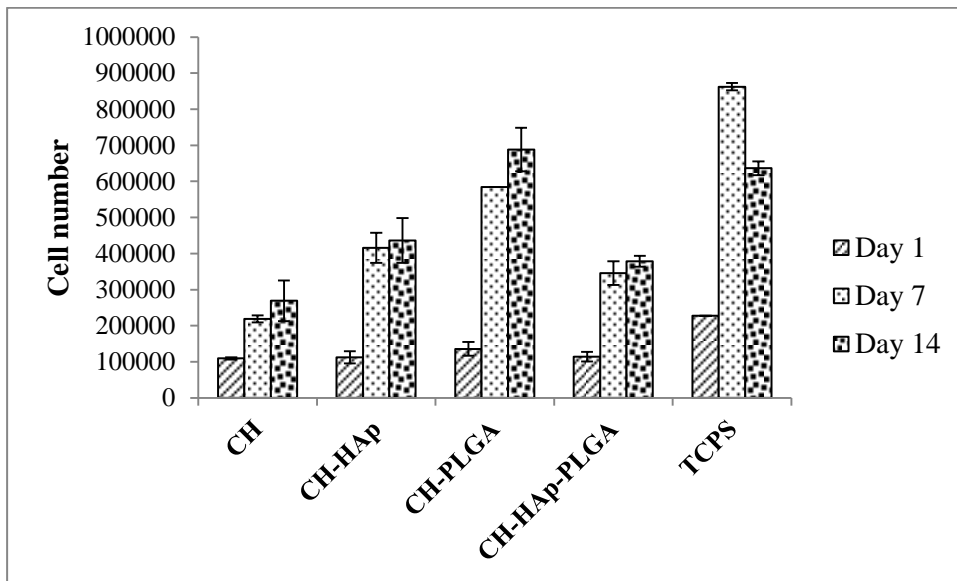


Figure 3.29 Proliferation of SaOs-2 cell line on the scaffolds

The morphology of cells on all the scaffolds was examined by SEM after 1 and 7 days of cell seeding (Figure 3.30 and Figure 3.31). After 1 day, the osteoblasts revealed a round shape. Cells were attached on scaffolds as well as within the pores. Then the cells proliferated and covered the surface of scaffolds forming multilayers after 7 days. The SEM images show cells attaching to the pore walls and making bridges between the pore walls (Figure 3.30 H). In addition, some cells could grow in the pores of the 3D scaffolds (Figure 3.30 F) and a number of filopodia extending on the scaffold were observed. Most of the cells were spread on day 7 as seen in the SEM micrographs.

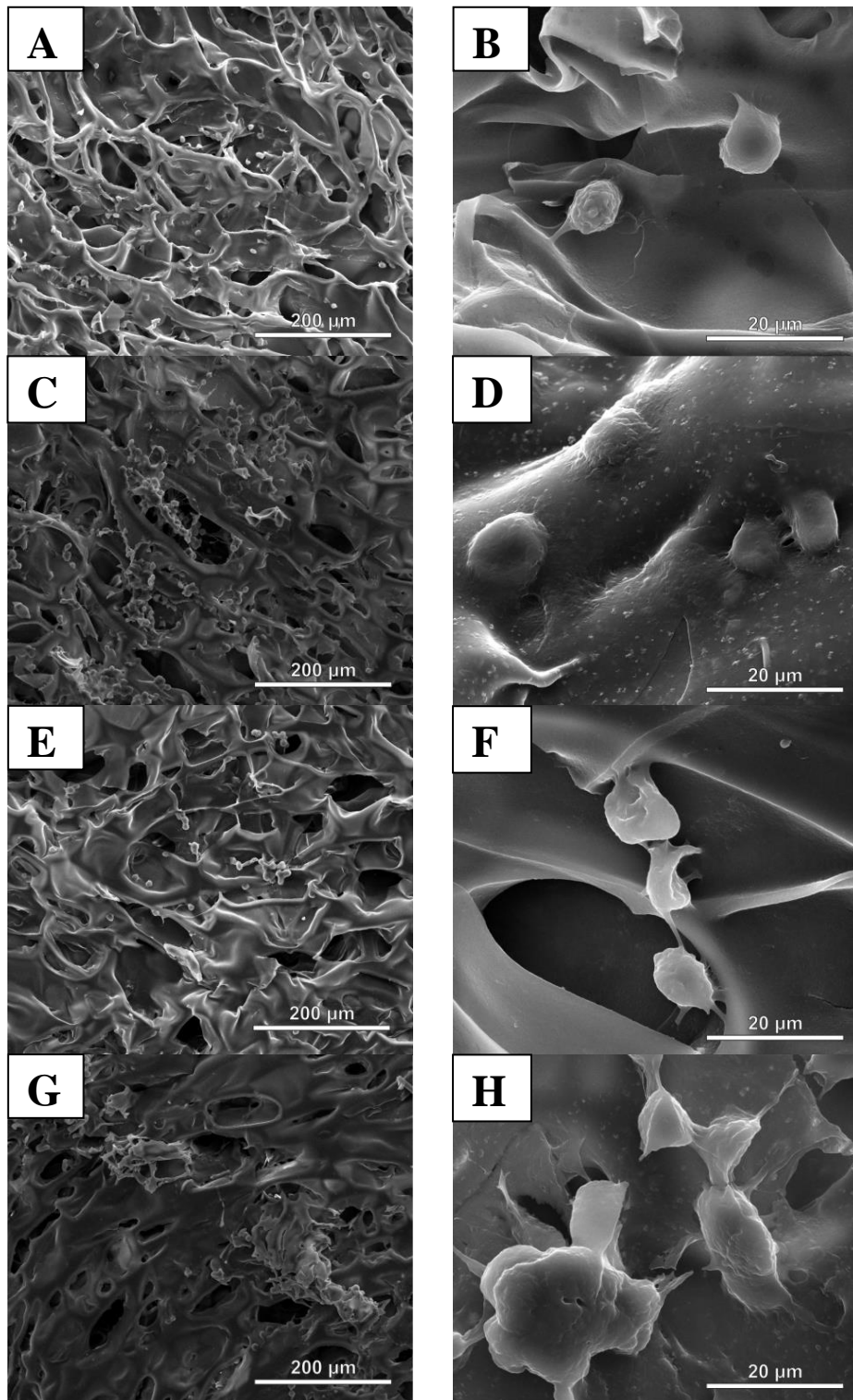


Figure 3.30 SEM micrographs of cell seeded foams. A, B) CH; C, D) CH-HAp; E, F) CH-PLGA; G, H) CH-HAp-PLGA. Day 1

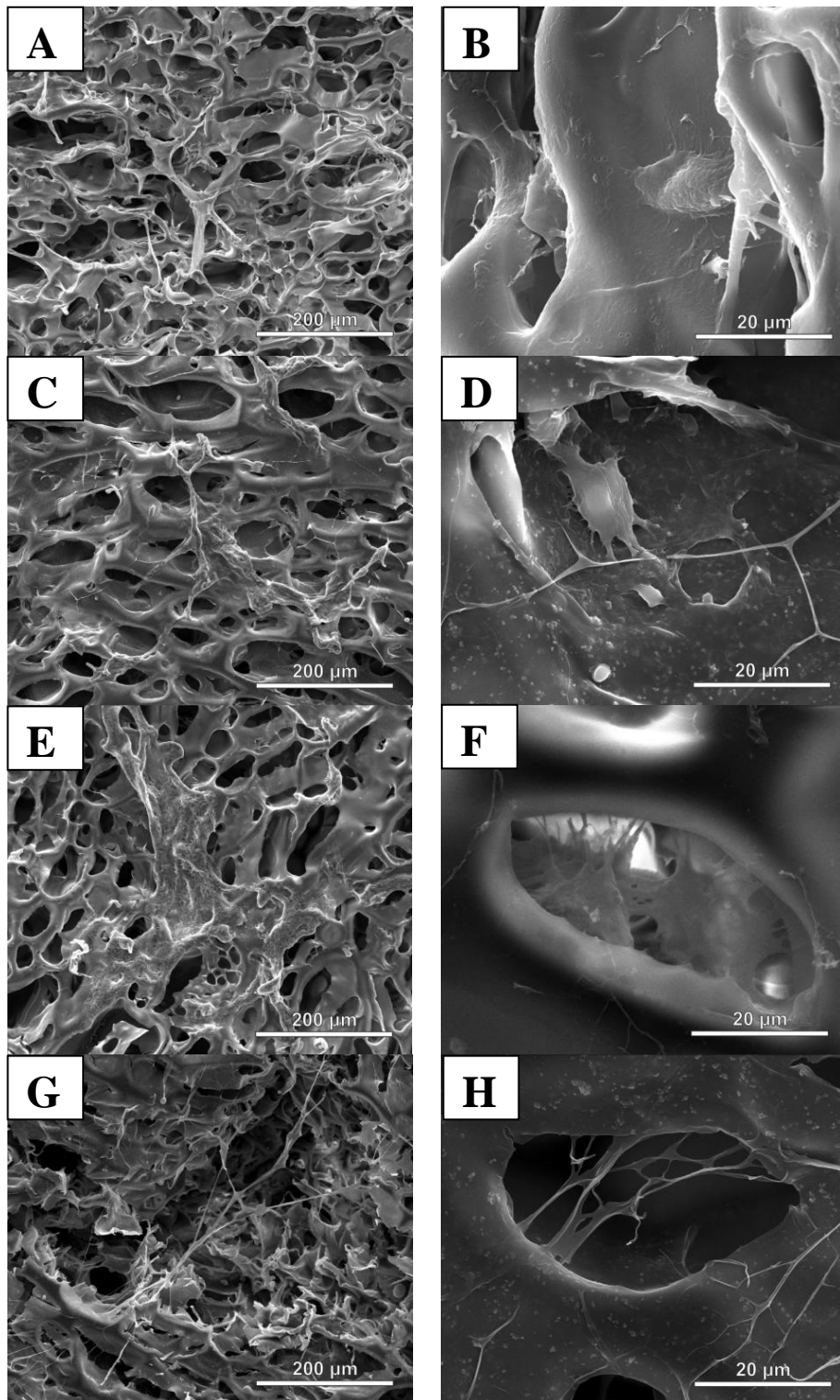


Figure 3.31 SEM micrographs of cell seeded foams. A, B) CH; C, D) CH-HAp; E, F) CH-PLGA; G, H) CH-HAp-PLGA. Day 7

In this part of the thesis, four different types of 3D polymeric scaffolds containing mainly chitosan and PLGA and/or HAp were prepared by freeze drying technique. All scaffolds had an interconnected macroporous structure with pore size ranging between 6 μm and 200 μm . Homogenous distribution of HAp particles was shown by SEM analysis in CH-HAp and CH-HAp-PLGA scaffolds. Porosity of the chitosan scaffold was found to be 89% and it decreased to 77% with PLGA and HAp incorporation due to increased hydrophobic polymer concentration and possible chemical interaction between the positive amine group of chitosan and negative groups of HAp. Addition of HAp particles in chitosan scaffold increased compressive modulus values of scaffolds, where crystalline HAp particles acted like a reinforcing agent. Incorporation of PLGA decreased the water uptake by the chitosan scaffold due to its hydrophobic nature, therefore, showed the highest compressive modulus value in hydrated state. When the degradation behavior of the scaffolds were examined we concluded that degradation rate of chitosan can be increased by incorporation of PLGA which has rapidly hydrolyzed lactide and glycolide components in the polymer chain. All the scaffolds were biocompatible, cell adhesion and proliferation were observed after cell seeding. Initial cell attachment was almost the same in all scaffolds but CH-PLGA scaffolds showed higher cell number compared to other scaffolds. Considering the interconnected porosity, high mechanical strength and in vitro cell proliferation CH-PLGA scaffolds appear to be the most suitable scaffold for bone tissue engineering applications.

3.3 Fibers Prepared by Electrospinning

Many extracellular proteins have a fibrous structure with fiber diameters varying from nanometer to submicrometer scales. For instance, the fiber diameter of collagen, which is the most abundant extracellular matrix (ECM) protein in the human body, changes between 50–500 nm. Electrospinning is a fiber fabrication technique which uses electrical forces to produce polymeric fibers with diameters ranging from 2 nm to several micrometers. Therefore, this technique can be used to prepare materials mimicking the fibrous extracellular matrix proteins for potential use as tissue engineering scaffolds.

3.3.1 Experimental

3.3.1.1 Materials

Poly(lactic acid-co-glycolic acid) (PLGA, type RESOMER® 503, 50:50 molar ratio D,L-lactic acid:glycolic acid, MW= 39.4 kDa) was purchased from Boehringer Ingelheim (Ingelheim, Germany). Chitosan (low viscosity, 75–85% deacetylated) was purchased from Fluka (Osaka, Japan). Acetic acid, trifluoroacetic acid (TFA) and 1,1,1,3,3,3-hexafluoro-2-propanol (HFIP) was obtained from Sigma Aldrich (Saint Louis, USA). Sodium hydroxide was obtained from J.T. Baker (Deventer, Holland). HAp particles used in the preparation of electrospun fibers were synthesized in the laboratory and the HAp synthesis was explained in freeze drying part in section 3.2.1.2. Calcium nitrate and ammonium phosphate were used in HAp synthesis and were purchased from Merck (Darmstadt, Germany). 25% ammonia solution was purchased from Carlo Erba. Lysozyme from chicken egg white (activity 96831 U.mg⁻¹) was bought from Fluka (Bornem, Belgium). Sodium azide was obtained from Scharlau (Barcelona, Spain). Roswell Park Memorial Institute (RPMI) Medium, fetal bovine serum (FBS) and penicillin/streptomycin (Pen/Strep) solution were obtained from Hyclone (Logan, UT, USA). Trypsin-EDTA (0.25%) was provided by Sigma (Utah, USA). Glutaraldehyde and cacodylic acid (sodium salt) were obtained from Sigma (Saint Louis, USA). Alamar Blue cell proliferation assay kit was from Biosource (Frederick, MD, USA).

3.3.1.2 Preparation of Electrospun Fibers

Chitosan was dissolved in TFA at a concentration of 3% (w/v). PLGA was dissolved in HFIP at a concentration of 15% (w/v). 6% (w/v) chitosan-PLGA blend solution (50:50 w/w) was prepared in HFIP:acetic acid (80:20 v/v). CH-PLGA-HAp fibers were electrospun from 6% (w/v) chitosan-PLGA blend solution containing HAp particles in 80:20 (w/w) ratio. All solutions were stirred at room temperature for 24 h to obtain a homogenous solution. These concentrations were chosen after optimization work carried out to produce fibers from polymer solutions.

The solutions were subjected to electrospinning at room temperature. Solutions were drawn into the syringe and the needle was attached. The syringe was then placed in the syringe pump and the flow rate on the pump was set. Then the high voltage supply was connected to the end of the needle and turned on. The electrospinning process was allowed to continue until the polymer solutions were finished. The polymer mats were collected on the collector plate. 5–15 $\mu\text{L}\cdot\text{min}^{-1}$ flow rate, 10–20 cm tip to collector distance and 21–27 kV voltage was applied to polymer solutions as process parameters. Chitosan containing fibers were crosslinked in a desiccator containing aqueous glutaraldehyde solution (10%, v/v) to preserve their form and to prevent them from disintegrating in the cell culture medium. Fiber mats were placed in a desiccator and crosslinked in the glutaraldehyde vapor at room temperature for 24 h. After crosslinking, the samples were kept under vacuum until use.

3.3.1.3 Characterization of Electrospun Fibers

3.3.1.3.1 Morphological Investigations

The electrospun fibers were examined with SEM (FEI, Quanta 400F, Eindhoven, Holland). For SEM examination, samples were mounted on aluminum stubs, sputter-coated with Au-Pd. The average fiber diameter of the electrospun fibers was measured from SEM micrographs using ImageJ programme.

3.3.1.3.2 Fourier Transform Infrared Spectroscopy

FTIR-ATR (Perkin Elmer, Spectrum BX-FTIR Spectrometer, Maryland, USA) analysis all samples were analyzed over 600-4000 cm^{-1} range with the resolution of 4 cm^{-1} . All spectra were averaged over 32 scans.

3.3.1.3.3 Differential Scanning Calorimetry

The thermal properties of the electrospun fibers were determined by differential scanning calorimetry (DSC, 910S/TA 2000, New Castle, USA). Approximately 5–10 mg samples were placed in aluminum DSC pans. Samples underwent two heating scans under nitrogen atmosphere from 0°C to 200°C. Heating rate was 10°C.min⁻¹.

3.3.1.3.4 In vitro Degradation Tests

The stability of the fibers was evaluated by incubating in aqueous media with the presence of lysozyme enzyme. For enzymatic degradation, matrices were placed into vials containing 5 mL of PBS (0.01 M, pH 7.4) with 0.5 mg.mL⁻¹ enzyme and 0.5 mg.mL⁻¹ of sodium azide to inhibit bacterial growth and incubated at 37°C within a water bath shaker. The solutions were changed every two days. Samples were removed periodically, washed with distilled water, freeze dried and weighed in order to examine the weight loss due to erosion of the samples. The weighed samples were then placed back into the fresh PBS medium containing enzyme and sodium azide. Three parallel experiments were carried out for samples of each type of sample and the measured values were averaged. Percentage weight loss was calculated as follows:

$$\text{Weight loss (\%)} = [(w_0 - w_1)/w_0] \times 100$$

where w_0 and w_1 are weight of dry samples before and after enzymatic degradation test, respectively.

3.3.1.3.5 Cell Culture Tests

Fibers were sterilized in 70% ethanol for 30 min and then washed 3 times with PBS (pH 7.4, 0.01 M) to remove remaining ethanol. Cell culture studies were conducted using human osteosarcoma cell line SaOs-2. Aliquots of 10 μL of cell suspension containing 20,000 cells were seeded dropwise on the scaffolds. After incubation for 30 min, complete RPMI medium (1 mL) was added and cells were maintained at 37°C in the CO₂ incubator. Medium was changed every two days.

Alamar Blue™ assay was used to determine cell numbers on the fibers after 1, 4, 7 days. The active ingredient of Alamar Blue (resazurin) is a nontoxic, cell penetrating compound that is virtually nonfluorescent. Upon entering the cells, resazurin is reduced to resorufin, which produces a very bright red fluorescence. Viable cells continuously convert resazurin to resorufin, thereby generating a quantitative measure of cell viability. After transferring of SaOs-2 seeded scaffolds into a new, sterile 24 well plate and washing with sterile PBS, 1 mL of Alamar Blue solution (10% in colorless medium) was added to each sample in the 24 well plate and incubated for 1 h at 37°C in the CO₂

incubator (all experiments were performed in triplicate). After 1 h incubation, 200 μ L of solution from each well was transferred to a new 96 well plate. Absorbance was measured at 570 nm and 595 nm using an Elisa Plate Reader (Molecular Devices, Vmax Microplate Reader, California, USA). The cell morphology was studied with SEM. For this, samples were fixed in 1% glutaraldehyde solution, rinsed with cacodylate buffer and freeze dried. After drying, the samples were mounted on aluminum stubs, sputter-coated with Au-Pd and examined.

3.3.2 Results and Discussion

3.3.2.1 Morphological Analysis Results

The morphology of the nanofibrous membranes are given in Figure 3.32. Average diameter of fibers measured from SEM micrographs is given in Table 3.4. Fibers with diameters in the range of nanometers to a few microns can be obtained by electrospinning technique. Applied voltage, polymer concentration, distance between the tip and collector and flow rate had important effects on fiber diameter. With increasing voltage, the polymer jet is discharged with a greater electrostatic repulsion that causes it to undergo higher levels of drawing stress resulting in the decrease of the fiber diameter. Moreover, increasing polymer concentration and decreasing the tip to collector distance increases fiber diameter. In this thesis randomly oriented nanofibrous fibers were obtained by electrospinning technique. For electrospinning of PLGA, HFIP was used as the solvent. Chitosan fibers were electrospun from 3% chitosan solution prepared in trifluoro acetic acid, and fibers had an average fiber diameter of 222 nm as measured from SEM micrographs. Chitosan was dissolved in aqueous acetic acid (5%, 80% and 90%), formic acid and trifluoro acetic acid. The electrospinning of chitosan solution prepared with mentioned solvents was performed with different process parameters. However, chitosan fiber could not be obtained with these solvents except TFA since it was not easy to obtain fibers from chitosan solution due to hydrogen bonds. It is reported in the literature that TFA forms salts with the amino groups of chitosan that destroys the rigid interaction between the chitosan molecules which makes it easy to be electrospun. Also TFA is a volatile solvent that is advantageous for electrospinning (Ohkawa *et al.* 2004). When TFA was used as a solvent chitosan fibers were deposited on the collector. However proper CH-PLGA fibers could not be electrospun from CH-PLGA solution prepared in TFA. Instead HFIP:acetic acid solvent couple yielded better fibers having less bead than blend fibers prepared in trifluoro acetic acid. A fiber diameter distribution from 85 nm to 365 nm with an average fiber diameter of 167 nm was observed for CH-PLGA-HAp fibers although some formation of beads as electrospinning defects was noticed in the membranes resulting from HAp particles. PLGA fibers with average fiber diameter of 525 nm were obtained, the fiber diameter was higher compared to other fibers since they were electrospun from a solution having higher polymer concentration.

Table 3.4 Average diameter of fibers

Sample	Average fiber diameter (nm)
CH	222 ± 91
CH-PLGA	183 ± 58
CH-PLGA-HAp	167 ± 52
PLGA	525 ± 151

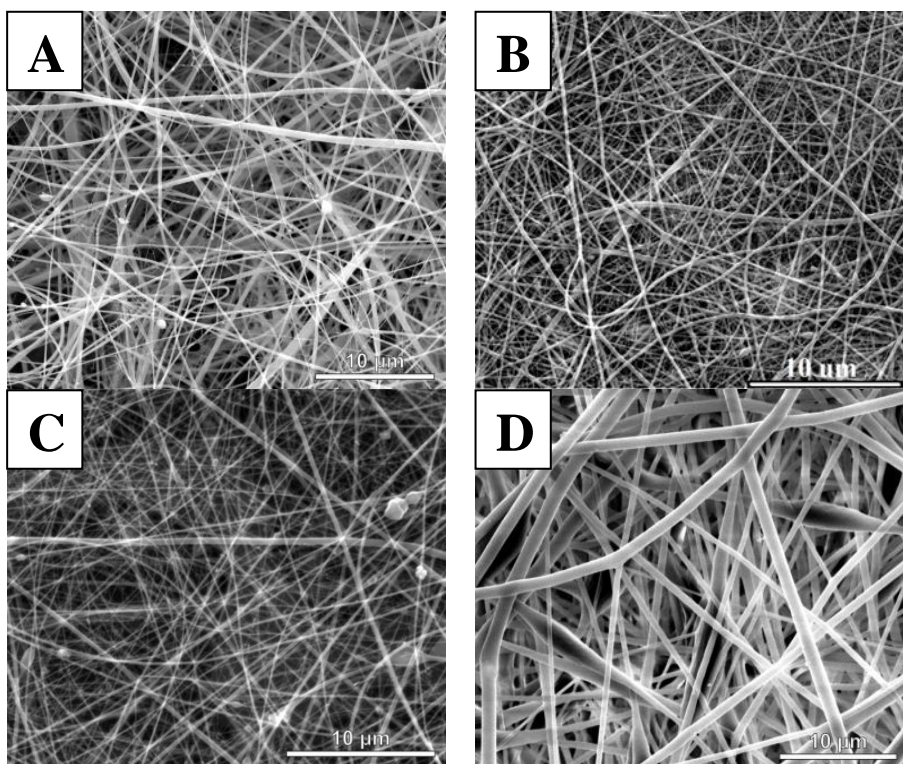


Figure 3.32 SEM micrographs of fibers A) CH; B) CH-PLGA; C) CH-PLGA-HAp; D) PLGA

3.3.2.2 Fourier Transform Infrared Spectroscopy Results

The FTIR-ATR spectra of fibers is given in Figure 3.33. For chitosan nanofibers, characteristic broad band around 3350 cm^{-1} are attributed to -OH linked to polymer, while 1660 cm^{-1} and 1560 cm^{-1} are the characteristic peaks of the stretching vibration of C=O amide bond and N-H bending vibration in amine groups, respectively. The peak at 2930 cm^{-1} corresponds to C-H stretching vibrations and cyclic -H stretching. The peaks at 1152 cm^{-1} , 1068 cm^{-1} and 1032 cm^{-1} correspond to C-O stretching vibrations. In the spectrum of PLGA fiber the peak at 1745 cm^{-1} is attributed to the carbonyl stretching of the ester. The peaks at about 2950 cm^{-1} correspond to CH stretching. The presence of a peak at 1452 cm^{-1} is due to CH_3 bending and a peak at 1130 cm^{-1} is due to the C-O stretching of the ester groups. When the FTIR-ATR spectrum of CH-PLGA fiber is examined characteristic peaks of both chitosan and PLGA were present. The position of the peaks almost didn't change which may be due to weak molecular interaction between chitosan and PLGA because PLGA does not have enough OH groups to form hydrogen bonds with OH groups and NH_2 groups in chitosan.

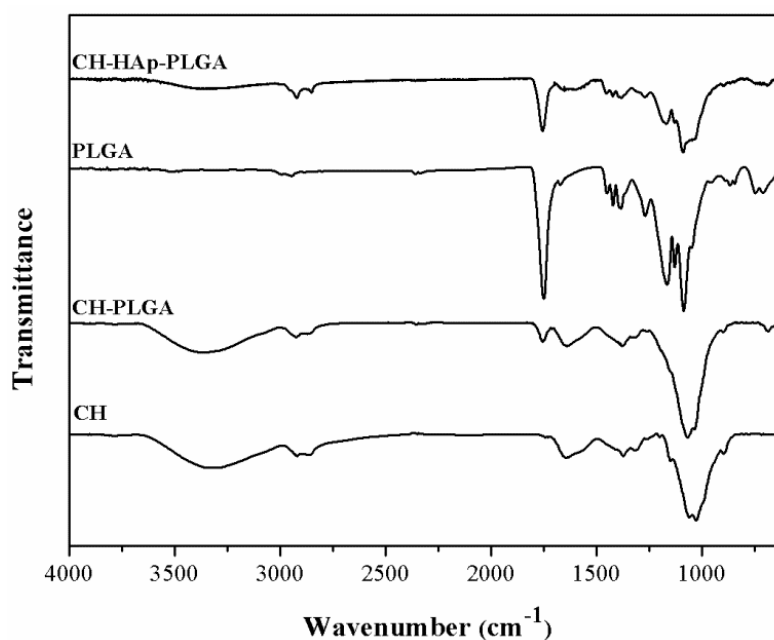


Figure 3.33 FTIR-ATR spectra of fibers

3.3.2.3 Differential Scanning Calorimetry Results

DSC thermograms and results of fibers are given in Figure 3.34 and Table 3.5. The pure PLGA fiber exhibited an endothermic event at 52°C referring to the aging peak that followed T_g in the first scan. There was no melting point for PLGA fibers since PLGA is amorphous. The DSC thermogram of chitosan fibers showed an endothermic peak at around 90°C in the first scan which was attributed to absorbed water in the polymer. In the second scan this endothermic peak disappeared since water was evaporated during the first heating. DSC thermograms of CH-PLGA and CH-PLGA-HAp fibers showed two endothermic peaks that referring to T_g of PLGA at about 50°C and evaporation of water at 90°C.

Table 3.5 Results of DSC analysis of fibers

	1st Scan		2nd Scan
	T _g (°C)	T _{peak} (°C)	T _g (°C)
CH	-	91.5	-
CH-PLGA	50.4	77.2	-
CH-HAp-PLGA	52.5	80.7	-
PLGA	51.9	-	45.3

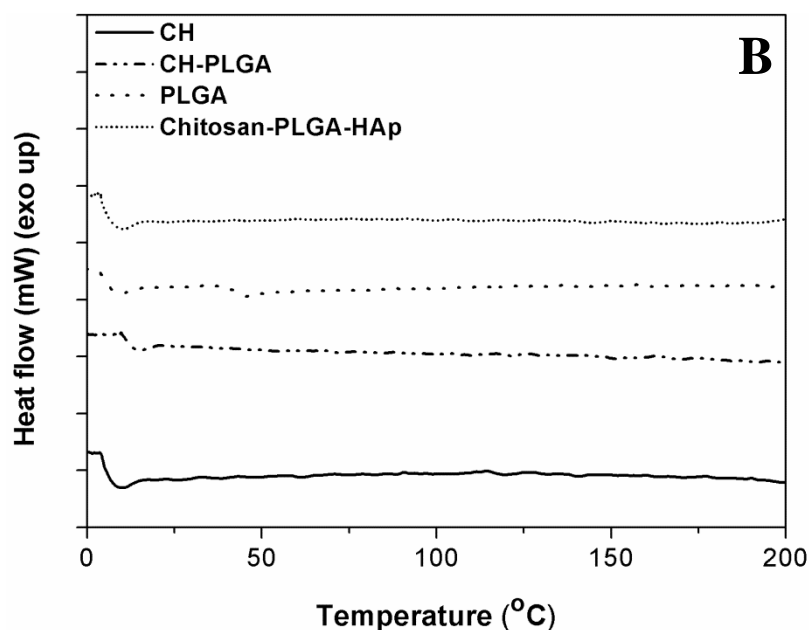
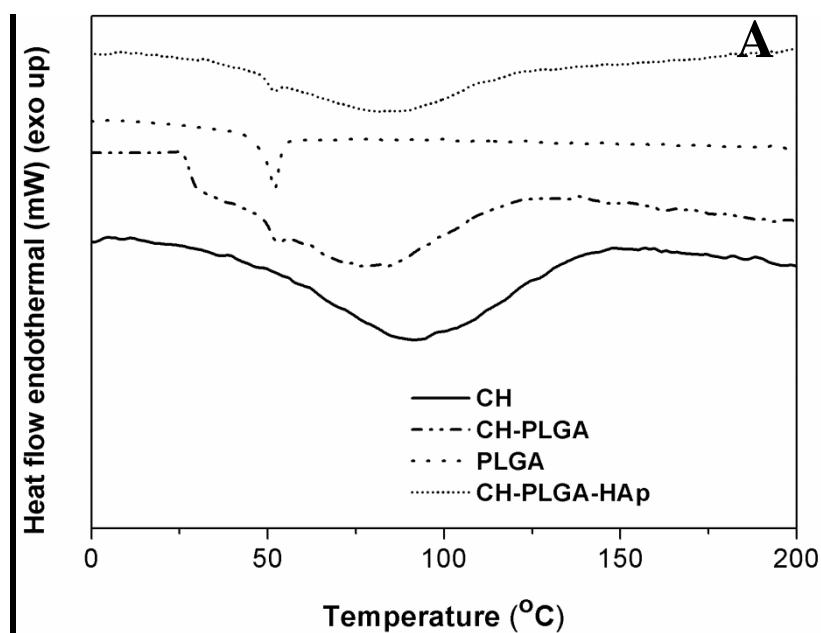


Figure 3.34 DSC thermograms of fibers A) 1st run, B) 2nd run

3.3.2.4 In vitro Degradation Results

The degradation behavior of fibers was studied by incubating them in lysozyme containing PBS for five weeks. The extent of degradation was expressed as percentage of weight loss of the fibers and degradation profile is given in Figure 3.35. Chitosan fibers retained 13% of their weight after 4 weeks of degradation while PLGA fibers exhibited significantly faster degradation. They started to disintegrate after 2 weeks and it was not possible to monitor its degradation afterwards. It was seen that introduction of PLGA into chitosan influenced degradation behavior and 50% of CH-PLGA

fibers was degraded after 4 weeks. It was concluded that the degradation rate of chitosan fibers can be tailored by addition of PLGA.

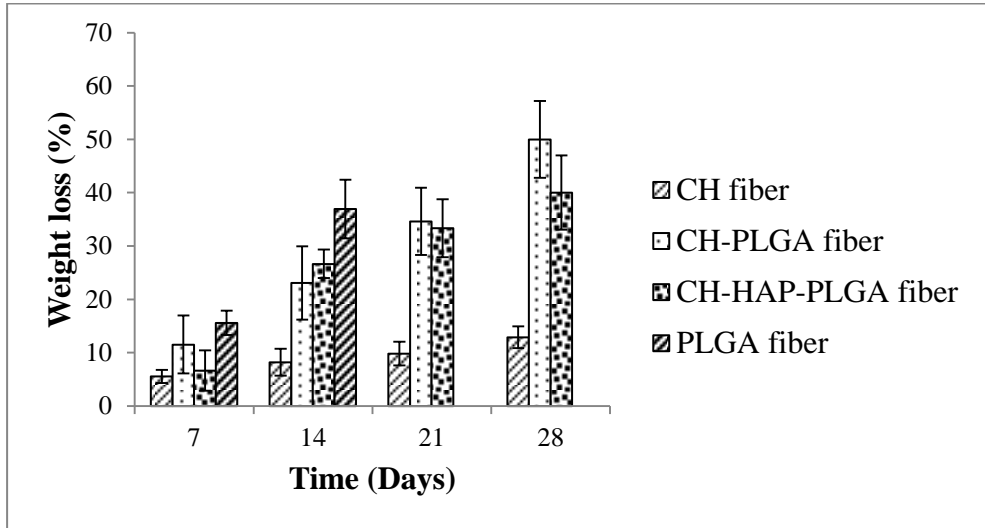


Figure 3.35 Degradation behavior of fibers in lysozyme containing PBS

3.3.2.5 Cell Culture Test Results

The viability measured by Alamar assay of SaOs-2 cells cultured on electrospun CH, CH-PLGA, CH-PLGA-HAp and PLGA fibers on days 1, 4 and 7 is shown in Figure 3.36. The number of osteoblasts cultured on each fiber increased on the fourth and seventh day compared to day 1 indicating that the ability of fibers to support growth of osteoblast cells (Figure 3.36). Cell number increased with incorporation of PLGA in chitosan fibers and cell number was higher on CH-PLGA-HAp fibers on day 7. Cell culture tests showed that all electrospun fibers promoted cell attachment and proliferation. SEM results are given in Figure 3.37 and Figure 3.38. Electrospun nanofibers provided a large surface area for cells to attach. It can be seen that SaOs-2 cells attached on all membranes and started to change their original round shape to elongated shape. On CH-PLGA-HAp fibers cells were round on day 1 and they were fully extended after 7 days. Some filopodia like extensions could be seen on fibers on some of the cells (Figure 3.37 F and H).

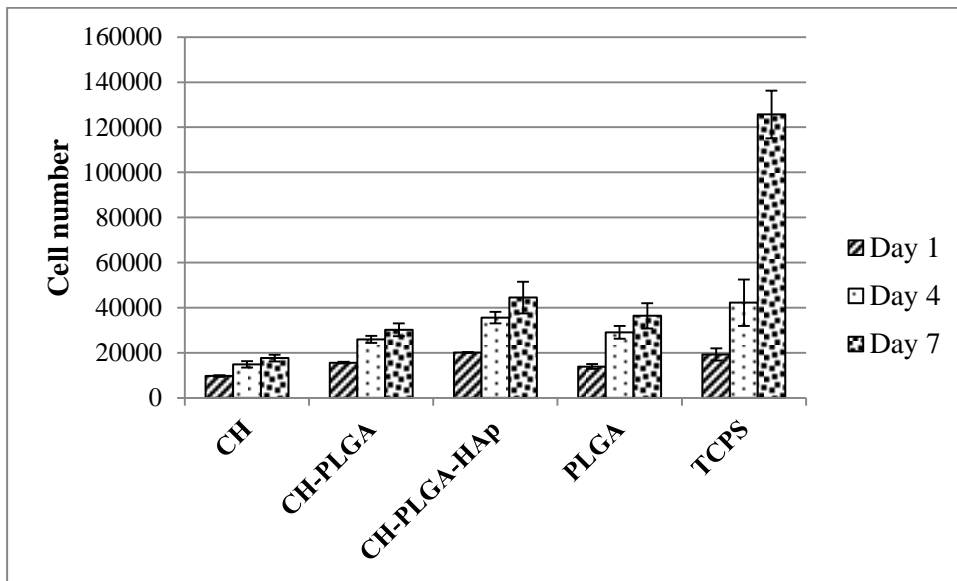


Figure 3.36 Proliferation of SaOs-2 cells on the electrospun fibers

The effect of chitosan on cell attachment and proliferation has been contradictory. Some studies reported that unmodified chitosan films exhibited poor cell adhesion. Different approaches have been used to improve cell-chitosan by changing the surface functionality with several techniques such as plasma modification, blending, and protein adsorption (Silva *et al.* 2008, Custodio *et al.* 2010, Lopez-Perez *et al.* 2010). In this study chitosan fibers were modified by blending with PLGA and HAp and cell culture tests showed that cell attachment on CH-PLGA-HAp fibers was higher compared to chitosan fibers. It was observed that cells seeded on fibers could interact with the surrounding fibers and cells. Favorable interaction between cell-cell and cell-matrix was shown by cell morphology. After 7 days of cell culture, cells were spread, they covered relatively larger area on a lot of nanofibers compared to day 1 and formed sheets on fibers. It was concluded that these fibers have the potential to serve as scaffolds for bone tissue engineering.

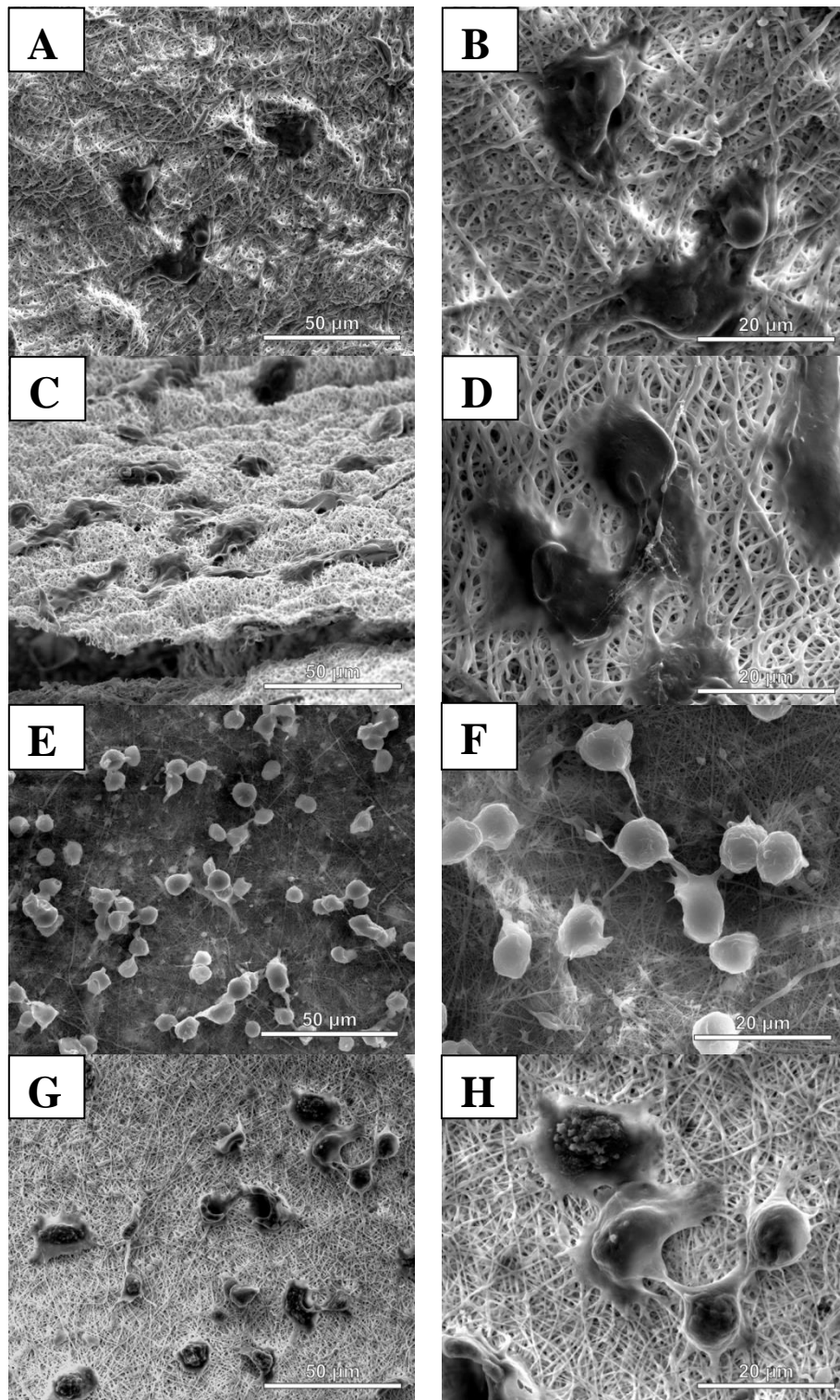


Figure 3.37 SEM micrographs of cell seeded fibers on day 1 A, B) CH; C, D) CH-HAp; E, F) CH-PLGA; G, H) CH-HAp-PLGA presented with different magnifications

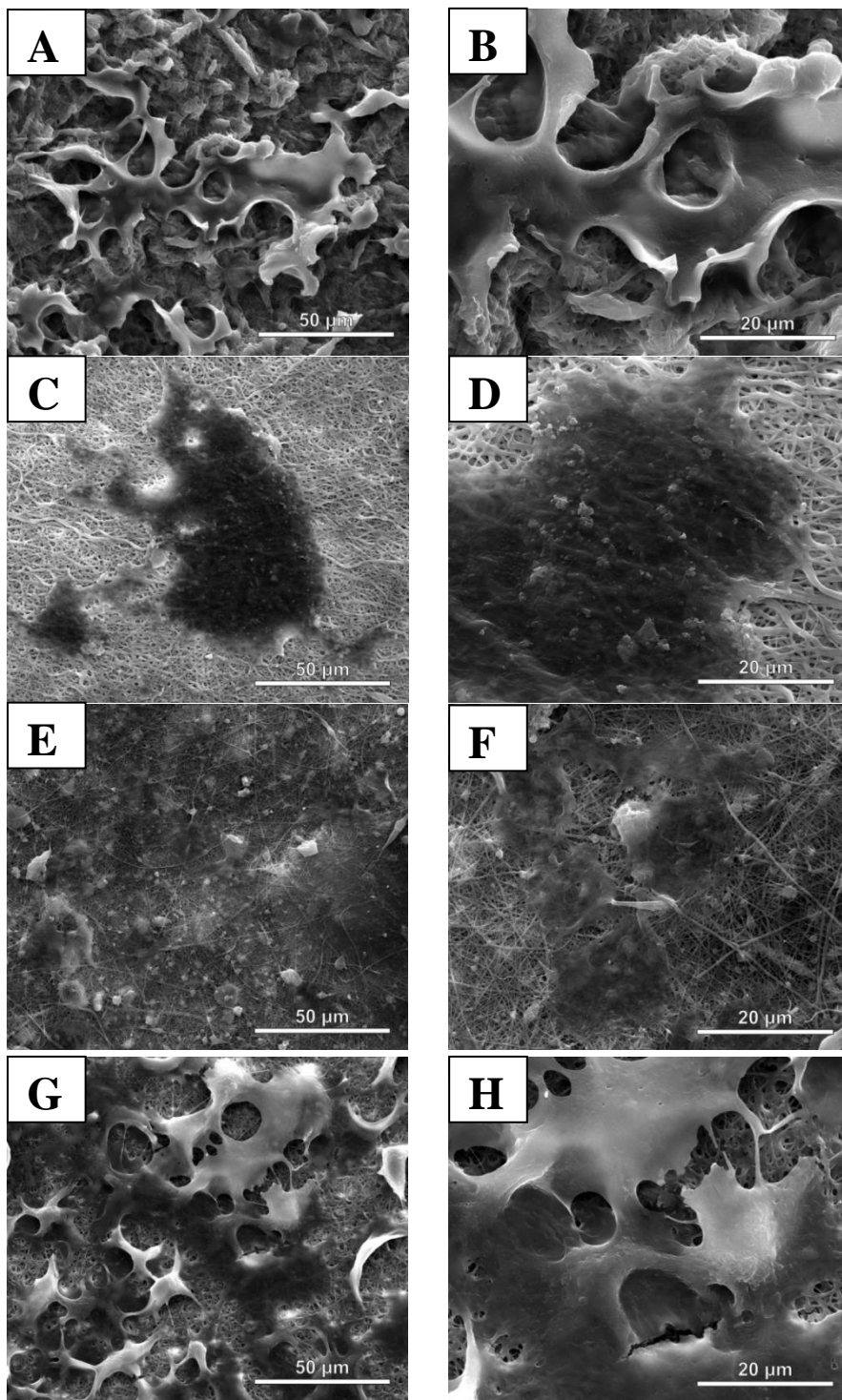


Figure 3.38 SEM micrographs of cell seeded fibers on day 7 A, B) CH; C, D) CH-HAp; E, F) CH-PLGA; G, H) CH-HAp-PLGA presented with different magnifications

CHAPTER 4

CONCLUSIONS

Bone replacement materials are needed for a variety of reasons. They are required when a part of a bone tissue is lost or damaged and the gap needs to be filled in, for example after an accident or after the removal of a tumour. There are several approaches for bone replacement like allografts, autografts and synthetic materials. Usage of artificial materials as bone substitute is an important alternative to bone grafting. Metals, ceramics, polymers and composites are commonly used either as supporting materials for the natural tissue, or as degradable scaffolds for tissue engineering purposes. There is extensive research on developing innovative bone support materials with new chemical, structural and biological properties in order to imitate the characteristics of the bone.

This thesis focused on preparation and characterization of polymeric bone supports for hard tissue applications. For this purpose in the first part of the thesis HAp containing acrylic based bone cements were prepared by using PMMA particles having three different particle size and adding various ingredients such as 1-dodecyl mercaptan (DDM), ammonium nitrate, zeolite or chitosan into the formulations. When effect of particle size of PMMA considered, it was observed that using PMMA particles with 50–150 μm particle size range would be more appropriate due to handling and setting properties while there was no significant difference in mechanical properties of bone cement prepared with PMMA having different particle size. As a novel approach oxygen plasma was applied to the powder part of bone cements in order to improve mechanical properties by increasing the compatibility of polymeric and inorganic components. In addition, zeolite was added and its effect on mechanical and curing properties of bone cement formulations was investigated for the first time in the literature. It was possible to decrease maximum curing temperature of bone cements to 71°C and 65°C with DDM and ammonium nitrate, respectively, however, there were undesirable decreases in mechanical strengths (almost 30%). That drawback was eliminated with zeolite addition by diffusion of methyl methacrylate monomer into pores of zeolites and incorporation of some polymer chains within the pores of zeolite particles during setting reaction of liquid part and powder part of bone cement and providing better mechanical interlock between resultant organic-inorganic composites. Furthermore incorporation of chitosan had improved ultimate compressive strength up to 97 MPa and decreased the maximum curing temperature of bone cements to 59°C and also induced new osteoid formation when applied to the defects in rat knee. The compressive strength of chitosan containing bone cement was above the required minimum value, its curing temperature was much lower than the commercial cement and new bone formation was observed. Therefore, considering mechanical, thermal and biological properties they can be good candidates as bone cements.

In the second part of the thesis 2D and 3D porous scaffolds were prepared for bone tissue engineering applications by using chitosan and PLGA as the biodegradable biopolymeric component and HAp as the mineral component through microfabrication, freeze drying and electrospinning techniques.

- By microfabrication technique, porous 2D membranes with regular square holes at micron level were obtained instead of 3D scaffolds because of collapsing of the polymer layers. It was concluded that this technique is not suitable for chitosan and PLGA polymers to produce 3D structures.
- By freeze drying technique, 3D scaffolds having interconnected macroporous structure with an approximate pore size ranging between 6 μm and 200 μm were obtained. Porosity of chitosan scaffold was found as 89%, but the porosity of CH-HAp-PLGA scaffold decreased to 77% with PLGA and HAp incorporation due to increased polymer concentration and

possible chemical interaction between amine group of chitosan and HAp. When mechanical properties compared addition of HAp had positive effect and in hydrated state CH-PLGA scaffolds had highest compressive strength (0.44 MPa) since hydrophobicity of PLGA decreased water uptake property and maintained its strength. It was shown that degradation behavior of chitosan scaffolds can be tailored with addition of PLGA. Alamar cell viability test showed that all scaffolds allowed cellular attachment and proliferation. CH-PLGA scaffolds showed higher proliferation rate compared to other scaffolds. Cell proliferation of CH-HAp-PLGA scaffold was not as high as CH-PLGA scaffolds despite the presence of HAp particles probably due to reduced porosity. Based on properties such as interconnected porosity, high mechanical strength and in vitro cell proliferation it can be concluded that CH-PLGA blend scaffolds have the potential to be used in hard tissue engineering applications among other scaffolds.

- By electrospinning technique, CH, CH-PLGA, CH-PLGA-HAp and PLGA nanofibers having fiber diameter between 180 nm and 525 nm were successfully prepared. It was observed that PLGA fibers disintegrated in aqueous media in two weeks. Therefore it was advantageous to prepare blend (CH-PLGA) and composite (CH-PLGA-HAp) fibers for stability and cell affinity properties.

It was concluded that CH-PLGA scaffolds prepared by freeze drying and CH-PLGA fibers prepared by electrospinning technique combine the advantages of both PLGA and chitosan polymers, which make them more suitable for non-load bearing bone tissue engineering applications. However in order to have detailed information about cell-material interaction, in vivo and histological examinations of the scaffolds and fibers are needed.

REFERENCES

- Agrawal C.M., Athanasiou K.A. Techniques to control pH in vicinity of biodegrading PLA/PGA implants. *J. Biomed. Mater. Res. Appl. Biomater.* 1997, 38(2): 105-114.
- Aiba S. Studies on chitosan: Lysozymic hydrolysis of partially N-acetylated chitosans. *Int. J. Biol. Macromol.* 1992, 14: 225-228.
- Alberto D.M., Sittinger M., Risbud M.V. Chitosan: a versatile biopolymer for orthopedic tissue-engineering. *Biomaterials.* 2005, 26: 5983-5990.
- Albrektsson T., Johansson C. Osteoinduction, osteoconduction and osseointegration. *Eur. Spine J.* 2001, 10: S96-S101.
- Aoki H. Medical applications of hydroxyapatite. Ishiyaku Euro America Inc., Tokyo, St. Louis, Takayama Press, 1994.
- Arens D., Rothstock S., Windolf M., Boger A. Bone marrow modified acrylic bone cement for augmentation of osteoporotic cancellous bone. *J. Mech. Behav. Biomed. Mater.* 2011, 4: 2081–2089.
- Bao C., Chen W., Weir M.D., Thein H.W., Xu H.H.K. Effects of electrospun submicron fibers in calcium phosphate cement scaffold on mechanical properties and osteogenic differentiation of umbilical cord stem cells. *Acta Biomater.* 2011, 7 (11): 4037-4044.
- Baron R. Anatomy and ultrastructure of bone. In M.J. Favus, ed. *Primer on the metabolic bone diseases and disorders of mineral metabolism.* Pages 3-10, Lippencott Williams&Wilkins, Philadelphia, Pennsylvania, 1999.
- Barrere F., Blitterswijk C.A.V., Groot K.D. Bone regeneration: molecular and cellular interactions with calcium phosphate ceramics. *Int. J. Nanomedicine.* 2006, 1(3): 317–332.
- Bergsma E.J., Brujn W., Rozema F.R., Bos R.M., Boering G. Late tissue response to poly(L-lactide) bone plates and screws. *Biomaterials.* 1995, 16(1): 25-31.
- Bhardwaj N., Chakraborty S., Kundu S.C. Freeze-gelled silk fibroin protein scaffolds for potential applications in soft tissue engineering. *Int. J. Biol. Macromol.* 2011, 49(3): 260-267.
- Bohner M. Design of ceramic-based cements and putties for bone graft substitution. *Eur Cells Mater.* 2010, 20: 1–12
- Bong-Soon C., Choon-Ki L., Kug-Sun H., Hyuk-Joon Y., Hyun-Seung R., Sung-Soo C., Kun-Woo P. Osteoconduction at porous hydroxyapatite with various pore configuration. *Biomaterials.* 2000, 21: 1291-1298.
- Bose S., Roy M., Bandyopadhyay A. Recent advances in bone tissue engineering scaffolds. *Trends Biotechnol.* 2012, 30(10): 546-554.
- Boxberger J.I., Adams D.J., Diaz-Doran V., Akkarapaka N.B., Kolb E.D. Radius fracture repair using volumetrically expanding polyurethane bone cement. *J. Hand. Surg. Am.* 2011, 36(8): 1294-1302.

- Brauer G.M., Steinberger D.R., Stansbury J.W. Dependence of curing time, peak temperature, and mechanical properties on the composition of bone cement. *J. Biomed. Mater. Res.* 1986, 20(6): 839-852.
- Canal C., Ginebra M.P. Fibre-reinforced calcium phosphate cements: a review. *J. Mech. Behav. Biomed. Mater.* 2011, 4: 1658-1671.
- Cao L., Zeng L., Huang J., Guo S., Zhang H. Preparation and property of short carbon fiber reinforced HA/PMMA bio-composites. *Fuhe Cailiao Xuebao/Acta Materiae Compositae Sinica.* 2009, 26: 138-142.
- Carletti E., Endogan T., Hasirci N., Hasirci V., Maniglio D., Motta A., Migliaresi C. Microfabrication of PDLA scaffolds. *J. Tissue Eng. Regen. Med.* 2011, 5: 569-577.
- Cervantes-Uc J.M., Vazquez-Torres H., Cauich-Rodriguez J.V., Vazquez-Lasa B., San Roman del Barrio J. Comparative study on the properties of acrylic bone cements prepared with either aliphatic or aromatic functionalized methacrylates. *Biomaterials.* 2005, 26: 4063-4072.
- Ceyhan T., Tatlier M., Akcakaya H. In vitro evaluation of the use of zeolites as biomaterials: effects on simulated body fluid and two types of cells. *J. Mater. Sci. Mater. Med.* 2007, 18: 1557-1562.
- Charnley J. Anchorage of the femoral head prosthesis to the shaft of the femur. *J. Bone Joint Surg. (Br).* 1960, 42-B: 28-30.
- Chen C.F., Shen H.H., Lin T.Y., Yu Y.J., Chen W.C., Chu I.M. Studies on the preparation and characterization of mPEG-polyester biodegradable biogluce for bone defect repair. *J. Med. Biol. Eng.* 2011, 31(1): 13-17.
- Chen G., Ushida T., Tateishi T. Poly(dl-lactic-co-glycolic acid) sponge hybridized with collagen microsponges and deposited apatite particulates. *J. Biomed. Mater. Res.* 2001, 57 (1): 8-14.
- Chen W.C., Lin J.H.C., Ju C.P. Transmission electron microscopic study on setting mechanism of tetracalcium phosphate/dicalcium phosphate anhydrous-based calcium phosphate cement. *J. Biomed. Mater. Res. A.* 2003, 64: 664-671.
- Chen Z., Mo X., Qing F. Electrospinning of collagen-chitosan complex. *Mater. Lett.* 2007, 61: 3490-3494.
- Cicek G., Aksoy E.A., Durucan C., Hasirci N. Alpha-tricalcium phosphate (α -TCP): solid state synthesis from different calcium precursors and the hydraulic reactivity. *J. Mater. Sci: Mater. Med.* 2011, 22: 809-817.
- Custodio C.A, Alves C.M., Reis R.L., Mano J.F. Immobilization of fibronectin in chitosan substrates improves cell adhesion and proliferation. *J. Tissue Eng. Regen. Med.* 2010, 4: 316-323.
- Dandurand J., Delpech V., Lebugle A., Lamure A., Lacabanne C. Study of the mineral-organic linkage in an apatitic reinforced bone cement. *J. Biomed. Mater. Res.* 1990, 24: 1377-1384.
- Danilchenko S.N., Kalinkevich O.V., Pogorelov M.V., Kalinkevich A.N., Sklyar A.M., Kalinichenko T.G., Ilyashenko V.Y., Starikov V.V., Bumeyster V.I., Sikora V.Z., Sukhodub L.F. Characterization and in vivo evaluation of chitosan-hydroxyapatite bone scaffolds made by one step coprecipitation method. *J. Biomed. Mater. Res. Part A*, 2011, 96A: 639-647.

- Daoud J.T., Petropavlovskaja M.S., Patapas J.M., Degrandpré C.E., DiRaddo R.W., Rosenberg L., Tabrizian M. Long-term in vitro human pancreatic islet culture using three-dimensional microfabricated scaffolds. *Biomaterials*. 2011, 32: 1536-1542.
- Deb S., editor. *Orthopedic Bone Cements*. Boca Raton, FL. CRC Press. 2008.
- Dhandayuthapani B., Yoshida Y., Maekawa T., Kumar D.S. Polymeric scaffolds in tissue engineering application: a review. *Int. J. Polym. Sci.* 2011, 2011: 1-19.
- Dong Y., Ruan Y., Wang H., Zhao Y., Bi D. Studies on glass transition temperature of chitosan with four techniques. *J. Appl. Polym. Sci.* 2004, 93: 1553–1558.
- Drosos G.I., Babourda E., Magnissalis E.A., Giatromanolaki A., Kazakos K., Verettas D.A. Mechanical characterization of bone graft substitute ceramic cements. *Injury*. 2012, 43: 266-271.
- Duan Y., Jia J., Wang S., Yan W., Jin L., Wang Z. Preparation of PLGA electrospun nanofibers for tissue engineering applications. *Journal of US-China Medical Science*. 2007, 4: 41-44.
- Dvir T., Tsur-Gang O., Cohen S. “Designer” scaffolds for tissue engineering and regeneration. *Isr. J. Chem.* 2005, 45: 487-494.
- Elsabee M.Z., Naguib H.F., Morsi R.E. Chitosan based nanofibers review. *Mater. Sci. Eng. C*. 32, 2012, 1711–1726.
- Endogan T., Serbetci K., Hasirci N. Effects of ingredients on thermal and mechanical properties of acrylic bone cements. *J. Appl. Polym. Sci.* 2009, 113: 4077–4084.
- Endres M., Huttmacher D.W., Salgado A.J., Kaps C., Ringe J., Reis R.L., Sittinger M., Brandwood A., Schantz J.T. Osteogenic induction of human bone marrow-derived mesenchymal progenitor cells in novel synthetic polymer–hydrogel matrices. *Tissue Eng.* 2003, 9: 689-702.
- Espigares I., Elvira C., Mano J.F., Vázquez B., Román J.S., Reis R.L. New partially degradable and bioactive acrylic bone cements based on starch blends and ceramic fillers. *Biomaterials*. 2002, 23: 1883-1895.
- Franco-Marques E., Mendez J.A., Girones J., Pelach M.A. Thermal and dynamic mechanical characterization of acrylic bone cements modified with biodegradable polymers. *J. Appl. Polym. Sci.* 2012, doi: 10.1002/app.38523.
- Fukuda C., Goto K., Imamura M., Nakamura T. Bioactive bone cement with a low content of titania particles without postsilanization: effect of filler content on osteoconductivity, mechanical properties, and handling characteristics. *J. Biomed. Mater. Res. Part B Appl. Biomater.* 2010, 95: 407–413.
- Fukuda C., Goto K., Imamura M., Neo M., Nakamura T. Bone bonding ability and handling properties of a titania–polymethylmethacrylate. *Acta Biomater.* 2011, 7: 3595–3600.
- Geng X., Kwon O.H., Jang J. Electrospinning of chitosan dissolved in concentrated acetic acid solution. *Biomaterials*. 2005, 26: 5427–5432.
- Goto K., Hashimoto M., Takadama H., Tamura J., Fujibayashi S., Kawanabe K. Mechanical, setting, and biological properties of bone cements containing micron-sized titania particles. *J. Mater. Sci. Mater. Med.* 2008, 19: 1009–1016.

Hamizah A. S., Mariatti M., Othman R., Kawashita M., Noor Hayati A. R. Mechanical and thermal properties of polymethylmethacrylate bone cement composites incorporated with hydroxyapatite and glass-ceramic fillers. *J. Appl. Polym. Sci.* 2012, 125: E661–E669.

Hansen D., Jensen J.S. Mixing does not improve mechanical properties of all bone cements. *Acta Orthop. Scand.* 1992, 63: 13-18.

He P., Sahoo S., Ng K.S., Chen K., Toh S.L., Goh J.C. Enhanced osteoinductivity and osteoconductivity through hydroxyapatite coating of silk-based tissue-engineered ligament scaffold. *J. Biomed. Mater. Res. A.* 2013, 101(2): 555-566.

He Y., Trotignon J.P., Tcharkhtchi A., Verdu J. Effect of antibiotics on the properties of poly(methylmethacrylate)-based bone cement. *J. Biomed. Mater. Res.* 2002, 63: 800-806.

Heini P.F., Berlemann U., Kaufmann M., Lippuner K., Frankhauser C., van Landuyt P. Augmentation of mechanical properties in osteoporotic vertebral bones: a biomechanical investigation of vertebroplasty efficacy with different bone cements. *Eur. Spine J.* 2001, 10: 164–171.

Hooy-Corstjens C.S.J.V., Govaert L.E., Spoelstra A.B., Bulstra S.K., Wetzels G.M.R, Koole L.H. Mechanical behaviour of a new acrylic radiopaque iodine-containing bone cement. *Biomaterials.* 2004, 25: 2657–2667.

Hsieh W.C., Chang C.P., Lin S.M. Morphology and characterization of 3D micro-porous structured chitosan scaffolds for tissue engineering. *Colloid Surface B.* 2007, 57: 250–255.

Hsiue G.H., Wang C.C. Functionalization of polyethylene surface using plasma-induced graft copolymerization of acrylic acid. *J. Polym. Sci. Polym. Chem.* 1993, 31: 3327–3337.

<http://www.sciencelab.com/msds.php?msdsId=9927336> (last visited on March 2013)

Huang Z.M., Zhang Y.Z., Ramakrishna S., Lim C.T. Electrospinning and mechanical characterization of gelatin nanofibers. *Polymer.* 2004, 45: 5361–5368.

Huang, Z. M., Zhang Y. Z., Kotaki M., Ramakrishna S. A review on polymer nanofibers by electrospinning and their applications in nanocomposites. *Compos. Sci. Technol.* 2003, 63: 2223-2253.

Hudson S.M., Jenkins D.W. Chitin and Chitosan. *Encyclopedia of Polymer Science and Technology*, 3rd Ed. Ed. Herman F. Mark. Hoboken, NJ: Wiley Interscience, 2001.

Hutmacher D.W. Scaffold design and fabrication technologies for engineering tissues — state of the art and future perspectives. *J. Biomater. Sci. Polymer Edn.* 2001, 12(1): 107–124.

Hutmacher D.W., Sittering M., Risbud M.V. Scaffold-based tissue engineering: rationale for computer-aided design and solid free-form fabrication systems. *Trends Biotechnol.* 2004, 22(7): 354-362.

Hutmacher D.W., Woodruff M.A. *Handbook of Engineering Biopolymers: Homopolymers, Blends and Composites.* In Fakirov S., Bhattacharyya D. eds. Pages 773-794, Chapter 26 Composite Scaffolds for bone engineering. Hanser Gardner Publications Ohio USA, 2007.

Isikli C., Hasirci V., Hasirci N. Development of porous chitosan-gelatin/hydroxyapatite composite scaffolds for hard tissue-engineering applications. *J. Tissue Eng. Regen. Med.* 2012, 6(2): 135-143.

- Itala A.I., Ylanen H.O., Ekholm C., Karlsson K.H., Aro H.T. Pore diameter of more than 100 micron is not requisite for bone ingrowth in rabbits. *J. Biomed. Mater. Res.* 2001, 58 (6): 679–683.
- Itoh M., Shimazu A., Hirata I., Yoshida Y., Shintani H., Okazaki M. Characterization of CO₃Ap-collagen sponges using X-ray high-resolution microtomography. *Biomaterials.* 2004, 25 (13): 2577–2583.
- Jang J., Yang H. The effect of surface treatment on the performance improvement of carbon fiber/polybenzoxazine composites. *J. Mater. Sci.* 2000, 35: 2297-2303.
- Jee W.. Structure and function of bone tissue. In F. Bronner and R.V. Worrell, ed. *Orthopedics-Principles of basic and clinical science.* Pages 3-27, CRC Press, Boca Raton, Florida, 1999.
- Johnson B.D., Beebe D.J., Crone W. Effects of swelling on the mechanical properties of a pH-sensitive hydrogel for use in microfluidic devices. *Mater Sci Eng C.* 2004, 24: 575–581.
- Jose M.V., Thomas V., Johnson K.T., Dean D.R., Nyairo E. Aligned PLGA/HA nanofibrous nanocomposite scaffolds for bone tissue engineering. *Acta Biomater.* 2009, 5: 305–315.
- Joshy M.I.A., Elayaraja K., Sakthivel N., Chandra V.S., Shanthini G.M., Kalkura S. N. Freeze dried cross linking free biodegradable composites with microstructures for tissue engineering and drug delivery application. *Mater. Sci. Eng. C.* 2013, 33(1): 466-474.
- Kane R.J., Roeder R.K. Effects of hydroxyapatite reinforcement on the architecture and mechanical properties of freeze-dried collagen scaffolds. *J. Mech. Behav. Biomed. Mater.* 2012, 7: 41-49.
- Karadas O., Yucel D., Kenar H., Kose G.T., Hasirci V. Collagen scaffolds with in situ-grown calcium phosphate for osteogenic differentiation of Wharton's jelly and menstrual blood stem cells. *J. Tissue Eng. Regen. Med.* 2012, doi: 10.1002/term.1555.
- Karageorgiou V., Kaplan D. Porosity of 3D biomaterial scaffolds and osteogenesis. *Biomaterials.* 2005, 26(27): 5474-5491.
- Katti K.S., Verma D., Katti D.R. *Materials for joint replacement* P.A. Revell (Ed.). in Chapter 4 *Joint Replacement Technology*, pages 90 Woodhead Publishing Limited, 2008.
- Kawashita M., Kawamura K., Li Z. PMMA-based bone cements containing magnetite particles for the hyperthermia of cancer. *Acta Biomater.* 2010, 6: 3187–3192.
- Kenar H., Kose G.T., Toner M., Kaplan D.L., Hasirci V. A 3D aligned microfibrillar myocardial tissue construct cultured under transient perfusion. *Biomaterials.* 2011, 32(23): 5320-5329.
- Khaled S.M.Z., Charpentier P.A., Rizkalla A.S. Physical and mechanical properties of pmma bone cement reinforced with nano-sized titania fibers. *J. Biomater. Appl.* 2011, 25: 515-523.
- Khang G., Yoon S.J., Song J.E., Iwasake Y., Lee D. Scaffold design for the, reduction of host tissue response. *Regenerative Research.* 2012, 1(1): 8-17.
- Kim H.D., Valentini R.F. Retention and activity of BMP-2 in hyaluronic acid-based scaffolds in vitro. *J. Biomed. Mater. Res.* 2002, 59 (3): 573–584.
- Kim H.Y., Yasuda H.K. Improvement of fatigue properties of Poly(methyl methacrylate) bone cement by means of plasma surface treatment of fillers. *J. Biomed. Mater. Res. Appl. Biomater.*

1999, 48: 135-142.

Kindt-Larsen T.K., Smith D.B., Jensen J.S. Innovations in acrylic bone cement and application equipment. *J. Appl. Biomater.* 1995, 6: 75-83.

Korach C.S., Halada G., Mubarez H. Effects of processing conditions on chitosan-hydroxyapatite biocomposite mechanical properties. *Conference Proceedings of the Society for Experimental Mechanics Series*, 2011, 2: 125-130.

Kuehn K.D., Ege W., Gopp U. Acrylic bone cements: composition and properties. *Orthop. Clin. North Am.* 2005, 36: 17-28.

Kühn K.D. *Bone Cements. Up-To-Date comparison of physical and chemical properties of commercial materials.* Berlin, Germany. Springer-Verlag, 2000.

Kumar A., Deka M., in: Ashok Kumar (Ed.), *Nanofibers*, page 17, Intech, 2010.

Kumar B.V.S., Siddaramaiah, Shayan M.B., Manjula K.S., Ranganathaiah C., Rao G.V.N., Basavalingu B., Byrappa K. Effect of zeolite particulate filler on the properties of polyurethane composites. *J. Polym. Res.* 2010, 17: 135-142.

Ladizesky N.H., Ward I.M. A review of plasma treatment and clinical application of polyethylene fibers to reinforcement of acrylic resins. *J. Mater. Sci. Mater. Med.* 1995, 6: 497-504.

Lam W.M., Pan H.B., Fong M.K., Cheung W.S., Wong K.L., Li Z.Y., Luk K.D., Chan W.K., Wong C.T., Yang C., Lu W.W. In Vitro characterization of low modulus linoleic acid coated strontium-substituted hydroxyapatite containing PMMA bone cement. *J. Biomed. Mater. Res. B Appl. Biomater.* 2011, 96(1): 76-83.

Langer R., Vacanti J. P., *Science.* 1993, 260, 920.

Lelovics H., Liptakova T. Time and mixing technique-dependent changes in bone cement smartest HV. *Acta Bioeng. Biomech.* 2010, 12: 63-67.

Lewis G. Properties of acrylic bone cement: State of the art review. *J. Biomed. Mater. Res. Appl. Biomater.* 1997, 38: 155-182.

Lewis G. Properties of antibiotic-loaded acrylic bone cements for use in cemented arthroplasties: a state-of-the-art review. *J. Biomed. Mater. Res. Part B: Appl. Biomater.* 2009, 89B (2): 558-574.

Lewis G. Viscoelastic properties of injectable bone cements for orthopedic applications: state-of-the-art review. *J. Biomed. Mater. Res. Part B Appl. Biomater.* 2011, 98: 171-191.

Li C., Mason L. Thermal characterization of PMMA-based cement curing. *J. Mater. Sci. Mater. M.* 2004, 15: 85-89.

Li D., Ouyang G., McCann J.T., Xia Y.N. Collecting electrospun nanofibers with patterned electrodes. *Nano Lett.* 2005, 5(5): 913-916.

Li Q., Grandmaison E.W., Goosen M.F.A., Dunn E.T. Applications and properties of chitosan. *J. Bioact. Compat. Pol.* 1992, 7(4): 370-397.

- Li Z., Kawamura K., Kawashita M., Kudo T., Kanetaka H., Hiraoka M. In vitro assessment of poly(methylmethacrylate)-based bone cement containing magnetite nanoparticles for hyperthermia treatment of bone tumor. *J. Biomed. Mater. Res. Part A.* 2012, 100A: 2537-2545.
- Li Z.S., Ramay H.R., Hauch K.D., Xiao D.M., Zhang M.Q. Chitosan–alginate hybrid scaffolds for bone tissue engineering. *Biomaterials.* 2005, 26: 3919-3928.
- Lieberman I.H., Togawa D., Kayanja M.M. Vertebroplasty and kyphoplasty: filler materials. *Spine J.* 2005, 5, 305S-316S.
- Litsky A.S., Rose R.M., Rubin C.T., Thrasher E.L. A reduced modulus acrylic bone cement: preliminary results. *J. Orthop. Res.* 1990, 8: 623–626.
- Liu C., Green S.M., Watkins N.D., Gregg P.J., McCaskie A.W. Some failure modes of four clinical bone cements. *Proceedings of the Institution of Mechanical Engineers, Part H: Journal of Engineering in Medicine*, 2001, 215: 359-366.
- Liu X., Ma P.X. Polymeric scaffolds for bone tissue engineering. *Ann. Biomed. Eng.* 2004, 32 (3): 477-486.
- Loh I.H., Sheu M.S. (1995). *Plasma Surface Modification in Biomedical Applications*. MRS Proceedings, 414, 43 doi:10.1557/PROC-414-43.
- Lopez-Perez P.M., da Silva R.M.P., Serra C., Pashkuleva I., Reis R.L. Surface phosphorylation of chitosan significantly improves osteoblast cell viability, attachment and proliferation. *J. Mater. Chem.* 2010, 20: 483–491.
- Lyons F., Partap S., O'Brien F.J. Part 1: scaffolds and surfaces. *Technol. Health Care.* 2008, 16: 305–317.
- Martin B. Aging and strength of bone as a structural material. *Calcif. Tissue Int.* 1993, 53(Suppl 1): S34-S40.
- Martini F.H. *Fundamentals of Anatomy and Physiology*, 3rd edition. Prentice-Hall, Inc., Englewood Cliffs, New Jersey, 1995.
- May-Pat A., Herrera-Kao W., Cauich-Rodríguez J.V., Cervantes-Uc J.M., Flores-Gallardo S.G. Comparative study on the mechanical and fracture properties of acrylic bone cements prepared with monomers containing amine groups. *J. Mech. Behav. Biomed. Mater.* 2012, 6: 95-105.
- Méndez J.A., Aguilar M.R., Abraham G.A., Vázquez B., Dalby M., DiSilvio L., San Román J. New acrylic bone cements conjugated to vitamin E: curing parameters, properties and biocompatibility. *J. Biomed. Mater. Res.* 2002, 62: 299-307.
- Meng Z.X., Zheng W., Li L., Zheng Y.F. Fabrication, characterization and in vitro drug release behavior of electrospun PLGA/chitosan nanofibrous scaffold. *Mater. Chem. Phys.* 2011, 125(3): 606-611.
- Mestres G., Ginebra M.P. Novel magnesium phosphate cements with high early strength and antibacterial properties. *Acta Biomater.* 2011, 7: 1853-1861.
- Meyer P.R., Lautenschlager E.P., Moore B.K. On the setting properties of acrylic bone cement. *J. Bone Joint Surg.* 1973, 55(A): 149–156.

- Mikos A.G., Thorsen A.J., Czerwonka L.A., Bao Y., Langer R., Winslow D.N., Vacanti J.P. Preparation and characterization of poly(L-lactic acid) foams. *Polymer*. 1994, 35(5):1068-77.
- Mohamed F., van der Walle C.F. Engineering biodegradable polyester particles with specific drug targeting and drug release properties. *J. Pharm. Sci.* 2008, 97, 71–87.
- Möller K., Bein T., Fischer R.X. Entrapment of pmma polymer strands in micro- and mesoporous materials. *Chem. Mater.* 1998, 10: 1841-1852.
- Moore W.R., Graves S.E., Bain G.I. Synthetic bone graft substitutes. *ANZ J. Surg.* 2001, 71: 354-361.
- Morejon L., Mendizabal E., Delgado J.A., Davidenko N., Lopez-Dellamary F., Manriquez R., Ginebra M.P., Gil F.J., Planell J.A. Synthesis and characterization of Poly(methyl methacrylate-styrene) copolymeric beads for bone cements. *Latin Am. Appl. Res.* 2005, 35: 175-182.
- Mori A, Ohtsuki C, Sugano A, Kuramoto K, Miyazaki T, Tanihara M, Osaka A. Bioactive PMMA-based bone cement modified with methacryloxypropyl-trimethoxysilane and calcium salts. *J. Ceram. Soc. Japan.* 2003, 111: 738–742.
- Mourino V., Cattalini J.P., Boccaccini A.R. Metallic ions as therapeutic agents in tissue engineering scaffolds: an overview of their biological applications and strategies for new developments. *J. R. Soc. Interface.* 2012, 9(68): 401-419.
- Murphy C.M., Haugh M.G., O'Brien F.J. The effect of mean pore size on cell attachment, proliferation and migration in collagen–glycosaminoglycan scaffolds for bone tissue engineering. *Biomaterials.* 2010, 31: 461–466.
- Nakayama M., Yano J., Nakaoka K., Ogura K. Spectroscopic studies on the incorporation of polypyrrole into zeolite channels. *Synth. Met.* 2003, 138: 419-422.
- Nalwa H. S., Ed., Nanostructured biomaterials, in *Encyclopedia of nanoscience and nanotechnology*, pages 595–613, California: American Scientific Publishers, 2004.
- Ndreu A., Nikkola L., Ylikauppila H., Ashammakhi N., Hasirci V. Electrospun biodegradable nanofibrous mats for tissue engineering. *Nanomed.* 2008, 3: 45-60.
- Nezafati N., Moztarzadeh F., Hesaraki S. Evaluation of a prepared sol-gel bioactive glass fiber-reinforced calcium phosphate cement. *J Ceram. Process. Res.* 2010, 11: 367-371.
- Nguyen H.Q., Deporter D.A., Pilliara R.M., Valiquettea N., Yakubovich R. The effect of sol–gel-formed calcium phosphate coatings on bone ingrowth and osteoconductivity of porous-surfaced Ti alloy implants. *Biomaterials.* 2004, 25(5): 865-876.
- Ni G.X., Lin J.H., Chiu P.K., Li Z.Y., Lu W.W. Effect of strontium-containing hydroxyapatite bone cement on bone remodeling following hip replacement. *J. Mater. Sci. Mater. Med.* 2010, 21(1): 377-384.
- Nien Y.H., Lin S., Hsu Y.N. Preparation and characterization of acrylic bone cement with high drug release. *Mater. Sci. Eng. C.* 2013, 33: 974–978.
- Niiranen H., Pyhalto T., Rokkanen P., Kellomäki M., Tormala P. In vitro and in vivo behavior of self-reinforced bioabsorbable polymer and self-reinforced bioabsorbable polymer/bioactive glass composites. *J. Biomed. Mater. Res. A.* 2004, 69(4): 699-708.

- Nishikawa H., Ueno A., Nishikawa S., Kido J., Ohishi M., Inoue H., Nagata T. Sulfated glycosaminoglycan synthesis and its regulation by transforming growth factor- β in rat clonal dental pulp cells. *J. Endod.* 2000, 26: 169–171.
- Nordin M., Frankel V.H. Basic biomechanics of the musculoskeletal system. Pages 22–30, 2nd edition, Lea and Fibiger, Philadelphia, 1989.
- Nordtveit R.J., Varum K.M., Smidsrod O. Degradation of partially N-acetylated chitosans with hen egg white and human lysozyme. *Carbonhyd. Polym.* 1996, 29: 163-167.
- Nwe N., Furuike T., Tamura H. The mechanical and biological properties of chitosan scaffolds for tissue regeneration templates are significantly enhanced by chitosan from *Gongronella butleri*. *Materials.* 2009, 2: 374-398.
- Ohkawa K., Cha D., Kim H., Nishida A., Yamamoto H. Electrospinning of chitosan. *Macromol. Rapid Comm.* 2004, 25: 1600–1605.
- Opara T.N., Dalby M.J., Harper E.J., Silvio L.D., Bonfield W. The effect of varying percentage of hydroxyapatite in poly(ethyl methacrylate) bone cement on human osteoblast-like cells. *J. Mater. Sci. Mater. Med.* 2003, 14: 277-282.
- Ozcan C. Surface free energy evaluation, plasma surface modification and biocompatibility studies of PMMA films. Master thesis, 2006.
- Ozgen O. Plasma surface modification and characterization of PMMA films. Master Thesis, 2011.
- Pallela R., Venkatesan J., Janapala V.R., Kim S.K. Biophysicochemical evaluation of chitosan-hydroxyapatite-marinesponge collagen composite for bone tissue engineering. *J. Biomed. Mater. Res. Part A.* 2012, 100A: 486-495.
- Park J.B., *Biomaterials in the Biomedical Engineering Handbook.* pages 529-536, Bronzino, J. D., (Eds.), CRC Press Inc., Boca Raton, Florida, USA, 1995.
- Park J.H., Olivares-Navarrete R., Wasilewski C.E., Boyan B.D., Tannenbaum R., Schwartz. Z. Use of polyelectrolyte thin films to modulate Osteoblast response to microstructured titanium surfaces. *Biomaterials.* 2012, 33(21): 5267-77.
- Pascual B., Gurruchaga M., Ginebra M.P., Goñi F.J., Planell J.A., Vázquez B., San Román J., Goñi I. Modified acrylic bone cement with high amounts of ethoxytriethyleneglycol methacrylate. *Biomaterials.* 1999, 20: 453–463.
- Pascual B., Vázquez B., Gurruchaga M., Goñi I., Ginebra M.P., Gil F.J., Planell J.A., Levenfeld B., San Román J. New aspects of the effect of size and size distribution on the setting parameters and mechanical properties of acrylic bone cements. *Biomaterials.* 1996, 17: 509-516.
- Patist C.M., Mulder M. B., Gautier S.E., Maquet V., Jérôme R., Oudega M. Freeze-dried poly(D,L-lactic acid) macroporous guidance scaffolds impregnated with brain-derived neurotrophic factor in the transected adult rat thoracic spinal cord. *Biomaterials.* 2004, 25(9): 1569-1582.
- Pavelić K., Hadžija M. Medical Applications of Zeolites. in *Handbook of Zeolite Science and Technology*, Auerbach S.M., Carrado C.A., Dutta P.K., Eds., pages 1453–1491, Marcel Dekker, Inc: New York, 2005.

- Pereira C.S., Cunha A.M., Reis R.L., Vazquez B., San Roman J. New starch-based thermoplastic hydrogels for use as bone cements or drug-delivery carriers. *J. Mater. Sci. Mater. Med.* 1998, 9: 825–833.
- Pourdeyhimi B., Wagner H.D. Elastic and ultimate properties of acrylic bone cement reinforced with ultra-high-molecular-weight polyethylene fibers. *J. Biomed. Mater. Res.* 1989, 23: 63–80.
- Provenzano M.J., Murphy K.P.J., Riley L.H. Bone cements: Review of their physiochemical and biochemical properties in percutaneous vertebroplasty. *AJNR Am. J. Neuroradiol.* 2004, 25: 1286–1290.
- Pulieri E., Chiono V., Ciardelli G., Vozzi G., Ahluwalia A., Domenici C., Vozzi F., Giusti P. Chitosan/gelatin blends for biomedical applications. *J. Biomed. Mater. Res.* 2008, 86A: 311–322.
- Race A., Miller M.A., Mann K.A. A modified PMMA cement (Sub-cement) for accelerated fatigue testing of cemented implant constructs using cadaveric bone. *J. Biomech.* 2008, 41(14): 3017-3023.
- Reflexive polymers and hydrogels: understanding and designing fast-responsive polymeric systems. N. Yui, R.J. Mersny, K. Park, eds. Pages 9-32, CRC Press LLC; Boca Raton, 2004.
- Ren D., Yi H., Zhang H., Xie W., Wang W., Ma X. A preliminary study on fabrication of nanoscale fibrous chitosan membranes in situ by biospecific degradation. *J. Membr. Sci.* 2006, 280: 99-107.
- Rentería-Zamarrón D., Cortés-Hernández D.A., Bretado-Aragón L., Ortega-Lara W. Mechanical properties and apatite-forming ability of PMMA bone cements. *Mater. Design.* 2009, 30: 3318–3324.
- Rocha L.B., Goissis G., Rossi M.A. Biocompatibility of anionic collagen matrix as scaffold for bone healing. *Biomaterials.* 2002, 23 (2): 449–456.
- Rojo L., Vazquez B., Deb S., Roman J.S. Eugenol derivatives immobilized in auto-polymerizing formulations as an approach to avoid inhibition interferences and improve biofunctionality in dental and orthopedic cements. *Acta Biomater.* 2009, 5: 1616-1625.
- Rosellini E., Vozzi G., Barbani N., Giusti P., Cristallini C. Three-dimensional microfabricated scaffolds with cardiac extracellular matrix-like architecture. *Int. J. Artif. Organs.* 2010, 33 (12): 885-894.
- Rouwkema J., Rivron N.C., van Blitterswijk C.A. Vascularization in tissue engineering. *Trends Biotechnol.* 2008, 26: 434–441.
- Saghiri M.A., Lotfi M., Aghili H. Dental Cement Composition. Pub. No. US Patent 2012/0012030.
- Saha S., Pal S. Mechanical properties of bone cement: A review. *J. Biomed. Mater. Res.* 1984, 18: 435-462.
- Sakurai K., Maegawa T., Takahashi T. Glass transition temperature of chitosan and miscibility of chitosan/poly(N-vinyl pyrrolidone) blends. *Polymer.* 2000, 41: 7051-7056.
- Salgado A.J., Coutinho O.P., Reis R.L. Bone tissue engineering: state of the art and future trends. *Macromol. Biosci.* 2004, 4: 74-765.

- Schrooten J., Helsen J.A. Adhesion of bioactive glass coating to Ti6Al4V oral implant. *Biomaterials*. 2000, 21, 1461.
- Seifu D.G., Isimjan T.T., Mequanint K. Tissue engineering scaffolds containing embedded fluorinated-zeolite oxygen vectors. *Acta Biomater*. 2011, 7: 3670-3678.
- Serbetci K., Korkusuz F., Hasirci N. Thermal and mechanical properties of hydroxyapatite impregnated acrylic bone cements. *Polym. Test*. 2004, 23: 145–155.
- Shikinami Y., Okuno M. Bioresorbable devices made of forged composites of hydroxyapatite (HA) particles and poly-L-lactide (PLLA): part I. Basic characteristics. *Biomaterials*. 1998, 20: 859-77.
- Silva S.S., Luna S.M., Gomes M.E., Benesch J., Pashkuleva I., Mano J.F., Reis R.L. Plasma surface modification of chitosan membranes: characterization and preliminary cell response studies. *Macromol Biosci*. 2008, 8(6): 568–576.
- Sin D.C., Miao X., Liu G., Wei F., Chadwick G., Yan C., Friis T. Polyurethane (PU) scaffolds prepared by solvent casting/particulate leaching (SCPL) combined with centrifugation. *Mater. Sci. Eng. C*. 2010, 30: 78–85.
- Spange S., Graser A., Muller H., Zimmermann Y., Rehak P., Jager C., Fuess H., Baetz C. Synthesis of Inorganic/Organic Host-Guest Hybrid Materials by Cationic Vinyl Polymerization within Y Zeolites and MCM-41. *Chem. Mater*. 2001, 13: 3698-3708.
- Spence A. *Basic Medical Anatomy*, 3rd ed. Redwood City, CA: Benjamin/ Cummings, 1990.
- Subbiah T., Bhat G.S., Tock R.W., Pararneswaran S., Ramkumar S.S. Electrospinning of nanofibers. *J. Appl. Polym. Sci*. 2005, 96: 557–569.
- Subramanian A., Lin H.Y. Crosslinked chitosan: Its physical properties and the effects of matrix stiffness on chondrocyte cell morphology and proliferation. *J. Biomed. Mater. Res. Part A*. 2005, 75: 742–753.
- Suh S.W., Shin J.Y., Kim J., Kim J., Beak C.H., Kim D.I., Kim H., Jeon S.S., Choo I.W. Effect of different particles on cell proliferation in polymer scaffolds using a solvent-casting and particulate leaching technique. *ASAIO J*. 2002, 48(5): 460-464.
- Sun Y., Haruman E. Influence of processing conditions on structural characteristics of hybrid plasma surface alloyed austenitic stainless steel. *Surf. Coat. Technol*. 2008, 202: 4069-4075.
- Tanase C.E., Popa M.I., Verestiuc L. Biomimetic chitosan-calcium phosphate composites with potential applications as bone substitutes: preparation and characterization. *J. Biomed. Mater. Res. Part B Appl. Biomater*. 2012, 100 B (3): 700-708.
- Thakur G., Mitra A., Basak A., Sheet D. Characterization and scanning electron microscopic investigation of crosslinked freeze dried gelatin matrices for study of drug diffusivity and release kinetics. *Micron*, 2012, 43(2–3): 311-320.
- Thein H.W.W., Kitiyanant Y. Chitosan scaffolds for *in vitro* buffalo embryonic stem-like cell culture: An approach to tissue engineering. *J. Biomed. Mater. Res*. 2006, 80B: 92-101.
- Thein H.W.W., Misra R.D.K. Biomimetic chitosan–nanohydroxyapatite composite scaffolds for bone tissue engineering. *Acta Biomater*. 2009, 5(4): 1182-1197.

Toksvig-Larsen S.T., Franzen S., Ryd L. Cement interface temperature in hip arthroplasty. *Acta Orthop. Scand.* 1991, 62: 102–105.

Topoleski L.D.T., Ducheyne P., Cuckler J.M. The effects of centrifugation and titanium fiber reinforcement on fatigue failure mechanisms in poly(methyl methacrylate) bone cement. *J. Biomed. Mater. Res.* 1995, 29: 299-307.

Travan, A., Marsich, E., Donati, I., Foulc, M.P., Moritz, N., Aro, H.T., Paoletti, S. Polysaccharide-coated thermosets for orthopedic applications: from material characterization to in vivo tests. *Biomacromol.* 2012, 13: 1564-1572.

Uchida M., Kim H.M., Kokubo T., Fujibayashi S., Nakamura T. Structural dependence of apatite formation on titania gels in a simulated body fluid. *J. Biomed. Mater. Res.* 2003, 64A: 164–170.

Urrutia J., Bono C.M., Mery P., Rojas C. Early histologic changes following polymethylmethacrylate injection (vertebroplasty) in rabbit lumbar vertebrae. *Spine.* 2008, 33: 877–882.

Van Mullen P.J., de Wijn J.R., Vaandrager J.M. Porous acrylic cement: evaluation of a novel implant material. *Ann. Plast. Surg.* 1988, 21: 576–582.

Venkatesan J., Ryu B.M., Sudha P.N., Kim S.K. Preparation and characterization of chitosan-carbon nanotube scaffolds for bone tissue engineering. *Int. J. Biol. Macromol.* 2012, 50: 393-402.

Vozzi G., Flaim C., Ahluwalia A., Bhatia S., Fabrication of PLGA scaffolds using soft lithography and microsyringe deposition. *Biomaterials.* 2003, 24: 2533-2540.

Vrana N.E., Elsheikh A., Builles N., Damour O., Hasirci V. Effect of human corneal keratocytes and retinal pigment epithelial cells on the mechanical properties of micropatterned collagen films. *Biomaterials.* 2007, 28: 4303–4310.

Wan Y., Fang Y., Wu H., Cao X. Porous polylactide/chitosan scaffolds for tissue engineering. *J. Biomed. Mater. Res.* 2007, 80A: 776-788.

Wan Jun T., Cunxin W., Donghua C. Kinetic studies of the pyrolysis of chitin and chitosan. *Polym. Degrad. Stabil.* 2005, 87: 389-394.

Woodard, J.R., Hilldore A.J., Lan S.K., Park C.J., Morgan A.W., Eurell J.A.C., Clark S.G., Wheeler M.B., Jamison R.D., Johnson A.J.W. The mechanical properties and osteoconductivity of hydroxyapatite bone scaffolds with multi-scale porosity. *Biomaterials.* 2007, 28: 45–54.

Wright D.D., Gilbert J.L., Lautenschlager E.P. The effect of processing temperature and time on the structure and fracture characteristics of self-reinforced composite poly(methyl methacrylate). *J. Mater. Sci. Mater. Med.* 1999, 10: 503–512.

www.btec.cmu.edu (last visited on October 2012)

www.roche.com (last visited on December 2012)

Xin X., Hussain M., Mao J.J. Continuing differentiation of human mesenchymal stem cells and induced chondrogenic and osteogenic lineages in electrospun PLGA nanofiber scaffold. *Biomaterials.* 2007, 28: 316–325.

- Xu L.X., Shi X.T., Wang Y.P., Shi Z.L. Performance of calcium phosphate bone cement using chitosan and gelatin as well as citric acid as hardening liquid. *Journal of Clinical Rehabilitative Tissue Engineering Research*. 2008, 12: 6381-6384.
- Yaylaoglu M.B., Korkusuz P., Ors U., Korkusuz F., Hasirci V. Development of calcium phosphate–gelatin composite as a bone substitute and its use in drug release. *Biomaterials*. 1999, 20: 711–719.
- Yilgor P., Sousa R.A., Reis R.L., Hasirci N., Hasirci V. 3D plotted PCL scaffolds for stem cell based bone tissue engineering. *Macromol. Symp.* 2008, 269: 92–99.
- Yucel D., Kose G.T., Hasirci V. Polyester based nerve guidance conduit design. *Biomaterials*. 2010, 31: 1596–1603.
- Yuzay I.E., Auras R., Selke S. Poly(lactic acid) and zeolite composites prepared by melt processing: Morphological and physical-mechanical properties. *J. Appl. Polym. Sci.* 2010, 115: 2262-2270.
- Zeltinger J., Sherwood J.K., Graham D.A., Mueller R., Griffith L.G. Effect of pore size and void fraction on cellular adhesion, proliferation, and matrix deposition. *Tissue Eng.* 2001, 7: 557-572.
- Zhang J., Zhang H., Wu L., Ding J. Fabrication of three dimensional polymeric scaffolds with spherical pores. *J. Mater. Sci.* 2006, 41: 1725-1731.
- Zhang R.Y., Ma P.X. Poly(a-hydroxyl acids) hydroxyapatite porous composites for bone-tissue engineering. I. Preparation and morphology. *J. Biomed. Mater. Res.* 1999, 44: 446-455.
- Zhang X., Ayers R.A., Thorne K., Moore J.J., Schowengerdt F. Combustion synthesis of porous materials for bone replacement. *Biomed. Sci. Instrum.* 2001, 37: 463–468.
- Zhang Y., Cheng X., Wang J., Wang Y., Shi B., Huang C., Yang X., Liu T. Novel chitosan/collagen scaffold containing transforming growth factor-beta1 DNA for periodontal tissue engineering. *Biochem. Biophys. Res. Commun.* 2006, 344(1): 362-369.
- Zhang Y., Venugopal J.R., El-Turki A., Ramakrishna S., Lim C.T. Electrospun biomimetic nanocomposite nanofibers of hydroxyapatite/chitosan for bone tissue engineering. *Biomaterials*. 2008, 29: 4314–4322.
- Zhang Y., Xu H.H.K. Effects of synergistic reinforcement and absorbable fiber strength on hydroxyapatite bone cement. *J. Biomed. Mater. Res. Part A*. 2005, 75A: 832-840.
- Zhao Y., Zhou Y., Wu X., Wang L., Xu L., Wei S. A facile method for electrospinning of Ag nanoparticles/poly (vinyl alcohol)/carboxymethyl-chitosan nanofibers. *Appl. Surf. Sci.* 2012, 258(22): 8867–8873.
- Zivic F., Babic M., Grujovic N., Mitrovic S., Favaro G., Caunii M. Effect of vacuum-treatment on deformation properties of PMMA bone cement. *J. Mech. Behav. Biomed. Mater.* 2012, 5: 129–138.
- Zou Q., Zhang L., Zuo Y., Wang H.N., Li Y.B., Li X.Y. Characterization and cytocompatibility of nano-hydroxyapatite/chitosan bone cement consisting of astragalus polysaccharides. *Gongneng Cailiao/Journal of Functional Materials*, 2008, 39: 1515-1521.

APPENDIX A

POLYMERIZATION REACTION

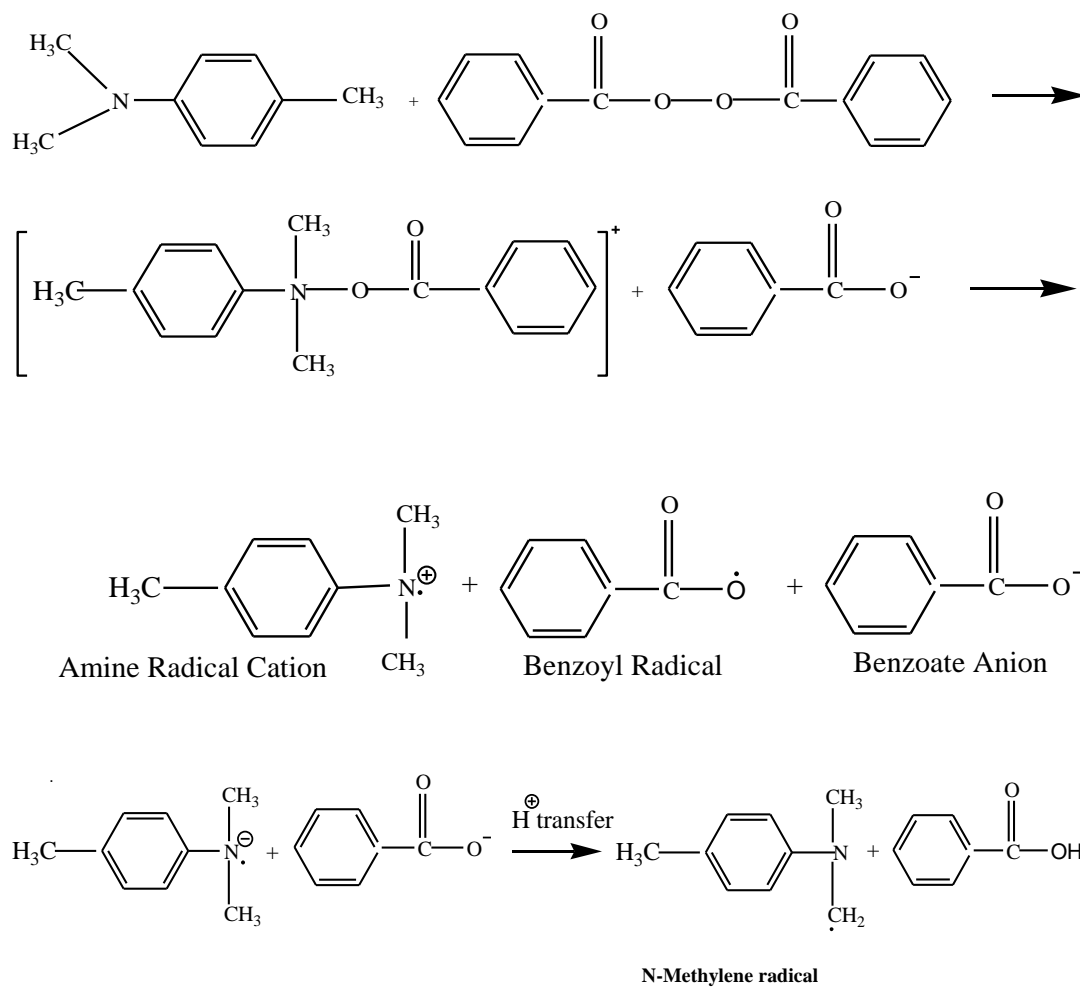


Figure A.1 Redox reaction between BPO and DMPT

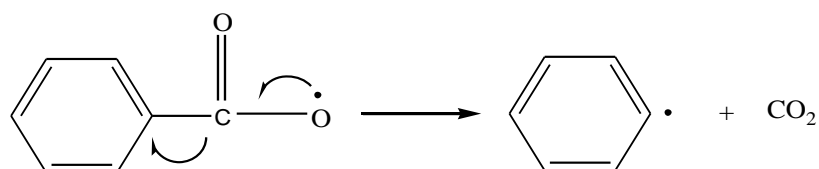


Figure A.2 Radical formation

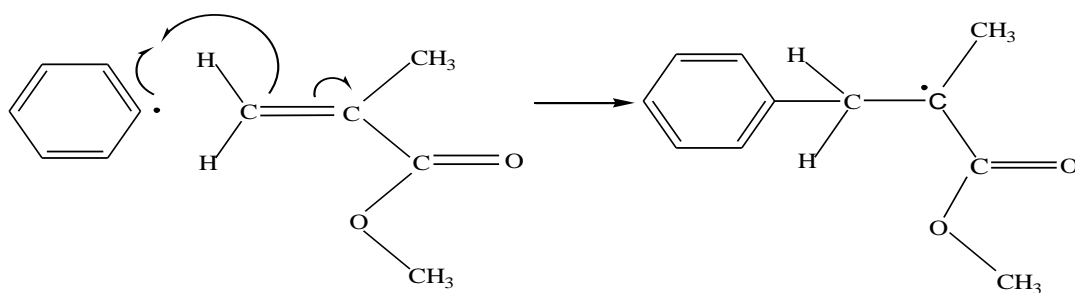


Figure A.3 Initiation step of MMA polymerization

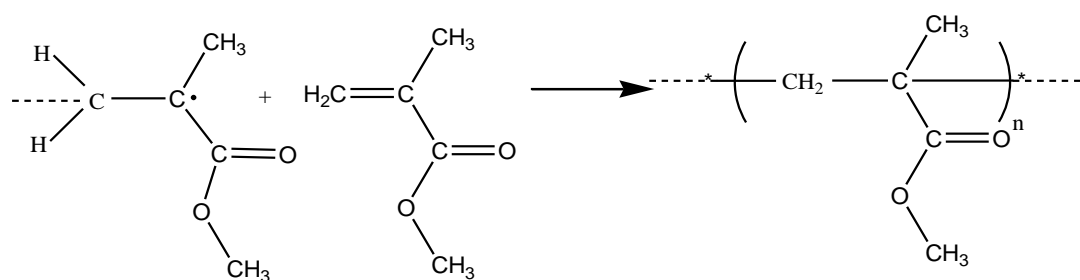


Figure A.4 Propagation step of MMA polymerization

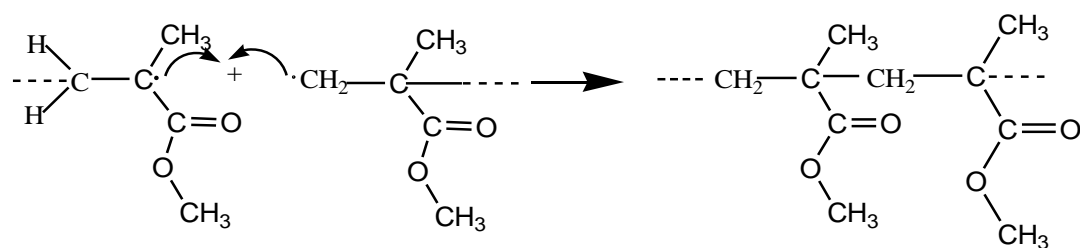


Figure A.5 Termination step

APPENDIX B

CALIBRATION CURVE

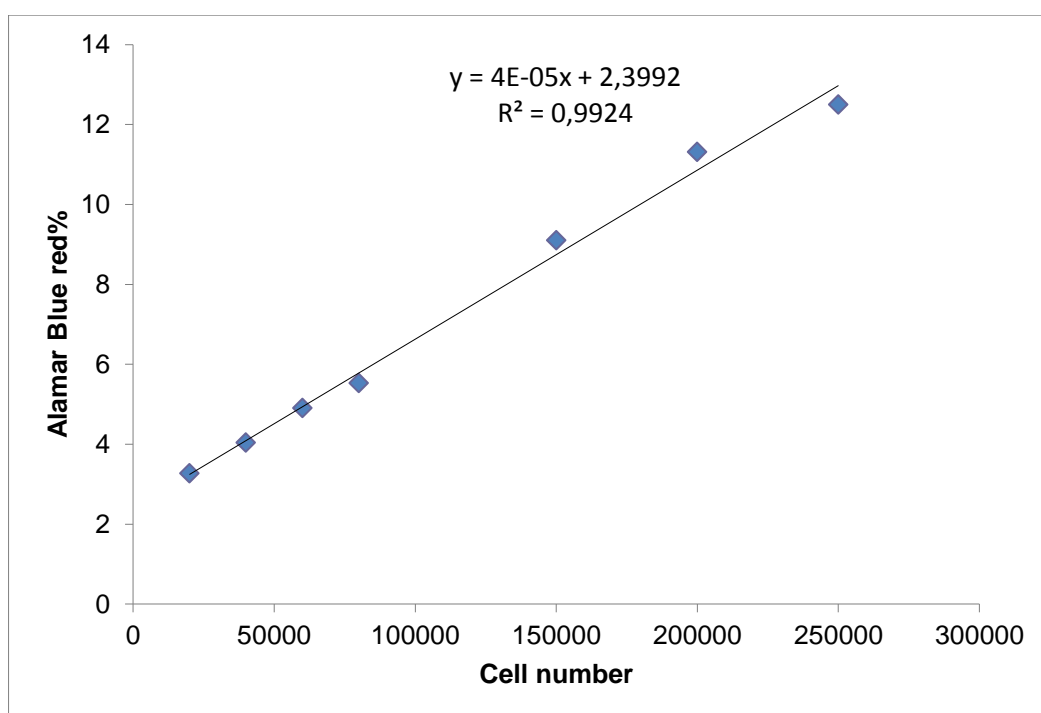


Figure B.1 Calibration curve of SaOs-2 with Alamar Blue assay

CURRICULUM VITAE

PERSONAL INFORMATION

Surname, Name: Endođan, Tuđba

Nationality: Turkish (TC)

Date and Place of Birth: 20 July 1980, Aydın

Marital Status: Single

Phone: +90 312 210 74 38

Fax: +90 312 210 64 25

E-mail: endogan@metu.edu.tr

EDUCATION

Degree	Institution	Year of Graduation
MS	METU Chemistry Dept.	2005
BS	METU Chemistry Dept.	2003
High School	Aydın Anadolu High School	1998

WORK EXPERIENCE

Year	Place	Enrollment
2010-	METU Central Laboratory	Research Associate

FOREIGN LANGUAGES: Advanced English

PUBLICATIONS

1. Endogan T., Kiziltay A., Torun Kose G., Comunoglu N., Beyzadeoglu T., Hasirci N. Acrylic Bone Cements: Effects of PMMA Powder Size and Chitosan Addition on Properties. Submitted to Journal of Applied Polymer Science
2. Bilgic H., Demiriz M., Ozler M., Ide T., Dogan N., Gumus S., Kiziltay A., Endogan T., Hasirci V., Hasirci N. Gelatin Based Scaffolds: Effect of EGF Dose on Wound Healing. Journal of Biomaterials and Tissue Engineering, 2012, accepted
3. Endogan T., Kiziltay A., Hasirci V., Hasirci N. Modification of Acrylic Bone Cements with Oxygen Plasma and Additives. Journal of Biomaterials and Tissue Engineering, 2012, 2: 236-243
4. Fedel M., Endogan T., Hasirci N., Maniglio D., Morelli A., Chiellini F., Motta A. Blood compatibility of polymers derived from natural materials. Journal of Bioactive and Compatible Polymers, 2012, 27 (4): 295-312
5. Hasirci V., Yilgor P., Endogan T., Eke G., Hasirci N. Polymer Fundamentals: Polymer Synthesis. In Comprehensive Biomaterials. Ed. P.Ducheyne, K.Healy, D.Hutmacher, J.Kirkpatrick, Elsevier Press, 2011, 1: 349-371, Book Chapter
6. Yucel D., Kenar H., Ndreu A., Endogan T., Hasirci N., Hasirci V. Nanotechnology in Biomaterials: Part I: Nanofibers in Tissue Engineering. In Bionanotechnology II: Global Prospects. Ed. D. E. Reisner, CRC Press, 2011, Book Chapter
7. Carletti E., Endogan T., Hasirci N., Hasirci V., Maniglio D., Motta A., Migliaresi, C. Microfabrication of PDLLA scaffolds. Journal of Tissue Engineering and Regenerative Medicine, 2011, 5: 569-577
8. Hasirci N., Endogan T., Vardar E., Kiziltay A., Hasirci V. Effect of oxygen plasma on surface properties and biocompatibility of PLGA films. Surface and Interface Analysis, 2010, 42: 486-491
9. Gulce Iz S., Deliloglu Gurhan S.I., Hakan Sen B., Endogan T., Hasirci N. Comparison of in vitro cytotoxicity and genotoxicity of MMA-based polymeric materials and various metallic materials. Turkish Journal of Medical Sciences, 2010, 40: 905-916
10. Bingol-Kologlu M., Bahadir G.B., Vargun R., Ilkay H., Bagriacik E.U., Yolbakan S., Guven C., Endogan T., Hasirci N., Dindar H. Effects of Local and Sustained Release of FGF, IGF, and GH on Germ Cells in Unilateral Undescended Testis in Rats. Urology, 2010, 75: 223-228
11. Endogan T., Serbetci K., Hasirci N. Effects of ingredients on thermal and mechanical properties of acrylic bone cements. Journal of Applied Polymer Science, 2009, 113: 4077-4084